NAVAL POSTGRADUATE SCHOOL
Monterey, California

DTIC
ELECTE
FEB 14 1991
S B D

THESIS

SATELLITE CHARGE CONTROL
WITH LITHIUM ION SOURCE AND ELECTRON
EMISSION

by

Ryu, Chong Soo

December 1990

Thesis Advisor	Richard C. Olsen

91 2 12 061

REPORT DOCUMENTATION PAGE

1a Report Security Classification Unclassified	1b Restrictive Markings

2a Security Classification Authority	3 Distribution Availability of Report
2b Declassification Downgrading Schedule	Approved for public release; distribution is unlimited.

4 Performing Organization Report Number(s)	5 Monitoring Organization Report Number(s)

6a Name of Performing Organization Naval Postgraduate School	6b Office Symbol (if applicable) Ph	7a Name of Monitoring Organization Naval Postgraduate School

6c Address (city, state, and ZIP code) Monterey, CA 93943-5000	7b Address (city, state, and ZIP code) Monterey, CA 93943-5000

8a Name of Funding Sponsoring Organization	8b Office Symbol (if applicable)	9 Procurement Instrument Identification Number

8c Address (city, state, and ZIP code)	10 Source of Funding Numbers

Program Element No	Project No	Task No	Work Unit Accession No

11 Title (Include security classification) SATELLITE CHARGE CONTROL WITH LITHIUM ION SOURCE AND ELECTRON EMISSION

12 Personal Author(s) Ryu, Chong Soo

13a Type of Report Master's Thesis	13b Time Covered From To	14 Date of Report (year, month, day) December 1990	15 Page Count 107

16 Supplementary Notation The views expressed in this thesis are those of the author and do not reflect the official policy or position of the Department of Defense or the U.S. Government.

17 Cosati Codes			18 Subject Terms (continue on reverse if necessary and identify by block number)
Field	Group	Subgroup	Satellite Charge Control, Lithium Ion Source, Electron Source

19 Abstract (continue on reverse if necessary and identify by block number)

A lithium ion source using thermal emission from a β-eucryptite structure has been investigated as a possible control device for spacecraft charging. This source can be used for control of positively charged spacecraft potentials in sunlight and differentially charged spacecraft surfaces in shadow. This thesis investigates the emission characteristics of lithium ion sources in conjunction with two kinds of electron sources and simulates spacecraft charge control. A 0.6″ lithium ion source produced currents up to 33 μA at a bias voltage of 100 V on the surface (strips) of the simulation body with extraction potentials of 200 V to the screen. Differential charging simulations produced currents up to 21 μA on the rear strip of the simulation structure at a bias voltage of 250 V. A directly heated tungsten dispenser cathode and a filament-type electron source were used to overcome space charge limiting effects ($I \propto V^{\frac{3}{2}}$). Space charge effects were studied with a 0.25″ lithium ion source in conjunction with the tungsten dispenser cathode. The average increase in current was approximately 50 %. Larger increases were found with the 0.6″ lithium ion source, using the filament electron source. The greatest effects occurred for low extraction voltages ($\lesssim 20V$). A typical increase was 400 % at 10 V. The vacuum chamber system and geometries for the simulation and investigation were very simple. However, we verified that the combined ion and electron sources could be used as a device for controlling a spacecraft potential in geosynchronous orbit.

20 Distribution Availability of Abstract ☒ unclassified unlimited ☐ same as report ☐ DTIC users	21 Abstract Security Classification Unclassified

22a Name of Responsible Individual Richard C. Olsen	22b Telephone (include Area code) (408) 646-2019	22c Office Symbol PhOs

DD FORM 1473, 84 MAR   83 APR edition may be used until exhausted   security classification of this page
All other editions are obsolete

Satellite Charge Control
with Lithium Ion Source and Electron Emission

by

Ryu, Chong Soo
Captain, Republic of Korea Army
B.S., Kum-Oh Institute of Technology, 1985

Submitted in partial fulfillment of the
requirements for the degree of

MASTER OF SCIENCE IN PHYSICS

from the

NAVAL POSTGRADUATE SCHOOL
December 1990
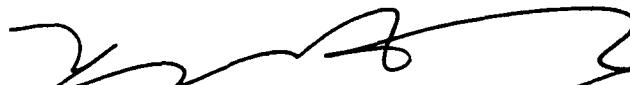
Author: _____
Ryu, Chong Soo
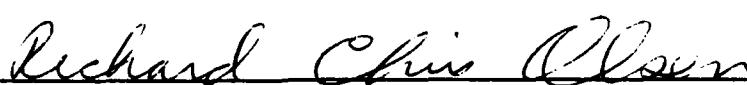
Approved by: _____
Richard C. Olsen, Thesis Advisor

_____
Otto Heinz, Second Reader

_____
Karlheinz E. Woehler, Chairman,
Department of Physics

ii

ABSTRACT

A lithium ion source using thermal emission from a β-eucryptite structure has been investigated as a possible control device for spacecraft charging. This source can be used for control of positively charged spacecraft potentials in sunlight and differentially charged spacecraft surfaces in shadow. This thesis investigates the emission characteristics of lithium ion sources in conjunction with two kinds of electron sources and simulates spacecraft charge control. A 0.6″ lithium ion source produced currents up to 33 μA at a bias voltage of 100 V on the surface (strips) of the simulation body with extraction potentials of 200 V to the screen. Differential charging simulations produced currents up to 21 μA on the rear strip of the simulation structure at a bias voltage of 250 V. A directly heated tungsten dispenser cathode and a filament-type electron source were used to overcome space charge limiting effects ($I \propto V^{\frac{3}{2}}$). Space charge effects were studied with a 0.25″ lithium ion source in conjunction with the tungsten dispenser cathode. The average increase in current was approximately 50 %. Larger increases were found with the 0.6″ lithium ion source, using the filament electron source. The greatest effects occurred for low extraction voltages ($\lesssim 20V$). A typical increase was 400 % at 10 V. The vacuum chamber system and geometries for the simulation and investigation were very simple. However, we verified that the combined ion and electron sources could be used as a device for controlling a spacecraft potential in geosynchronous orbit.

iii

TABLE OF CONTENTS

LIST OF TABLES

LIST OF FIGURES

ACKNOWLEDGMENTS

I. INTRODUCTION

A. SPACECRAFT CHARGING

Spacecraft charging is the development of a potential difference between a spacecraft and its plasma environment. Nonzero spacecraft potentials have been noted since the beginning of satellite flights. Large negative potentials (hundreds to thousands of volts) were first observed on the ATS-5 (Applied Technology Satellite-5) in eclipse at geosynchronous orbit. The majority of spacecraft charging events have been reported on satellites in geosynchronous orbit. Subsequently, similar results have been observed and investigated on the ATS-6 and SCATHA (Spacecraft Charging at High Altitude) satellites. The largest potential observed to date was -19 kV on ATS-6 during eclipse, but even in sunlight potentials as high as -2.2 kV have been observed. [Refs. 1, 2 , 3]

Spacecraft charging is important because it has been associated with anomalous satellite behavior, and even system failure. A satellite anomaly is an undesired event in a satellite subsystem such as a spurious detector signal, or an unintended logic reset in an electronic system [Ref. 4]. Anomalies or malfunctions and negative charging events are strongly concentrated in the midnight to dawn local time sectors, as shown in Figure 1. Spacecraft charging and resulting discharges as the cause for the anomalies depend on the degree of magnetospheric disturbance and local time. [Refs. 5, 6]

The basic spacecraft charging equation, in terms of the current densities (or number fluxes) is

$$J_E(V) - \{J_I(V) + J_{SE}(V) + J_{BSE}(V) + J_{PH}(V) + J_B(V) + J_{SI}(V) + J_{RLC}(V)\} = J_T(V) \quad (1)$$
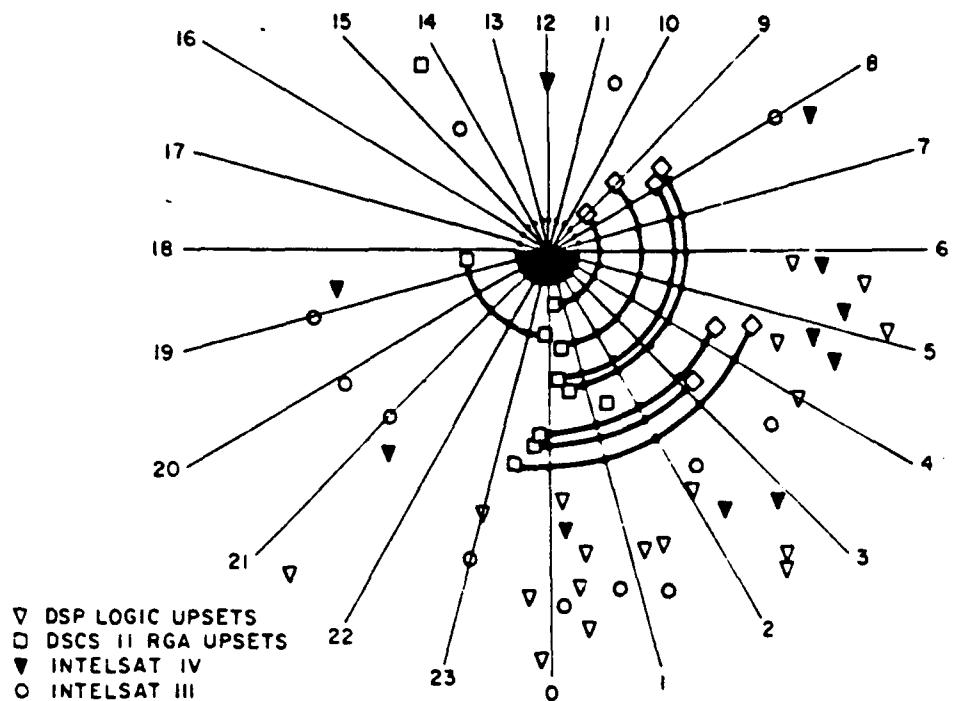
Figure 1.   Occurrences of satellite operational anomalies: plotted as a function

of local time in the geostationary orbit. [Ref. 6]

where

V = satellite potential

J_E = ambient electron flux to a point on satellite surface

J_I = ambient ion flux to a point on satellite surface

J_{SE} = secondary electron flux due to J_E

J_{SI} = secondary ion flux due to J_I

J_{BSE} = backscattered electrons due to J_E

J_{PH} = photoelectron flux

J_B = active current sources such as charged particle beams or ion thrusters

J_{RLC} = resistive, capacitive, and inductive coupling currents between a point and adjoining surfaces

J_T = total current density

The spacecraft charging problem consists of two phases: (1) the determination of the J's as functions of ambient conditions and potential, and (2) the determination of V so that $J_T = 0$ at every point on the satellite surface in the case of a nonconducting satellite, or for the entire satellite for a conducting satellite. As in any complex physical situation, the solution of the Equation (1) can be carried out at different levels of sophistication. [Ref. 6]

There are three main cases of charging on geosynchronous satellites. The first is negative charging in eclipse. Typical values for spacecraft potential in eclipse are from -1 to -10 kV. This results in current flows are shown in Figure 2(a). The remaining two cases involve sunlight conditions. Figure 2(b) shows the situation in sunlight outside the plasmasphere when photoemission is relatively important. An equilibrium potential is achieved when the flow of escaping photoelectrons is equal to the difference between the flows of plasma electrons and ions which reach the surface. In order to fulfill this condition the potential of the surface must be positive and a significant fraction of the emitted photoelectrons must return to the surface.

Considering further the case of a spacecraft in sunlight, Figure 3(a) illustrates the situation of a body with a conductive and equipotential surface when photoemission is dominant. On the shadowed side of the spacecraft plasma ion and electron currents are the only contributers; on the sunlight side photoemission plays an important role. As long as the total photoelectron current emitted on one side exceeds the difference be-

3
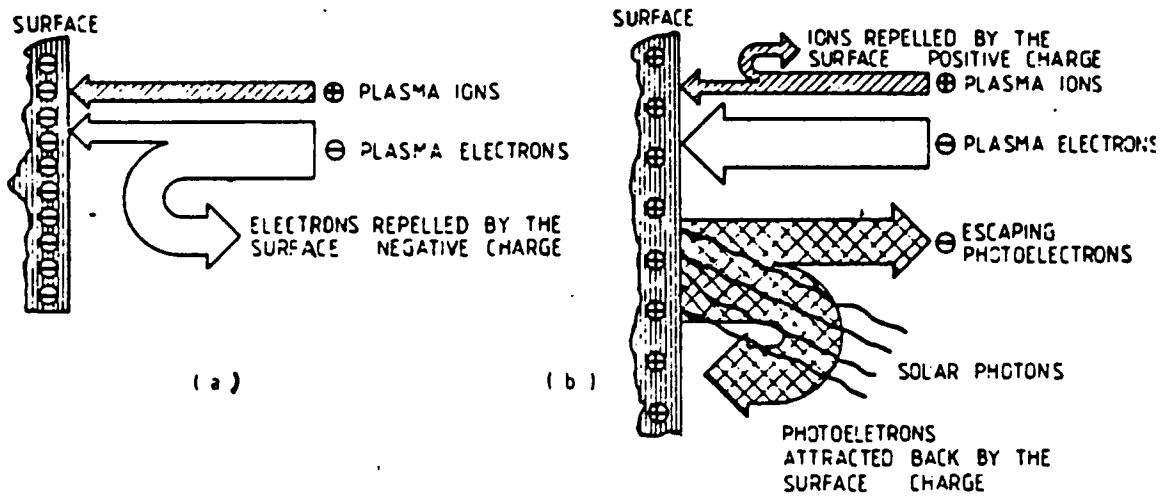
Figure 2. Qualitative illustration of the charging: of a surface by a plasma. (a) Surface in shadow. (b) Surface in sunlight. [Ref. 5]

tween plasma electron and ion currents collected on both sides, the satellite charges to a positive potential. The magnitude of the charge is governed by the mean photoelectron energy and corresponds to a potential of the order of few volts. Figure 3(b) represents a satellite with an insulating surface(SiO_2) in sunlight. The current exchange on the sunlight side remains unchanged. For the shadowed side, however, the incoming electron plasma current cannot be conducted across the surface to the front side and be released by photoemission. So the dark side can adopt a negative potential. The magnitude of the potential in the plasmasheet is a negative potential which can vary from -100 V to -1 kV. [Ref. 5]

4
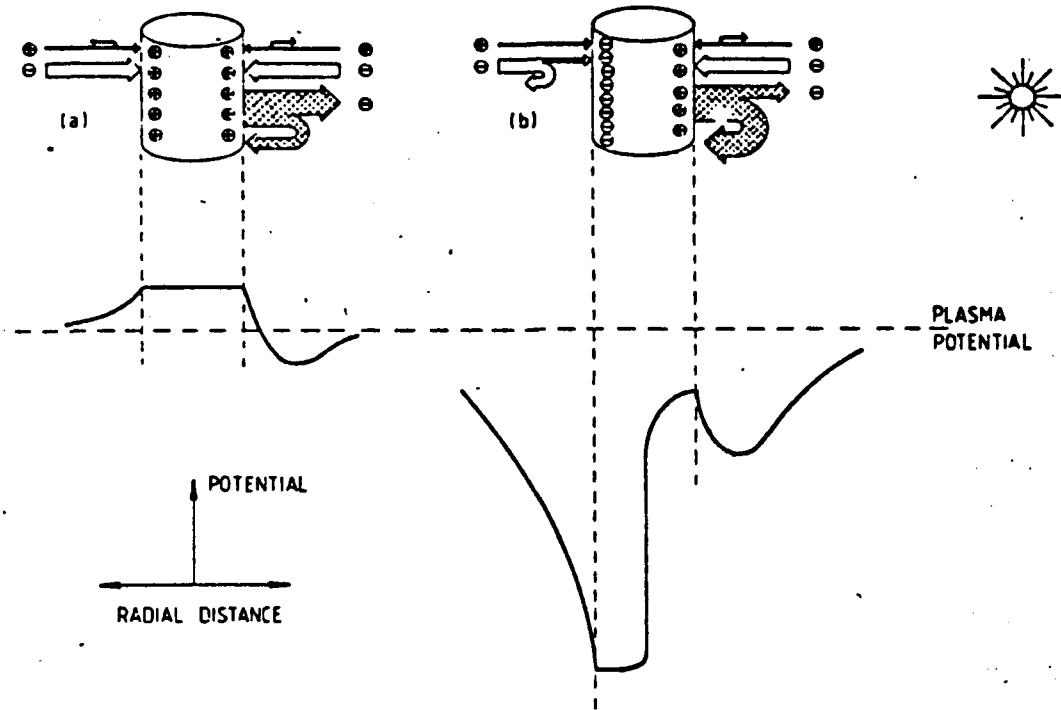
Figure 3.   **Schematic representation of particle flows:**   (a) A conductive surface.

(b) An insulator surface. [Ref. 5]

B.   SPACECRAFT CHARGE CONTROL

It is desirable to control the charge on a satellite or satellite surfaces, because a spacecraft will be generally charged positively in sunlight due to the emission of photoelectrons. Hence, an ion emitter is capable of neutralizing the charge. Negative satellite potentials that would require an electron emitter will occur during eclipses, in the very dense plasmas of the near-perigee part of the orbit, and perhaps in very hot

plasmas during magnetospheric storms. Differential charging (negatively charged dielectric surfaces) require a low energy ion or plasma source to be discharged.

The basic approach to the active control of spacecraft potential involves the emission of charges from the spacecraft sufficient to balance the excess of charge accumulating on the vehicle from the environment. By providing a positive emission current on the order of a few tens of μA, the spacecraft potential can thus be adjusted near to zero. [Refs. 7, 8]

This thesis work used a simulation for a satellite with charge control. This thesis provides the emission characteristics of ion and electron sources for active charge control of the spacecraft body potential (positively or differentially charged). Lithium ion emitters developed by O. Heinz and R. T. Reaves in 1968 and two kinds of electron sources were used. The purpose of the electron sources was to study effects on space charge limited current collection. Lithium ion emitters of 0.25 and 0.6 inch diameter were used. A directly heated tungsten dispenser cathode of barium impregnated 31180, particularly ordered and manufactured by Spectra-Mat, Inc., was investigated. A filament type electron source was used to improve the characteristics of ion current from lithium ion source. [Refs. 9, 10, 11]

II. THEORY AND BACKGROUND

A. PLASMA CHARACTERISTICS IN GEOSYNCHRONOUS ORBIT

At or near geosynchronous orbit, a satellite is usually in the plasmasphere or plasma sheet, two very different regimes. The plasmasphere lies closest to and corotates with the earth. Its particle population is cold (average temperature $\sim 1 eV$) and dense (10 to 1000 particles/cm^3). The boundary of the plasmasphere is the plasmapause, beyond which is a transition region. Steep spatial and temporal gradients in the plasma density

SCALE IN EARTH RADII

‑‑‑ SCATHA ORBIT RANGE
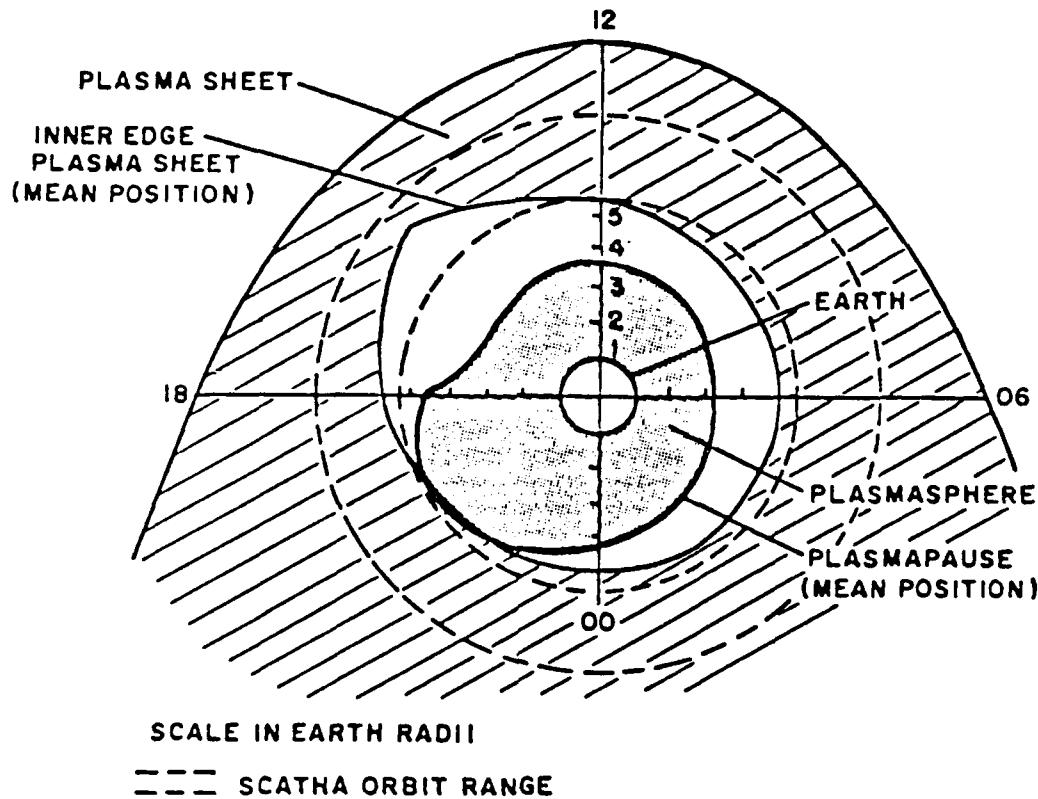
Figure 4.   Schematic of the major magnetospheric plasma regimes: [Ref. 12]

7

Table 1.   TYPICAL SPACE PLASMA ENVIRONMENTS.

Parameter	Plasmasphere	Plasma sheet	Solar wind
Plasma density, cm^{-3}	$10-10^3$	1	6
Electron mean kinetic energy, eV	1	1000	15
Ion mean kinetic energy, eV	1	6000	10
Electron random current density, $\mu A\ m^{-2}$	0.25-25	0.85	0.62
Ion random current density, $\mu A\ m^{-2}$	0.006-0.6	0.05	0.012
Electron Debye length, m	2.5-0.25	240	12

occur here. The boundary is not well defined and varies with local time and magnetic activity. Outside the plasmasphere is the plasma sheet, which in general begins at distances of 3 to 7 R_E (Earth Radii), characterized by a plasma which is hot (average temperature is 1 to 10 keV) with very low plasma densities (0.1 to 1 cm^{-3}). The plasma regions encountered by most satellites and the approximate position of the plasmapause are shown in Figure 4. [Refs. 13, 12]

Typical values for plasma parameters at different locations in space are given in Table 1. In the vicinity of the geostationary orbit, the ambient charged particle population originates from both the plasmasphere and the plasma sheet. In the sunward hemisphere and during quiet time conditions the relatively cold plasma of the plasmasphere is dominant. On the night-side, especially in a magnetically disturbed situation, the inner edge of the plasmasphere may cross the geostationary altitude and the

8

plasma environment becomes more energetic. The electron energy distributions which characterize the magnetically quiet and disturbed environments in this orbit are illustrated in Figure 5 [Ref. 5].
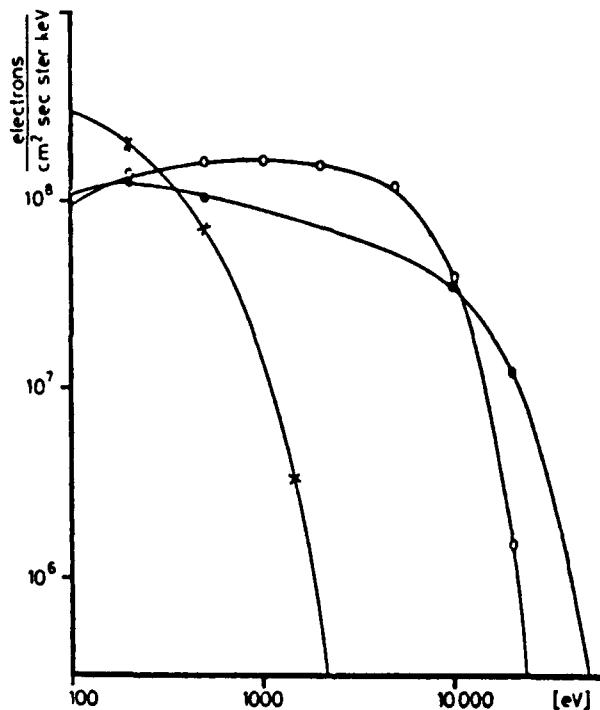
Figure 5.   Electron spectra encountered at the geostationary orbit: during quiet(crosses) and disturbed(circles) periods [Ref. 5].

So far, only the geostationary orbit has been discussed because the most severe environment is imposed by the plasma sheet and because many application satellites are placed in this orbit. Magnetospheric and interplanetary plasma environments other than the plasma sheet cause much smaller potentials, as shown in Table 2 [Ref. 5]; it is seen

Table 2.   EXTREME POTENTIALS FOR SATELLITES IN DIFFERENT
PLASMA ENVIRONMENTS.

Environment	Satellite in eclipse, or insulated surface in shadow (V)	Sunlit satellite with conductive surfaces (V)
Plasmasphere (out to ~ 5 R_E)	−2	+2
Dayside magnetosphere (~ 5 to ~ 10 R_E)	−5 to −100?	+10
Nightside magnetosphere (~ 5 to ~ 15 R_E)	−20000 (1)	+30 (2)
Dayside magnetosheath (~ 10 to ~ 15 R_E)	−200	+5
Solar wind	−20	+10 (2)

(1) During magnetospheric storms.
(2) In a tenuous plasma (under average conditions, potentials are 1/3−1/2 of these values).

that a satellite with a conductive surface floats at relatively small positive potentials in these environments. [Ref. 13]

B.   HIGH VACUUM SPACE CHARGE

The application of a solid-state ion source results in a pure ion plasma. Current extraction from such devices is largely determined by space-charge current limiting effects. These effects have been observed in practical devices such as vacuum tubes for decades. [Ref. 14]

In a region where there is a concentration of ions of one sign. the geometric electrostatic field is distorted at the anode and cathode principally. The physical situation is similar for either ion or electron transport. A rough physical picture of the

reason for the limitation of space current at low voltages electric fields may be obtained by examining the forces acting upon a single electron as it passes from the emitter to the plate of a two-electrode tube, or diode, as shown in Figure 6.
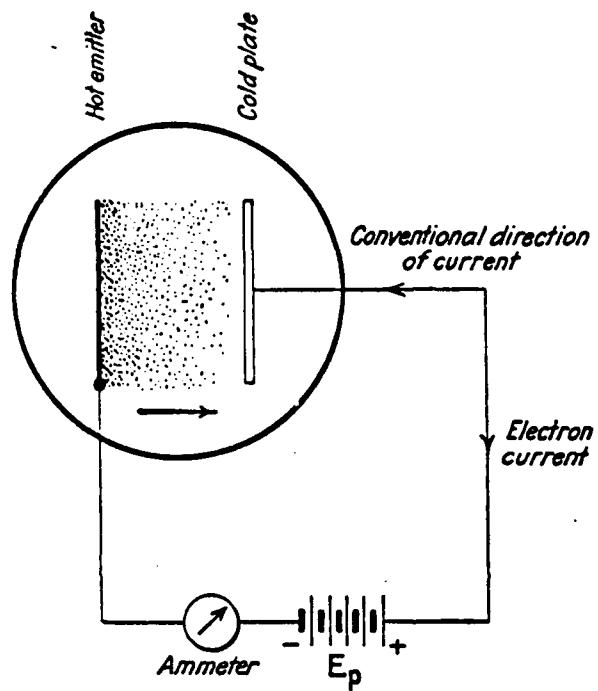
Figure 6.   Diagrammatic illustration of space charge: [Ref. 14]

The cloud constitutes a negative space charge, which exerts a force on each electron according to its position. An electron just emerging from the emitter is attracted toward the plate by the electric field caused by the voltage applied between emitter and plate, but is repelled back toward the emitter by the space charge. The potential distribution for three cases including space-charge limited effect is shown in Figure 7. When the emission is very low, every electron emitted will reach the anode (curve A). When only

11
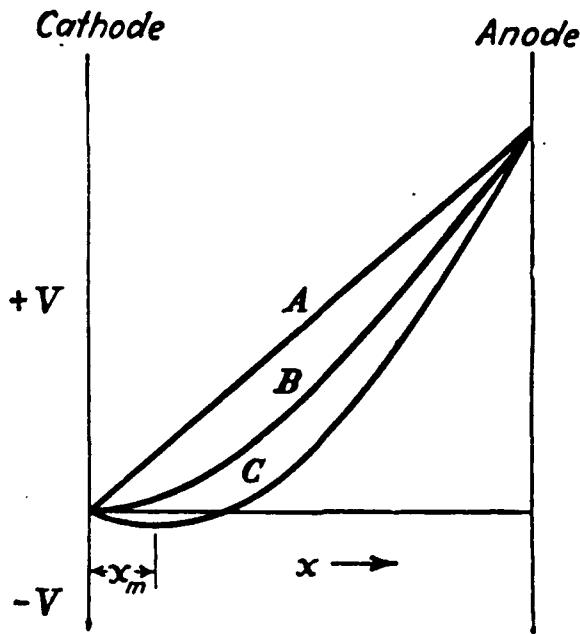
Figure 7. Parallel-plate potential distribution: (A) no space charge; (B) space charge, no initial velocity of electrons; (C) space charge, with initial velocity of electrons. [Ref. 11]

as many electrons are emitted, having no initial velocity, as can reach the anode, the field at the cathode is zero (curve B). If an excess of electrons is being emitted, only electrons having a certain minimum energy will be able to traverse the field of the electron space charge and reach the anode (curve C).

The electron cloud is most dense near the emitter. It is evidently impossible for a current to pass to the plate which is greater than that giving a space charge which just

12

neutralizes the force at the emitter due to the plate. This leads to a maximum value of current known as the *saturation current* corresponding to each plate voltage. [Ref. 14]

The space charge effect was studied for infinite plane-parallel electrodes in a vacuum, with one of the electrodes emitting electrons thermionically by Child in 1911. Space charge effects were later independently derived and extended to a cylindrical geometry by Langmuir The electron current density is

$$j = \frac{1}{9\pi} \sqrt{\frac{2e}{m}} \frac{V^{3/2}}{x^2} \qquad (2)$$

where x is the seperation distance between plates, V is the potential at the point x, m is the mass of the electron, and e is charge. This is known as the space-charge equation, or Child's law.

It was shown that this law holds in a vacuum for any electrode configuration by Langmuir and Compton in 1931. Thus, regardless of the electrode configuration,

$$j \propto V^{3/2} \qquad (3)$$

For concentric cylinders with an emitter of radius r_0 and a collector of radius r, the space-charge equation is

$$j = 14.65 \times 10^{-6} \frac{V^{3/2}}{r\beta^2} \qquad (4)$$

where β^2 is a constant of the geometry for the ratio $\frac{r_0}{r}$ and $\frac{r}{r_0}$, as given in Figure 8. When the inner cylinder is the emitter, $r_0 < r$, the (β^2) curve is used. When the outer

cylinder is the emitter, $r < r_0$, the curves $(-\beta)^2$ are used. Only the case of $r_0 < r$ is meaningful for our purposes. The constant $\beta^2 \simeq 1$ for values of $r \simeq 10 r_0$ or greater.
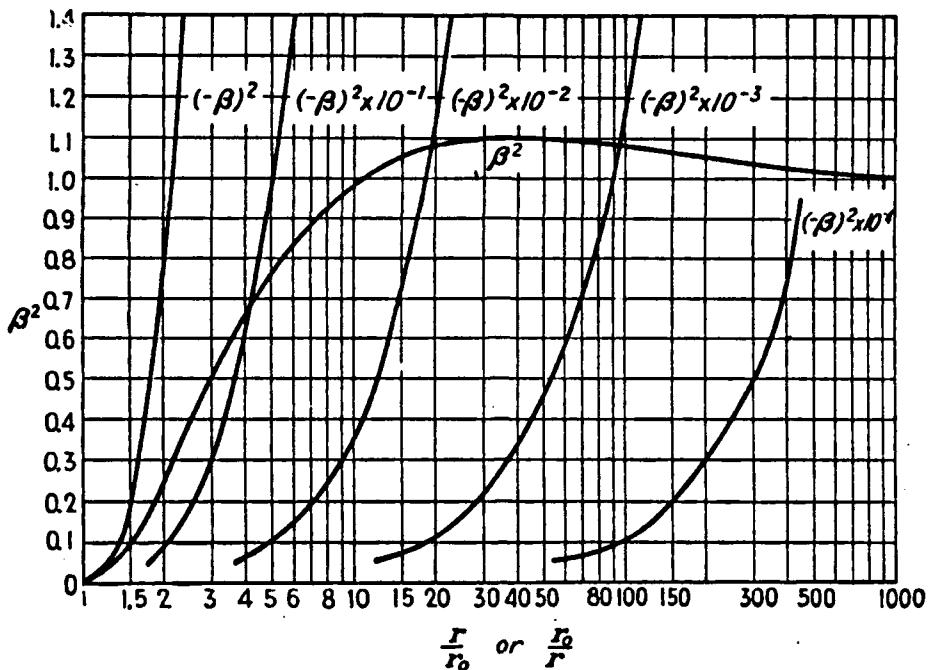
Figure 8.   Geometric factor for space-charge equation for cylinders: [Ref. 11]

This law has been verified by experiments over a wide range of conditions and is true for any electrode, even a cold one, that permits electrons or ions to escape from it. If an excess of electrons is being emitted, only electrons having a certain minimum energy will be able to traverse the field of the electron space charge and reach the anode.

The space-charge equation may be applied to ions as well as to electrons if the same boundary conditions hold. For ions,

$$ j = 2.33 \times 10^{-6} \frac{V^{3/2}}{(1823.3 M)^{1/2} x^2} \tag{5} $$

14

where M is the molecular weight of the ions, V is in volts, x is in centimeters, and j is in amperes per square centimeter. This equation holds in the dark spaces of gas discharges when conditions are such that the ions are not hindered in their motion by collisions with the gas molecules, or in other words the equation holds for a region whose length is of the order of an mean free path (m.f.p). [Ref. 11]

Langmuir has discussed the possibility of increasing the space charge limited electron current between two electrodes by injecting positive ions into the electron space charge and thereby partially neutralizating its detrimental effect on electron extraction. [Ref. 15]

In this thesis work we use the complementary idea of neutralizing a positive ion space charge by injecting negative charges into the region between the current collecting grid and ion emitter. This could lead to an increased ion current density for the spacecraft charge control.

C.   THERMIONIC ELECTRON EMISSION

Electrons may be emitted by surfaces at high temperature in a process, called *thermionic emission*. Richardson derived an equation for thermionic emission of electrons as a function of the temperature of the emitter. But, Richardson's theory was incorrect because of discrepancies between the theory and certain experimental facts.

Dushman derived a form for the thermionic emission equation which rests on sounder theoretical principles than does Richardson's first equation. The Dushman equation is

$$j = AT^2 e^{-\frac{b_0}{T}} \tag{6}$$

15

j = the saturation current density ($amp./cm^2$)

T = the absolute temperature of the emitter (°K)

b_0 = a constant of the emitting surface such that $b_0 k = \phi_0 e$, where k is Boltzmann's constant, e is the electronic charge, and ϕ_0 is known as the thermionic work function which is the work in volts necessary to remove unit charge of electrons from the surface.

A = a universal constant whose value is $(2\pi e m k^2 / h^3) = 60.2$ amp./$(cm^2)(deg.^2)$. where m is the mass of the electron and h is Planck's constant.

Modern theory requires that this value be doubled to take account of the spin of the electron. However, the constant A has the value of approximately 60 for most metals. The theoretical value 120.4 should hold for pure surfaces of a single crystal face. Values of the thermionic constants are given in Table 3. [Ref. 11]

In spite of some uncertainties, the thermionic emission equation holds within the accuracy with which the temperatures can be determined. As the voltage between a thermionic cathode and anode is increased, the current to the anode increases according to Child's law (Eq.2), the space charge equation; but at a certain value of anode voltage the current should cease to increase for all thermionically emitted electrons are then being drawn to the anode. In other words the saturation current has been reached. It is this saturation current which obeys the thermionic emission equation (Eq.6) for various cathode temperatures. If the voltage is increased beyond the saturation value, it has been found experimentally that the current will continue to increase. This effect was first studied by Schottky and is often called the Schottky effect. For the effective work function of the cathode in the presence of an electric field in the thermionic emission equation gives the Schottky equation:

$$j = j_0 e^{4.389 \frac{\sqrt{E}}{T}}$$

(7)

16

Table 3. ELECTRON EMISSION CONSTANTS.

A in amp./(sq. cm.)(deg.^{2}); ϕ_0 in volts; [ ] = uncertain; __ = best out-gassed value; b_0 in degrees Kelvin

Material	A	ϕ_0		b_0	Boiling point, °C.	Effect of gas on ϕ_0	
		Therm-ionic	Photoelectric			Increase	Decrease
Ag	60.2	4.08	4.73–3.85	......	1950	H₂	O₂, N₂, CN
Al	....	....	4.56(600°) 3.57[2.5–3.6]		1800		
Al₂O₃	1.4	3.77	....	43,700			
Au	60.2	4.42	4.73 (740°)	......	2600	H⁺	Air
BaO	2.5	(1050°) 3.44–1.66	4.82 (20°)	19,700			
Bi	....	....	4.4–4.0	......	1450		Air
C	5.93	3.93	4.82[4.7]	46,500	4200	NH₃, H₂, CO₂, Air	
Ca	60.2	3.02–2.24	[2.7]	26,000	1170		
CaO	25.7	2.24	....	26,000			
Cd	....	....	[4.0]	......	767		
CdO	1.65 × 10⁻⁶	2.43					
Co	....	....	4.25–4.12		3000		
Co₂O₃	2.17 × 10⁻²	4.06					
Cu	65(1316°)	4.38	4.5–4.1	......	2300		
CuO	1.55 × 10⁻⁸	1.76					
Cs	162	1.81	1.9	21,000	670		
Fe	....	....	4.72–4.2	......	3000	O₂, H₂	
Fe₂O₃	1.16 × 10⁻²	3.82					
Hf	14.5	3.53	....	41,000			
Hg	....	....	4.53	......	357	Wax vapor H₂O vapor	H₂O (trace)
K	....	....	2.25–1.76	......	760	H₂, O₂, H₂O, S, NO	
Li	....	....	2.9–2.1	......	>1220		
Mg	....	....	[<3.4]	......	1110		
MgO	1.1 × 10⁻⁵	....	3.19	33,100			
Mo	60.2	4.41–3.48	4.33–3.22	51,300	3700	H₂O	
Na	....	....	2.46–1.90	......	880	O₂, S, H₂O	
Ni	26.8	2.77	5.01–4.12	32,100	2900	H₂O	Air, O₂
NiO	9.1×10⁻²	4.87					
Pb	....	....	[4.1–3.5]	......	1620		
Pd	....	4.99	4.96	......	2200	H₂, O₂	O₂
Pt	1.7 × 10⁴	6.27	6.3 × 4.40	72,500	4300	H₂, NH₃	O₂
Rb	....	....	2.2–1.8	......	700		
Rh	....	4.58	4.57 (20°)	......	......	....	H₂, O₂
SiO₂	5.0	4.58					
Sn:							
β	....	....	4.5				
γ	....	....	4.38				
Liquid	....	....	4.21	......	2260		
SrO	6.9	1.99	....	23,100		H₂O	
Ta	60.2	4.18–4.07	4.05 (20°)	47,200	......	H₂O	
Th	60.2	3.35	3.92 (700°) [3.6–3.3]	38,900			
ThO₂	0.015	2.94	....	34,700			
W	60.2	4.52–4.40	4.80–4.52	52,400	5900	H₂O	O₂
Zn	....	....	3.68–3.32	......	907		
Zr	330	4.13		51,000	>2900		
ZrO₂	0.35	3.4	....	39,400			

where j_0 is the thermionic emission when the field at the cathode is zero. E is an external accelerating field in *volts/cm* which is proportional to the applied voltage V for a given electrode configuration. [Refs. 11, 14]

D. LITHIUM ION EMISSION

Certain materials when present as impurities on the surface of a heated metallic filament can be evaporated as positive ions. For this phenomenon to take place the work function of the surface must exceed the ionization potential of the atom that is to be evaporated as an ion. [Ref. 11]

J. P. Blewett and E. J. Jones were among the first to recognize the excellent ion-emission properties of β-eucryptite and in fact hypothesized that in the crystal lattice the lithium ions are situated in large *"holes"* . An alkali ion is therefore comparatively free to migrate within the lattice, and with the aid of small electrolytic potentials which are bound to be present, it migrates to the surface and is emitted easily as indicated by the low work function. The work function for ions determined by F. M Johnson on a large number of samples of sintered β-eucryptite were all in the neighborhood of 2.0 eV in contrast to 2.7 - 4.0 eV as determined by Blewett and Jones. [Refs. 16, 20]

F. M. Johnson studied ion emission by means of simple diode structures with an emitter collector spacing of about 1 millimeter. The ion emission data could be fitted to a Schottky-type equation:

$$\log_{10}I_s = \log_{10}I_{so} + \frac{1.9}{T_s}(\frac{V}{d})^{1/2} \qquad (8)$$

18

where V is measured in volts, d in centimeters, I_{so} is the saturated ion current at zero biased voltage, and T_t is the apparent Schottky temperature. The second term in Equation (8) arises from the fact that an ion includes an image charge in the material as it leaves the surface and hence modifies the potential distribution immediately outside the material. The values of Schottky temperature, T_t , range from 210 to 430 °K depending on the emitter temperature, whereas the actual temperature of the ion emitter was in the 1300 to 1600 °K range. Figure 9 shows the I-V diode characteristics for a sample which had 50 % lithium composition, 50 % inert materials. [Ref. 16]
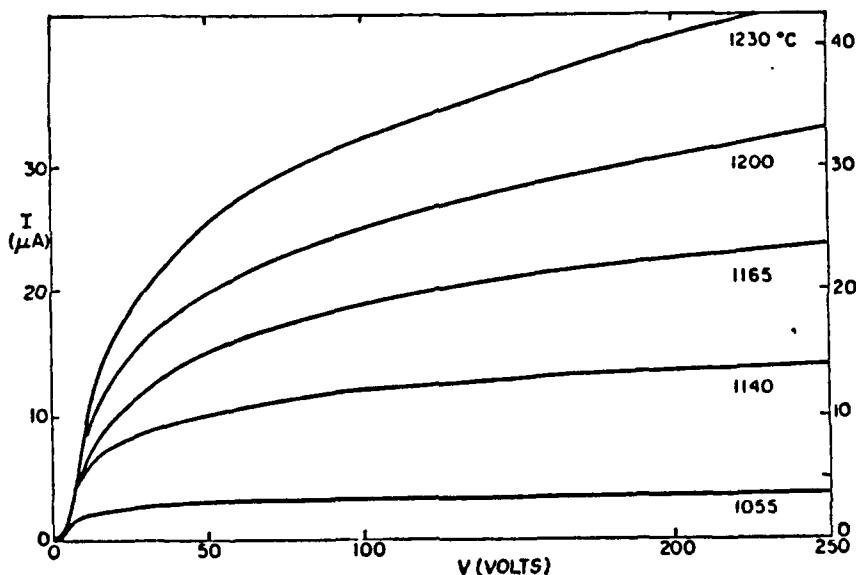
Figure 9.   Typical diode characteristics of current vs. voltage: [Ref. 16]

The ion emission data in the high voltage region and 1300 to 1600 °K temperature range may be fitted to the following equation, for a 50 % lithium sample:

$$\log_{10}I_s = \log_{10}I_{so} + \frac{1.9}{1375 - 0.726T}\left(\frac{V}{d}\right)^{\frac{1}{2}} \qquad (9)$$

19

In the low-voltage region, the lithium ion emission should be space charge limited, which implies that the ion current is governed by the Child-Langmuir equation (Eq.5). The equation is the appropriate form for calculating the space charge limited current for the lithium ion source used in this experiments. A typical graph of $I^{2/3}$ vs. V is shown in Figure 10.

In the space-charge limited region, the experimental points are expected to lie on the theoretical curve, which is drawn as a dashed line in Figure 10 and marked "perveance" line. The derivations from the straight line are interpreted as being due to the resistance of the thermionic emitter. The ion current is then given by

$$I = P(V - IR)^{3/2} \qquad (10)$$

where P is the perveance of the diode, i.e.,

$$P = 2.33 \times 10^{-6} \frac{S}{d^2} \sqrt{\frac{m}{M}} \qquad (11)$$

V is the plate voltage, S is the emitting area in cm^2, d is the electrode spacing in centimeters, m/M is the ratio of the electron mass to the ion mass, and R is the initial resistance of the ion emitter. [Refs. 11, 16]

E.   HISTORY OF ACTIVE EXPERIMENTS

Active spacecraft charge control encompasses the use of a wide range of charged particle emitters, including electron, ion and plasma emitters. But, the history of flight experiments in charge control is brief. Sounding rockets experiments with electron beams have been conducted since the late 1960's, primarily with the objective of gener-
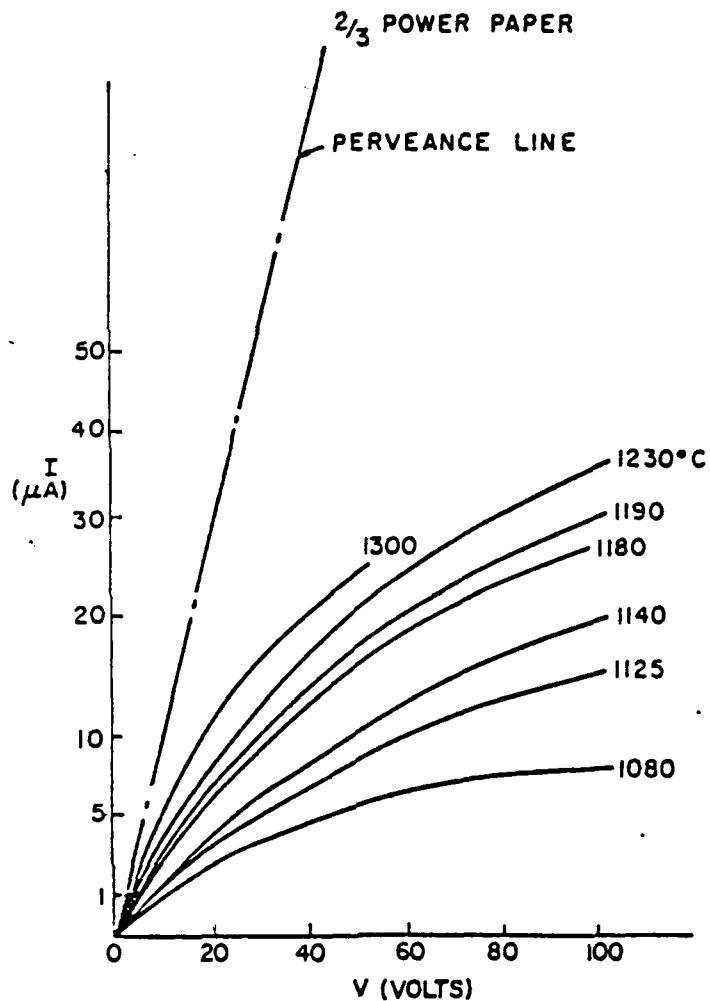
Figure 10.   Typical plot of I vs. V for a lithium emitter: The perveance line ap-

plies to the Child-Langmuir equation. [Ref. 16]

ating artificial aurora. These sounding rocket experiments were interpreted as being

successful in coupling currents of several hundred miliamperes to the ambient, with rel-

atively low potentials resulting.

Satellite charge control at high altitude has primarily been demonstrated in exper-

iments on ATS-5, ATS-6, and SCATHA (P 78-2).

1. Electron Sources

ATS-5 carried filament electron sources as part of an ion engine experiment. The ion engines were small cesium thrusters with filament neutralizers. The filaments, illustrated in Figure 11, can be seen near the outer edge of the thruster. The filament neutralizer was used as an electron emitter at microampere current levels at geosynchronous orbit. The electron emitter was operated hundreds of times over 4-year period, primarily during eclipses. These operations succeeded in reducing the magnitude of the negative eclipse charging potentials on an satellite, but rarely discharged the spacecraft completely, as shown in Figure 12.

Modeling of the current balance to the spacecraft showed that less than 1 % of the emitted current was escaping the spacecraft at equilibrium. Three-dimensional modeling of the potentials and currents with NASA Charging Analyzer Program (NASCAP) showed the development of differential potentials on the order of 100 V to be developed on the spacecraft surfaces, limiting the emission of the filament. The limitation was sufficient to explain the equilibrium potentials seen and would apply to most spacecraft with insulating surfaces.

The experience obtained with ATS-5 data and modeling were directly applicable to the data obtained from the electron gun experiments on the SCATHA satellite with a more powerful electron source. The SCATHA satellite generally was similar to ATS-5, i.e., cylindrical, and dominated by insulating surfaces. The electron emitter was considerably more sophiscated, however. The experimental results from SCATHA were similar to the ATS-5 results qualitatively. Electron emission initially caused to satellite potential to rise toward zero, but limiting processes prevented the full electron beam from escap-
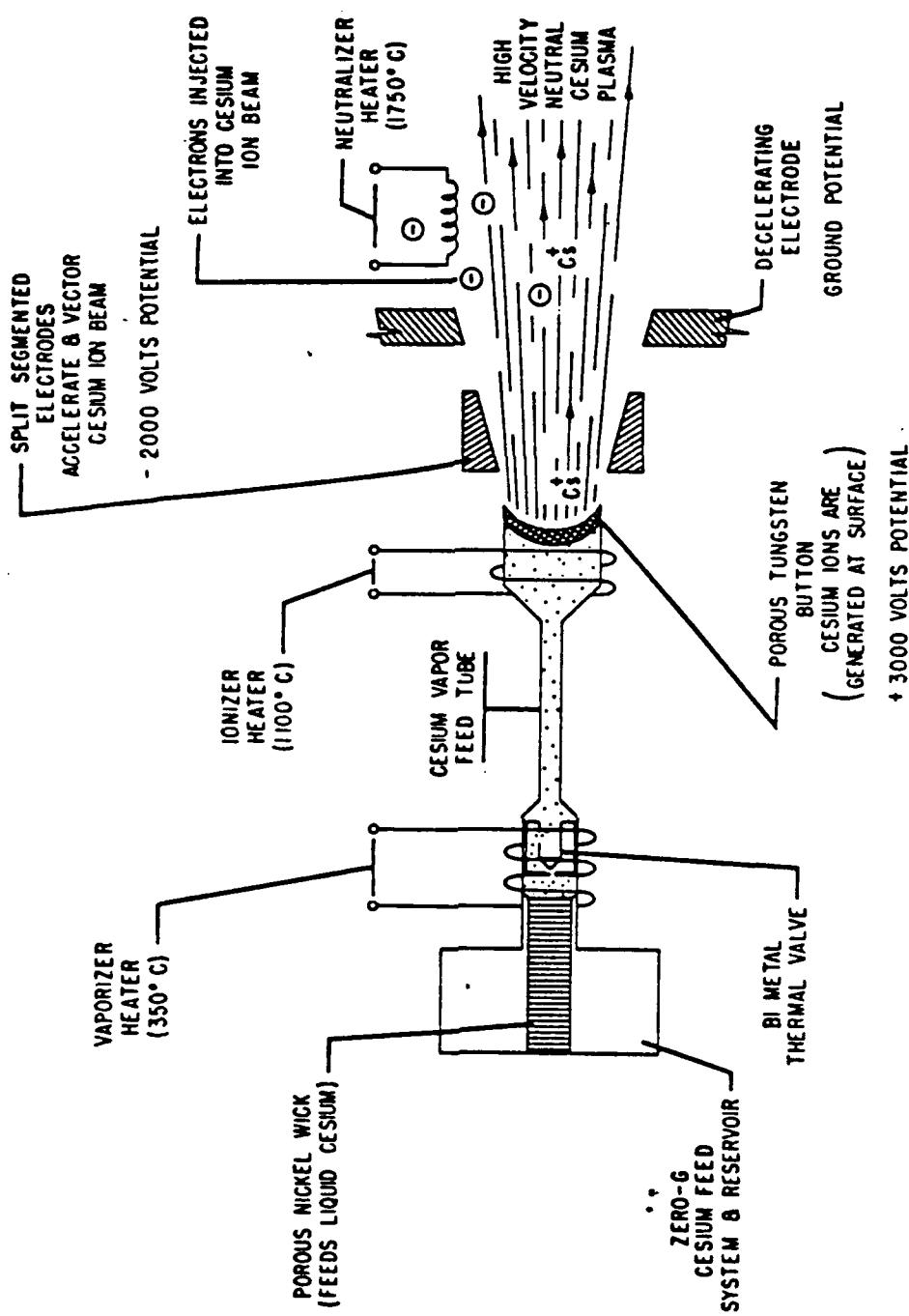
Figure 11. ATS-5 ion engine with filament neutralizer: [Ref. 17]
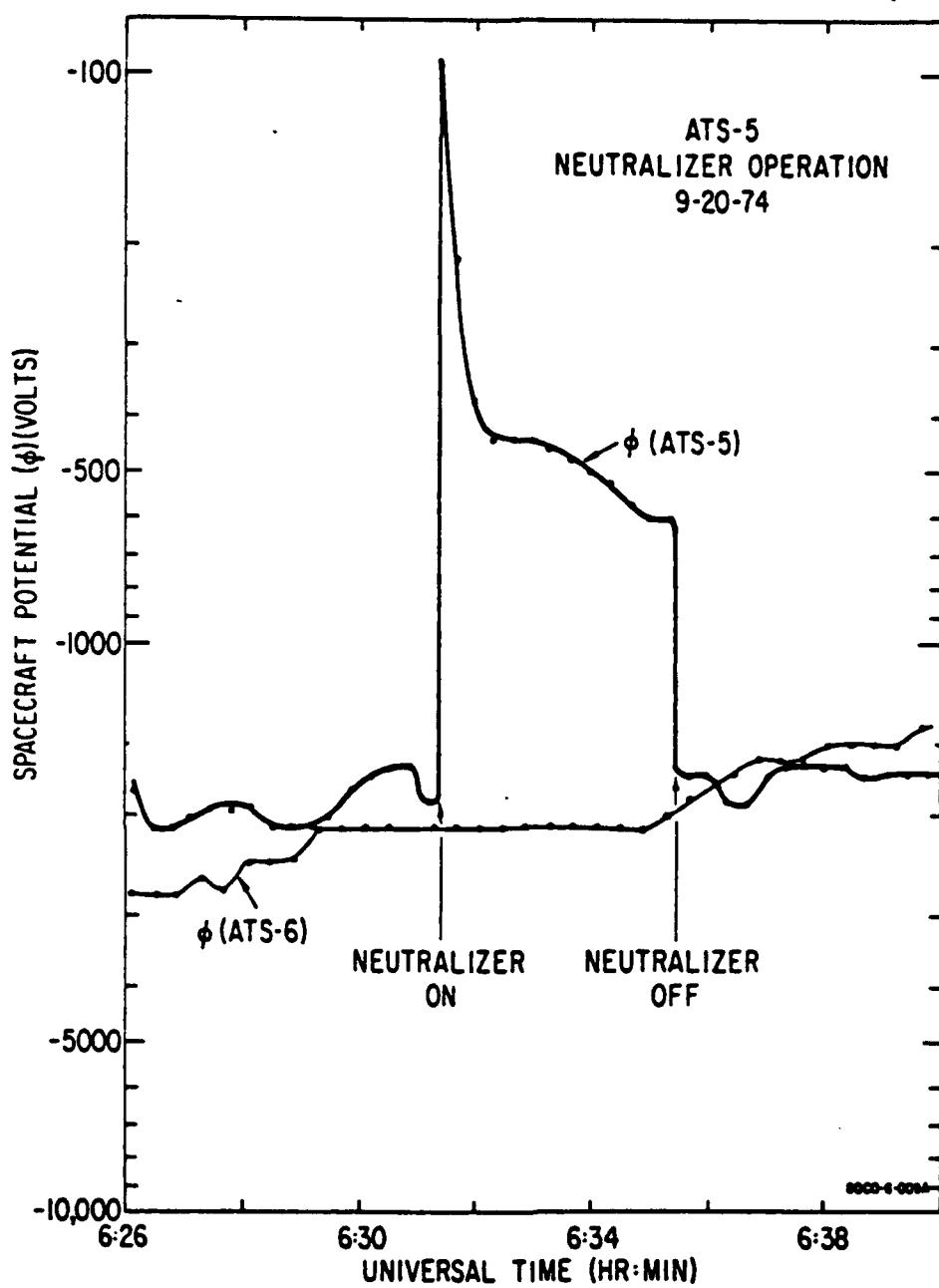
Figure 12.   ATS-5 neutralizer operation (Sep.20, 1974):   [Ref. 17]

24

ing. The satellite did not necessarily discharge any further with increasing current and voltage. Those operations confirmed the need to provide a means of discharging the dielectric surfaces, since increasing the electron gun accelerating voltage will only increase the magnitude of the differential potentials on the spacecraft surface. [Ref. 17]

2. Plasma Sources

An ion engine is a device which combines an ion beam with a charge and current balancing electron source. ATS-6 carries two ion trusters of the type illustrated in Figure 13. Two grids are used to extract and accelerate the plasma. Neutralizing electrons are supplied by a plasma bridge neutralizer which generates its own cesium plasma at the plasma probe potential. This plasma provides the necessary electrons to the ion beam. The neutralizer is the main link between the engine, beam, and the spacecraft mainframe. Operation of the ATS-6 engines and plasma bridge neutralizer had major effects on the spacecraft potential with respect to the ambient plasma as well as on the differential potentials on the spacecraft surface.

The ion engine operations on ATS-6 altered the charge state of the spacecraft, charging the spacecraft surface potentials with respect to the distant plasmas. Plasma emission in quiet environments (plasma temperatures below 1 keV) caused the spacecraft potential to shift from a few volts positive to a few volts negative. A net ion current is emitted in such cases. The emission of the plasma or beam in energetic environments (plasma temperatures in the 5-10 keV range) in sunlight caused larger changes. Typical equilibrium potentials for ATS-6 in such environments were on the order of a hundred volts negative, with variations in potential across the spacecraft surface of comparable magnitude. Engine operations under such conditions raised the mainframe potential to

25
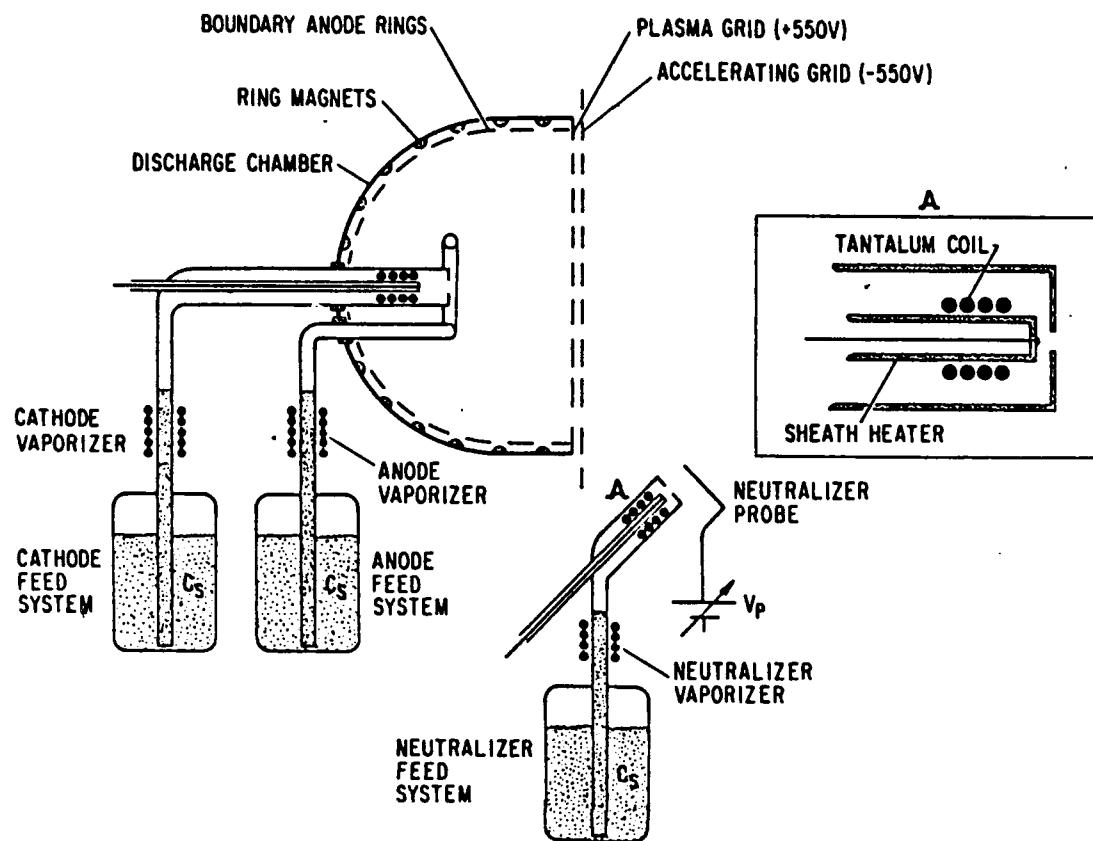
Figure 13. ATS-6 ion engine with hollow cathode neutralizer: [Ref. 18]

near zero volts, and discharged the differential potentials on the dielectric surfaces.

Plasma emission by the plasma bridge was an effective method of discharging kilovolts

potentials in eclipse. Figure 14 shows the plasma bridge operation for eclipse discharg-

ing. Based on the analysis, it is believed that a low energy plasma discharge provides an

effective means for controlling spacecraft potentials. [Refs. 17, 18, 19]

The success of plasma sources in controlling satellite charging have led to their

continued development for charge control. A hollow cathode based on plasma source

ATS-6 NEUTRALIZER/ECLIPSE OPERATION
DAY 97/77
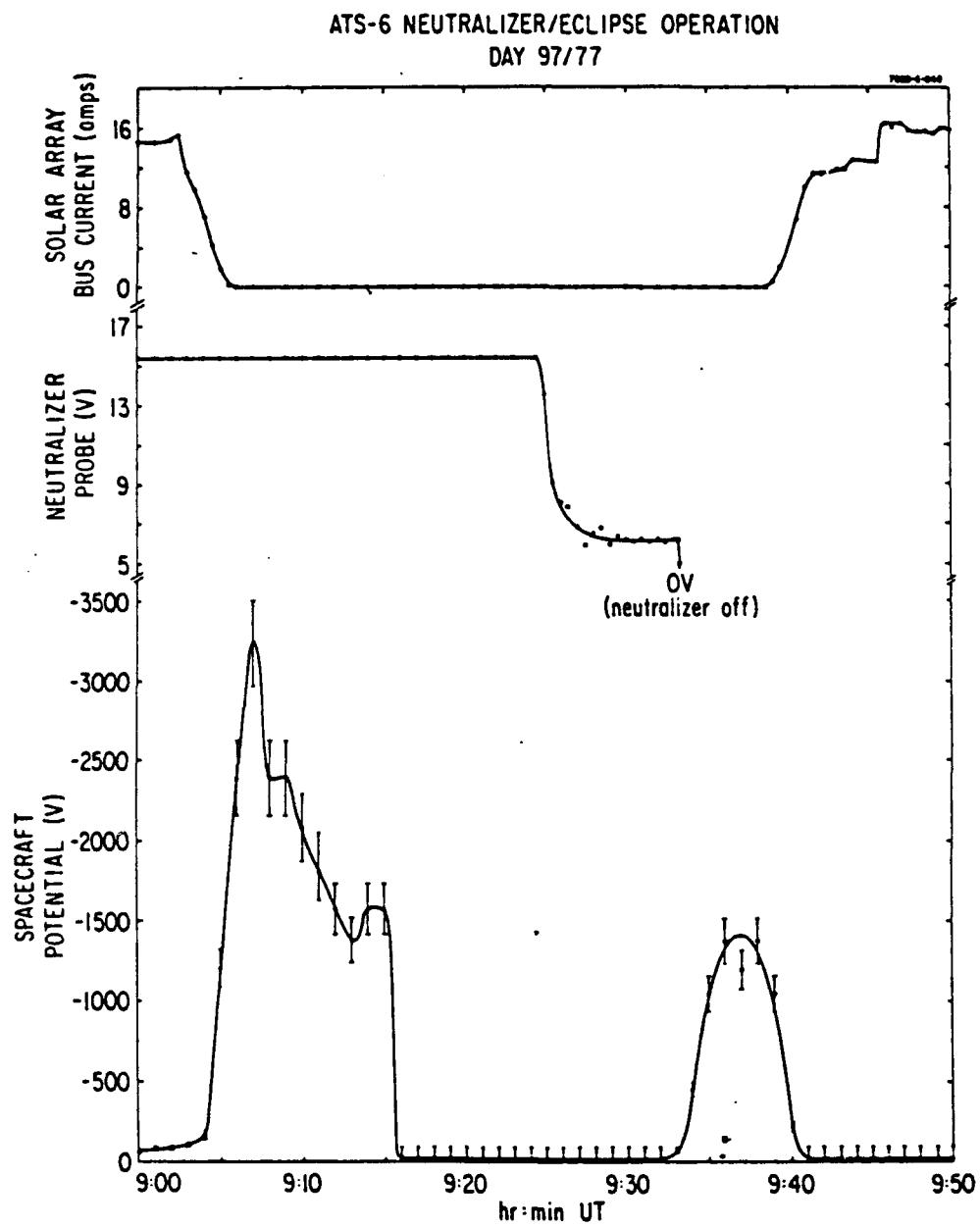
Figure 14. Plasma bridge operation (Apr.7, 1977): [Ref. 18]

27

will be flown on the NASA POLAR satellite, to be launched in 1993. The problem with this technology is that it is heavy (10-20 Kg payload weight), uses large amounts of power (10-20 W), and is electromagnetically noisy. These problems motivate a continued effort to find alternate forms of charge control technology.

III.   LITHIUM ION AND ELECTRON SOURCES

A.   LITHIUM ION SOURCE

1.   Introduction

In 1936, J. P. Blewett and E. J. Jones studied the emission of the lithium sources as a function of composition, and they reported the β-eucryptite $Li_2O{:}Al_2O_3{:}2SiO_2$ is the most satisfactory ion emitter as a filament sources of positive ions. When heated to temperatures in the range 1000-1300°C, lithium ions are emitted. [Refs. 16, 20]

The lithium ion emitters which used in our experiment were developed by Otto Heinz and R. T. Reaves in 1968. The ion emitters are particularly suited for low energy experiments ($E \lesssim 100 eV$) where ion beams with small energy spreads are essential. [Ref. 9]

2.   Structure of Beta-eucryptite

Beta-eucryptite is a ceramic material (Aluminosilicate) in which lithium is stored. The crystal structure, shown in Figure 15, is similar to a high-temperature quartz structure, yet differs from it in that half of the silicon atoms are replaced by aluminum atoms in alternate layers along the c-axis.

The lithium ions are in the interstitial space on the level where the substitution takes place, surrounded by four oxygen atoms. This arrangement has a very satisfactory Pauling electrostatic bond structure. The oxygens surrounding the Li are shared by one Si and one Al , so that they receive electrostatic bonds of strength $1\frac{3}{4}$ from this source. The tetrahedrally coordinated Li atoms contribute the remaining $\frac{1}{4}$.

a = 5.27 A.
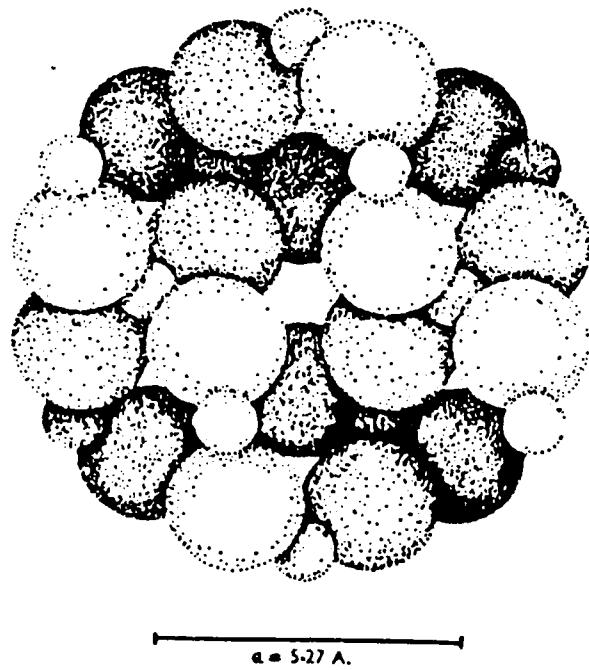
Figure 15.   Crystal structure of β-eucryptite viewed along c axis: Large spheres represent oxygen atoms, small spheres either Si or Al atoms. The lithium ions are situated in center opening. [Ref. 16]

Beta-eucryptite is extremely anisotropic in thermal expansion, with coefficients of thermal expansion in the a and c crystallographic directions of $+ 82 \times 10^{-7}$ and $- 176 \times 10^{-7}$ per °C, respectively. The net effect of this anisotropic expansion is to enlarge the openings of the crystal lattice in which the lithium ions are situated. This is the reason why lithium ions are readily emitted from this type of crystal structure if the material is sufficiently heated. [Ref. 16]

3. Construction of Lithium Ion Emitter

Figure 16 shows the emitter consisting of an indirectly heated, highly porous, tungsten plug into which the emitter material has been fused. The molybdenum body holding the plug is machined with a solid partition for complete isolation between the emitter and the heater cavity. The three rhenium support struts are brazed at a 120° spacing with a moly/ruthenium eutectic at 2100°C in hydrogen, yielding a ductile and
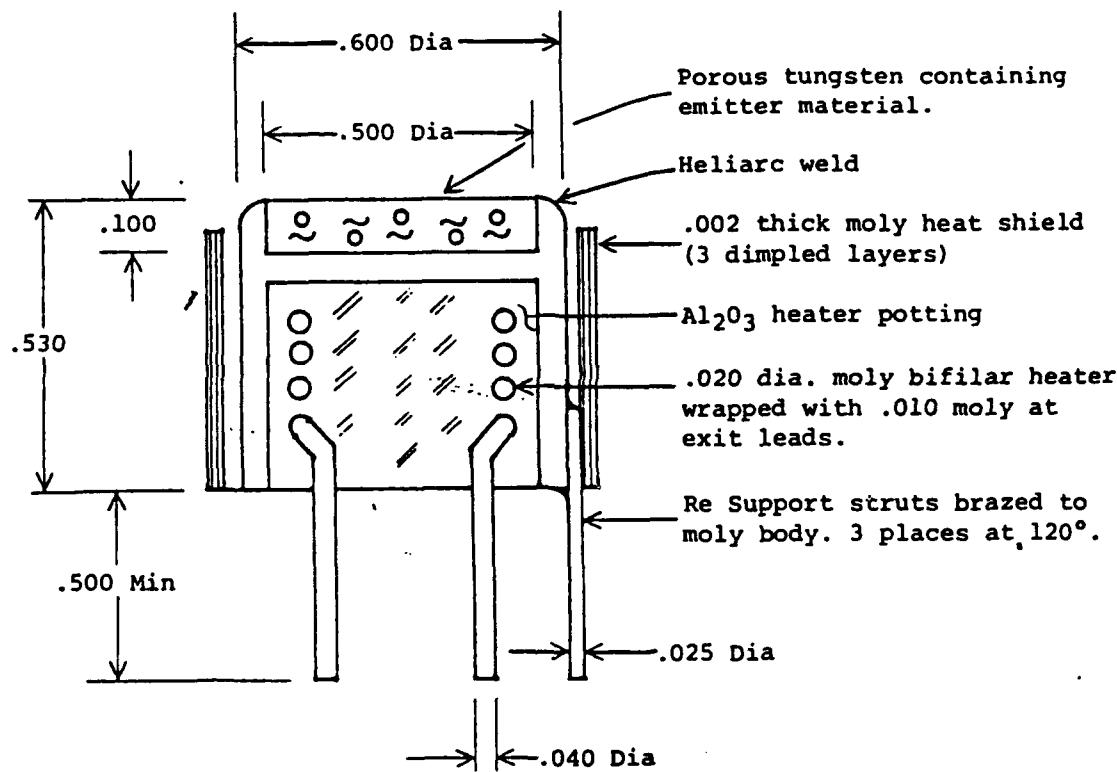
Figure 16. Construction of lithium ion emitter: [Ref. 21]

versatile mounting tripod. The heater is a noninductively wound bifilar coil with heliarc welded rhenium leads solidly potted into the body cavity. The high purity Al_2O_3 potting

mix is H_2 fired at 1900°C which completely immobilizes the heater. The emitter matrix, a specially prepared, extremely porous, tungsten disc with a density of 30% (70% porosity) is heliarc welded to the moly body. The β-eucryptite powder is placed on the face in controlled amounts and melted into the porous disc at approximately 1650°C in a hydrogen atmosphere. The lifetime of this $^6Li^+$ ion emitter was about 200 h. [Ref. 9]

4. Ion Emission Characteristics

The observed total emission current as a function of emitter power and emitter surface temperature (as measured with an optical pyrometer) for a 0.6 inch diameter source is shown in Figure 17. Although the currents are small they are more than adequate for most low energy beam experiments where space charge limitations usually restrict the beam to lower values than those shown in Figure 17. A mass analysis of the beam indicates that there are small amounts of other alkali ions present ($\sim 1\%$) when the emitter is first fired up, but that after a few hours of running the impurities decrease to about 0.01% resulting in a lithium ion beam of very high purity [Ref. 9]. The impurity fraction of the ion beam decreases as the temperature of the ion emitter material increases. At high pulse voltages, the emitted ion current exhibits the Schottky effect; that is, increasing ion current with increasing extraction voltage. While the exact ratio of ions to neutral atoms emitted is not known, it appears that ions dominate by a very large factor. Negative ion and primary electron emission are not normally observed. Current densities of 1-10 mA/cm^2 are achieved at operating temperatures between 950°C and 1100°C. [Ref. 21]
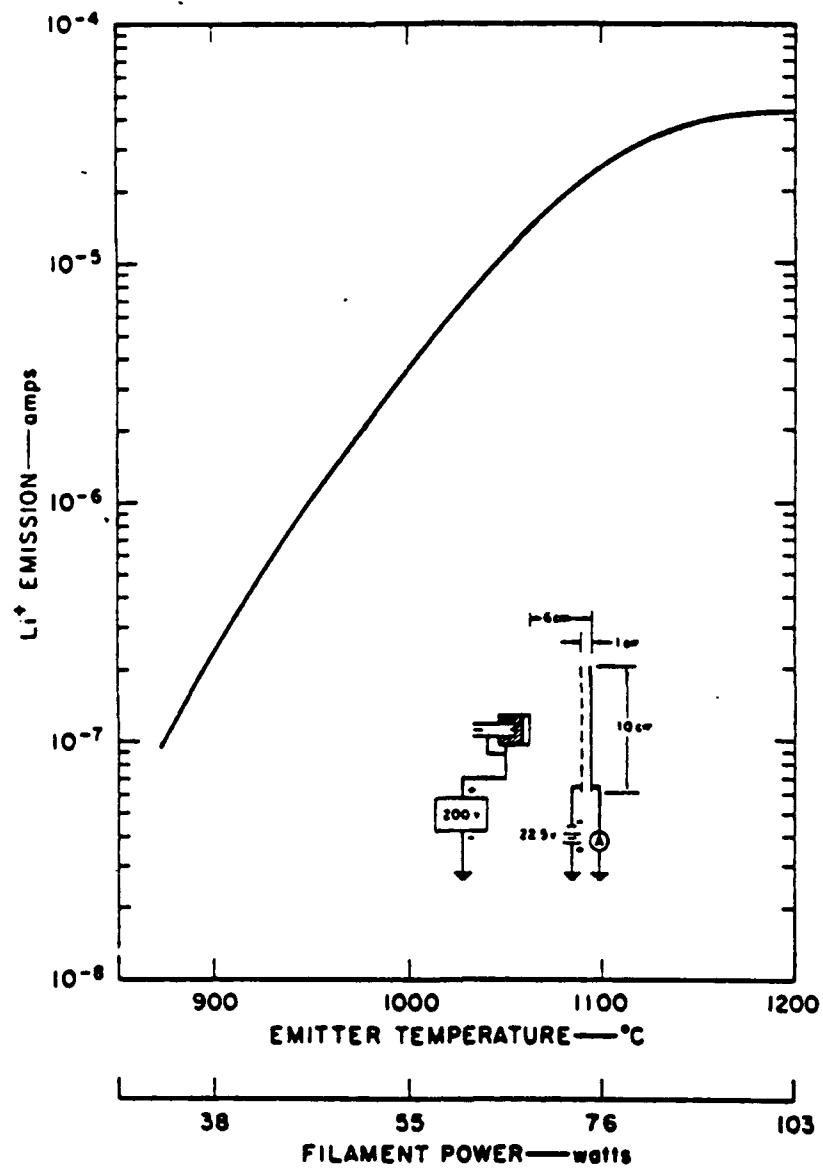
Figure 17. Total emission current as a function of power and temperature: Insert shows experimental arrangement. [Ref. 9]

33

5. Other Designs for Low Energy Ion Beams

O. Heinz, D. C. Lorents, and G. Black presented results of a measurement of the absolute charge transfer cross section for the reaction between *Li* ions and *Li* atoms for incident ion energies from 14 to 1000 eV. They used the lithium ion source to produce a intense and pure alkali-ion beams as shown in Figure 18. The ion gun consists
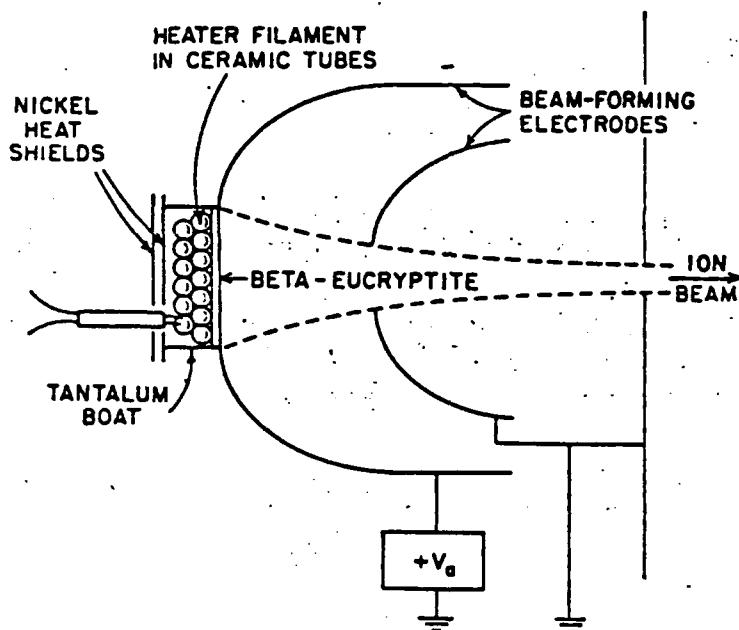
Figure 18.   Lithium ion source for charge transfer: [Ref. 22]

of the emitter and accelerating electrodes mounted on a Lavite holder designed to provide adjustment of the source parameters. The dimensions of the emitter surface are $1.5 \times 1 cm$. A tungsten wire grid spot-welded to the boat assisted adhesion of the coating and served to maintain the β-eucryptite surface at the same potential and temperature as the boat. [Ref. 22]
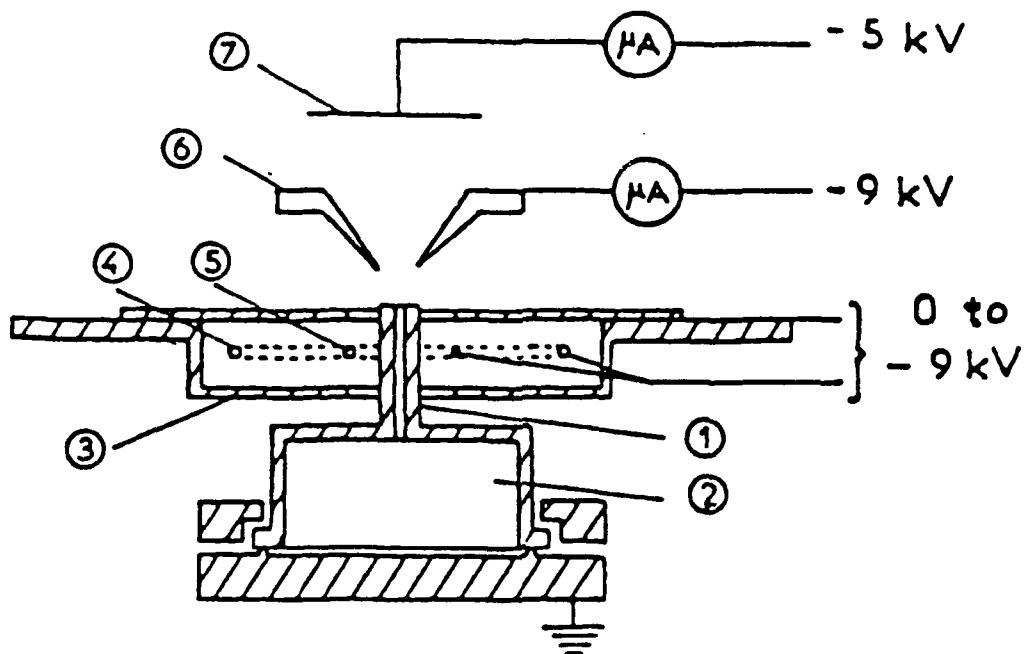
Figure 19. Cross section of the lithium capillary ion source: (1) Capillary tube, (2) lithium reservoir, (3) electron reflector, (4) hot tungsten filament, (5) cold filament, (6) ectractor, (7) collector. [Ref. 23]

M. Remy and R. Haug constructed a capillary ion source using surface ionization of lithium on rhenium in 1969. Figure 19 shows the cross section of the lithium capillary ion source device. The utilization of surface ionization for the production of lithium ions has some advantages. The life of the ion source is limited only by the capacity of the lithium reservoir. The temperature of the lithium reservoir can be increased using a heat reflector around the reservoir. A current of 400 μA was obtained with the 0.5 g capacity lithium reservoir for 300 h, and 100 μA was obtained for 1000 h. [Ref. 23]

OXYGEN SPRAY — OXYGEN INLET

RESERVOIR — HEAT SHIELD — DECEL ELECTRODE

VAPORIZER HEATER — IONIZER HEATER

ION BEAM

LIQUID-VAPOR INTERFACE

VAPOR

FEED TUBE
WIRE BUNDLE

POROUS TUNGSTEN IONIZER

Li OR Na LIQUID

BEAM FORMING ELECTRODE

ACCEL ELECTRODE
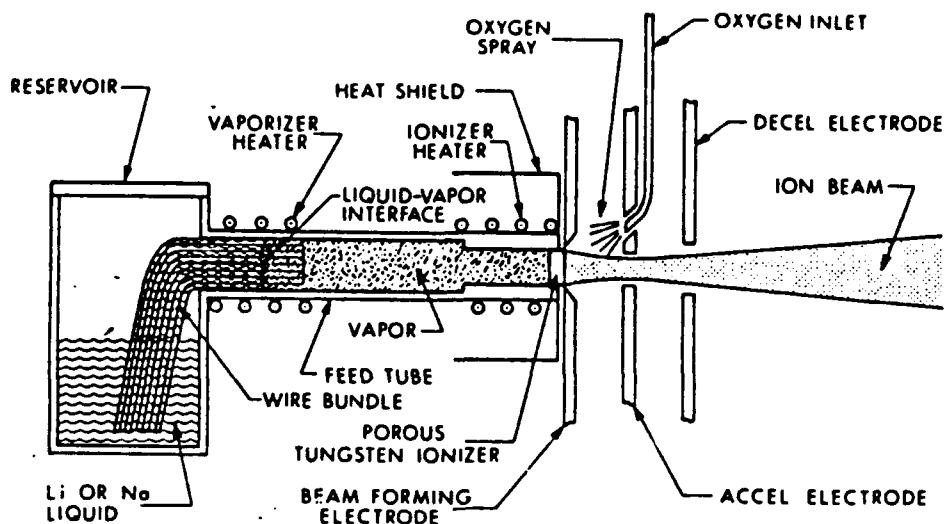
Figure 20.   Schematic representation of the ion source configuration: used to

generate lithium and sodium ions. [Ref. 24]

Howard L. Daley and J. Perel developed an ion source which used direct sur-

face ionization from oxygenated tungsten to generate lithium or sodium ions with high

efficiencies, as shown in Figure 20. The theoretical efficiency of the source depends upon

the difference between the work function (ϕ_w) of the surface and the ionization potential

(ϕ_i) of the desired species. When ϕ_w is $\geq \phi + 0.5eV$, the surface ionization process is very

efficient. The measured efficiencies are more than 70% for both Li and Na using this

type source. This is much greater than that of the capillary ion source ($< 5\,\%$) developed

by M. Remy and R. Haug in 1969. [Ref. 24]

R. K. Feeney and William E. Sayle used a varity of aluminosilicate sources of

positive ions for atomic collision experiments. The most copious thermionic-type ion
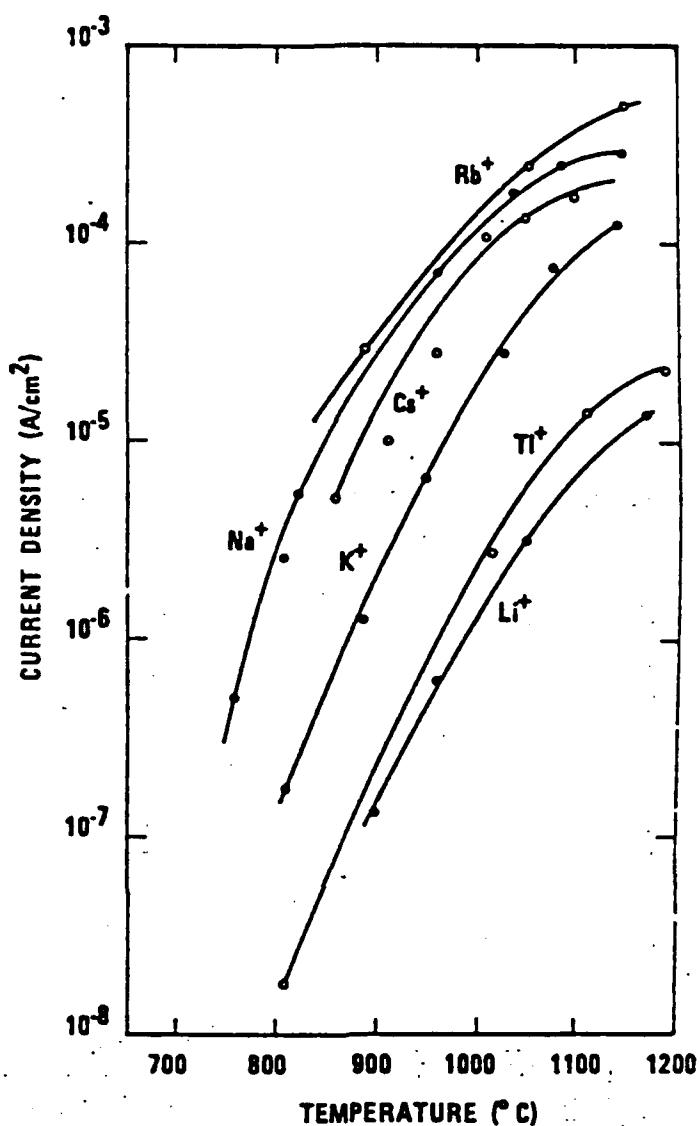
Figure 21.   Typical current densities obtained from the various emitters: as a

function of temperature. [Ref. 25]

emitters have been observed to be the aluminosilicates. Figure 21 shows the typical total

current densities obtained from the 6 emitters as a function of temperature for an ex-

traction electric field of 500 V/cm. This shows that the various aluminosilicate-type ion

emitters did not give equal emission currents for the same conditions. Emitters produc-

ing colimated beams of Li^+, Na^+, K^+, and Tl^+ ions operated for about one month. The failure of a filament can terminate the emission earlier than original life time. [Ref. 25]

Table 4.   SUMMARY OF DESIGNS FOR LOW ENERGY ION BEAM EXPERIMENTS.

Ions	Techniques	Currents	Advantages/Disadvantages
Li^+	Crossed-beam	Ion density $10^{13} atoms/cm^3$	Low Energy spread (< 3 %). High density collimated beams. Slow ions collected.
Li^+	Capillary surface ionization	100 μA, 400 μA	Limited lifetime with reservoir capacity. Low ionization efficiency (< 5 %).
Li^+, Na^+	Direct surface ionization	Several hundred μA to several mA	High efficiency ($\geq$ 70 %). Accel-decel electrode system used to overcome space-charge effects.
Na^+, K^+ Li^+, Tl^+ Cs^+, Rb^+	Aluminosilicate sources	Several hundred μA (see Figure 21)	Obtained various emission currents. Low Li^+, Tl^+ current obtained. Emitter lifetime terminated by failure of Pt-Rh gauze filament.

Table 4 shows a summary of other designs for low energy ion beam experiments which containing icns observed, techniques, currents obtained, and remarkable results.

6.   Applications of the Spectra-Mat. Design

The design to be used in the work has been utilized by others, primarily to produce atomic/ionic beams.

In certain applications the linear arrangement of ion source and charge exchange chamber in standard charge exchange sources for neutral atomic beams leads to undesirable stray light. To avoid this problem a modified design was developed by S. Kita et al., in 1980. In order to prolong its lifetime the emitter surface of 15 *mm* diam-

eter was masked by a cover which had an opening of 3 *mm* diameter, made of 0.1 *mm* tantalum sheet. [Ref. 26]

In 1981, G. Conforti *et al.*, developed a low energy (25-500 eV) alkali ion gun for use in collision experiments using the same lithium ion source. Using the *Li* -ion emitter, currents up to 10^{-5} A at 500 eV ion energy were obtained. [Ref. 27]

D. M. Thomas and W. P. West used a lithium ion emitter for plasma diagnostics. They needed an ion beam of 2-3 times higher intensity than the parent emitter for the diagnostic systems. With enlarged 15 *cm²* of emitter area, they could get a lithium ion emission current of 20 mA. [Ref. 28]

These applications illustrate the wide range of physical application for which this lithium ion source design has been used. The work designated here is intended to extend these applications in space physics.

B. ELECTRON SOURCE

1. Introduction

Two types of electron sources are applied in this thesis work. The first is a dispenser cathode. The first stage in the development of the modern dispenser cathode was the transition from an oxide coating on nickel to $(BaSr)CO_3$ in a cavity behind a porous tungsten plug. This new cathode was termed the 'L' cathode and its development was attributed to Philips Research Laboratories in Holland around 1950. The structure is shown in Figure 22. A porous tungsten disc is attached in a vapour-tight manner to a molybdenum support sleeve. Behind the tungsten disc is an enclosure containing a charge of $(BaSr)CO_3$. Behind this enclosure is an ordinary alumina-insulated heater. The L cathode provided good emission-current capability and long life but had several dis-

POROUS TUNGSTEN DISC

(Ba Sr) CO₃
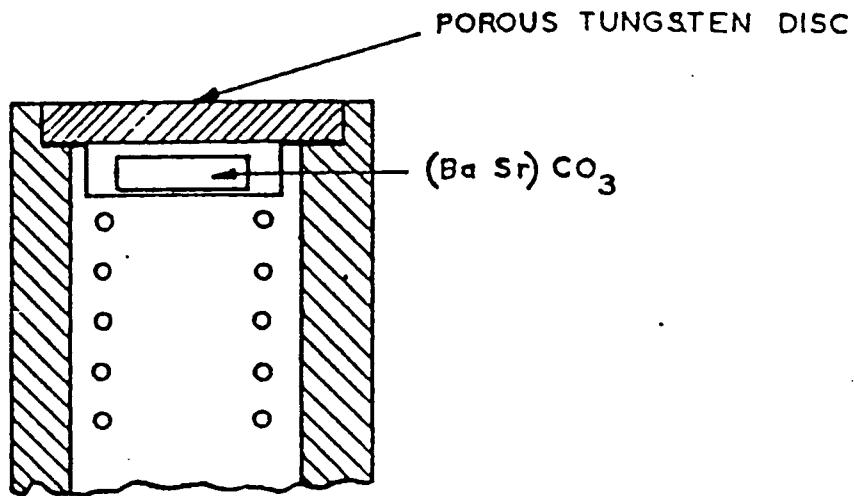
Figure 22. Diagram of L-cathode: [Ref. 29]

advantages. It proved difficult to make a barium vapour leak-tight seal between the porous tungsten emitter and the molybdenum support body. Obtaining uniform cathodes temperatures was difficult because there is little heat transfer through the cavity containing the emissive mix to the porous tungsten plug. Further, it was found that outgassing and activation processing had to be carried out in a narrow temperature range for good emission.

Between 1964 and 1968, R. J. Bondley and M. J. Slivka developed techniques to produce a tungsten matrix dispenser cathode capable of 8 A/cm^2 while operating at 1000°C in a close-packed diode. This event represented an advance in the state of the art for high current density emitters. [Ref. 30]

40

A tungsten dispenser cathode is a thermionic electron emitter used in gas and vacuum tubes. In 1969, R. T. Reaves and S. M. Jarrett found that a directly heated, barium impregnated, tungsten dispenser cathode is an excellent choice for a thermionic cathode in an ion laser plasma tube and in other experimental tubes. One reason is that cathode activation is easily performed. A situation often encountered in evaluating new tube structures is the poisoning of the cathode due to outgassing of tube parts. Here the ability to reactivate is important for efficient experimentation. In addition, tube failure in operation of experimental devices need not require cathode replacement. [Refs. 31, 29]

We used the tungsten dispenser cathode as an electron emitter which was designed for this work and manufactured by Spectra-Mat, Inc.. We will discribe the design and fabrication of the directly heated tungsten dispenser cathode, and we will discuss newly designed electron emitter for this experiment.

2. Directly Heated Tungsten Dispenser Cathodes

A tungsten-base dispenser cathode is basically porous tungsten impregnated with an emissive material. The porous tungsten matrix acts as a reservoir from which the emitting material can diffuse to the surface, maintain an active layer and, consequently, provide a low work-function surface for the thermionic emission of electrons [Ref. 30]. When heated, the material diffuses to the surface forming a low work function emitter (1.7 eV approximately). These cathodes are normally operated between 950°C and 1200°C (surface brightness values) depending upon the emissive current required and environmental conditions. [Ref. 31]

The emission current capability of the tungsten dispenser cathode is dependent on several variables: (1) emitter temperature, (2) work function of emitting surface, (3) tungsten-matrix pore size, (4) pore density (pores per unit surface area), (5) uniformity of pores. Reliable electron current over a long period of time is a function of the equilibrium established between the rate of arrival of barium at the emitting surface and the rate of evaporation of barium from the emitting surface. The barium is produced in the pores of the tungsten matrix by the reaction of the impregnant and the tungsten. [Ref. 30]

Examples of a directly heated cathode are shown in Figure 23. Life expectancy of these cathodes exceeds 10,000 hours in vacuum tubes. Total emitting current can be calculated by the multiplication of current density, emitting surface area per turn, and the number of turns.

3. Fabrication

The directly heated cathode fabrication starts by blending high purity tungsten powders with particles in the 1 to 15 μm range. Exact particle size and distribution is of importance in maintaining a final interconnecting, open pore structure while optimizing physical strength in the 80% of theoretical density range. Table 5 [Ref. 30] lists the important characteristics of tungsten powder used for dispenser cathode fabrication. Figure 24 shows a 5000x SEM of typical tungsten powder.

The powder is sealed in plastic or rubber molds and isostatically pressed at 20,000 psi. The resulting pellet will possess a density of approximately 60% (11.6 g/cm^3). Subsequent hydrogen sintering at 2500°C for 30 minutes will raise the density to 80%. The next step is machining the sintered pellet to the helical form. The sintered

Figure 23. Examples of directly heated tungsten dispenser cathodes: [Ref. 31]

pellet must first be infiltrated with an inert plastic filler. This is done to aid in machining and to maintain an open pore structure. Table 6 [Ref. 30] lists the important parameters of porous tungsten made from the powder characteristerized in Table 5.

Rhenium has been selected for the lead material because of its compatibility with the cathode and its conformance with some critical design parameters. Other lead materials such as molybdenum may be used as well for less critical assembly procedures. The impregnant is made by converting a mixture of $BaCO_3$, $CaCO_3$, and Al_2O_3 to $3BaO \cdot CaO \cdot Al_2O_3$. The CO_2 is driven off during air firing and the resulting oxide composite melted into the porous tungsten matrix at 1700°C in a hydrogen atmosphere. The
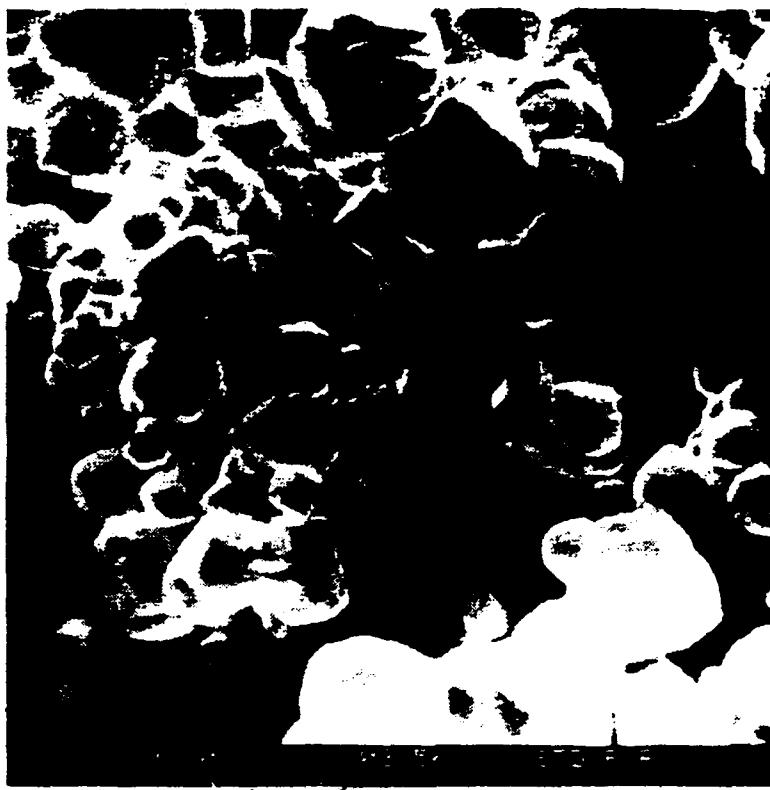
Figure 24. Tungsten powder, 5000 magnification: [Ref. 30]

impregnated cathode needs to be protected from long periods of atmospheric exposure as the barium, calcium, aluminate is quite hydroscopic. It will readily absorb moisture resulting in a volume expansion and an exuding of the impregnant from the pores of the tungsten body. This *blooming* can be easily brushed away should it occur. The only negative effect caused by *blooming* will be an initial gas burst larger than normal during the first cathode heating. The cathode is protectively packed in either individual vacuum glass vials or in an argon atmosphere. [Refs. 31, 30]

Table 5. TUNGSTEN POWDER CHARACTERISTICS.

Type	hydrogen-reduced tungstic acid
Particle size	Fisher subsieve — average between 6.0 μm and 8.0 μm photelometer — average between 7.0 μm and 9.0 μm minimum 90% between 2.0 μm and 14.0 μm
Shape	angular

Typical impurities

Element	Maximum impurities	Element	Maximum impurities
	ppm		ppm
Al	10	Mn	10
C	10	Mo	200
Ca	10	Ni	40
Co	10	O$_2$	1000
Cr	30	Pb	10
Cu	10	Si	10
Fe	50	Sn	10
Mg	10	Ti	20

Table 6. HYDROGEN SINTERED TUNGSTEN: TYPICAL CHARACTERISTICS.

Density	(15.44 ± 0.39) g/cm^3 (or 80% ± 2% of the theoretical density of tungsten)
Average pore diameter	3 μm (maximum)
Pore diameter range	1–7 μm
Mean pore area	(16 ± 8) μm^2
Pore density	8 000–36 000 pores per mm^2

4. Newly Designed Electron Source

Porous tungsten with a formula of barium oxide dispersed throughout the matrix is the essential form of the dispenser cathodes. Figure 25 shows a diagram of the tungsten dispenser cathode which has been designed as an electron source for this experiment.

Table 7. BARIUM-CALCIUM-ALUMINATE IMPREGNANT COMPOSITION.

	BaO	:	CaO	:	Al_2O_3
Molar ratio	4	:	1	:	1
Molar weight %	79.5		7.3		13.2
Molar ratio	3	:	1	:	1
Molar weight %	74.4		9.1		16.5
Molar ratio	5	:	3	:	2
Molar weight %	67.3		14.8		17.9

This is a directly heated, barium impregnated, standard '31180' tungsten dispenser cathode which is manufactured by Spectra-Mat, Inc.. The designation of the model '31180' contains two implicit meanings, '80' represents the density of porous tungsten matrix by volume ratio to pores, and '311' stands for the molar ratio of the barium-oxide to calcium-oxide and aluminum-oxide which is mixture as an impregnant material seen in Table 7.

Pure molybdenum leads are welded to the terminal ends to form a ductile mounting support. To insure optimum performance, cathodes should not be exposed to atmospheric conditions even though it does not interact strongly with atmosphere. It should be kept in a partial vacuum of 10^{-3} torr or better.
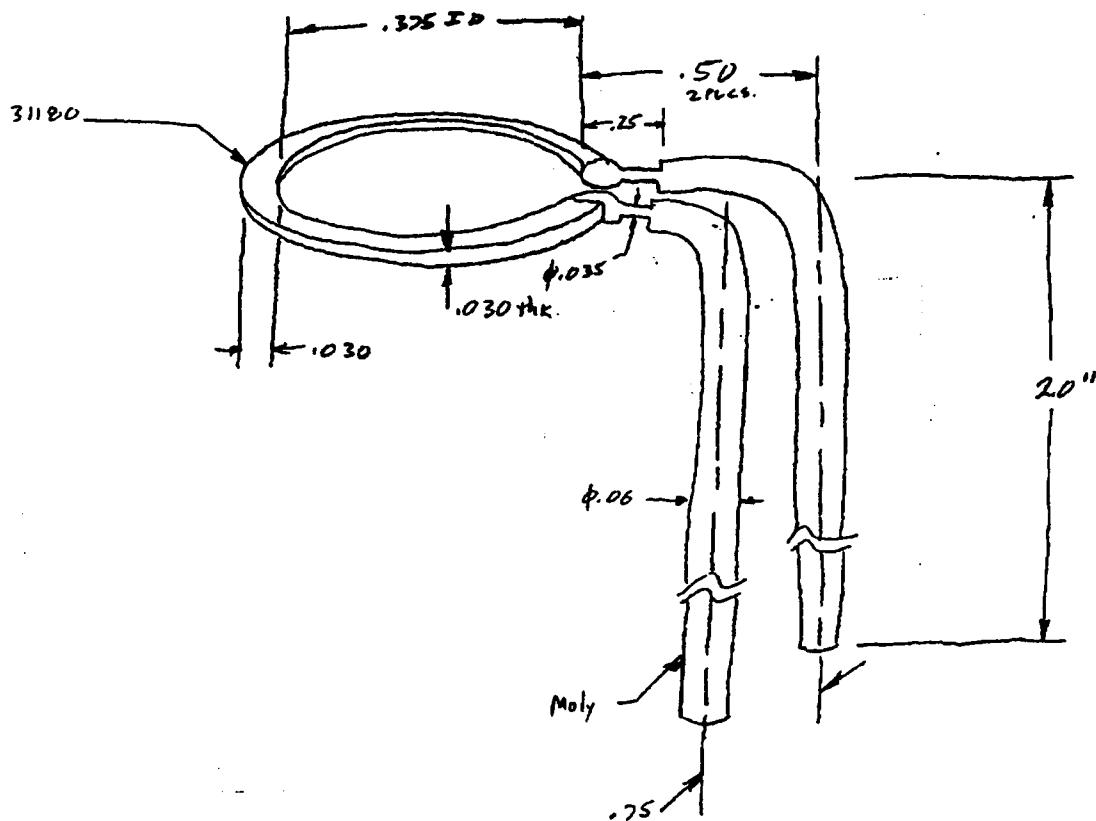
Figure 25. 31180 tungsten dispenser cathode: manufactured by Spectra-Mat, Inc..

Figure 26 shows the emission characteristics of several tungsten dispenser cathodes involving the standard model '31180'. It compares the zero-field emission of the M family (improved version) of cathodes to that of the family of barium calcium aluminate impregnated tungsten dispenser cathodes. [Refs. 30, 31, 32]
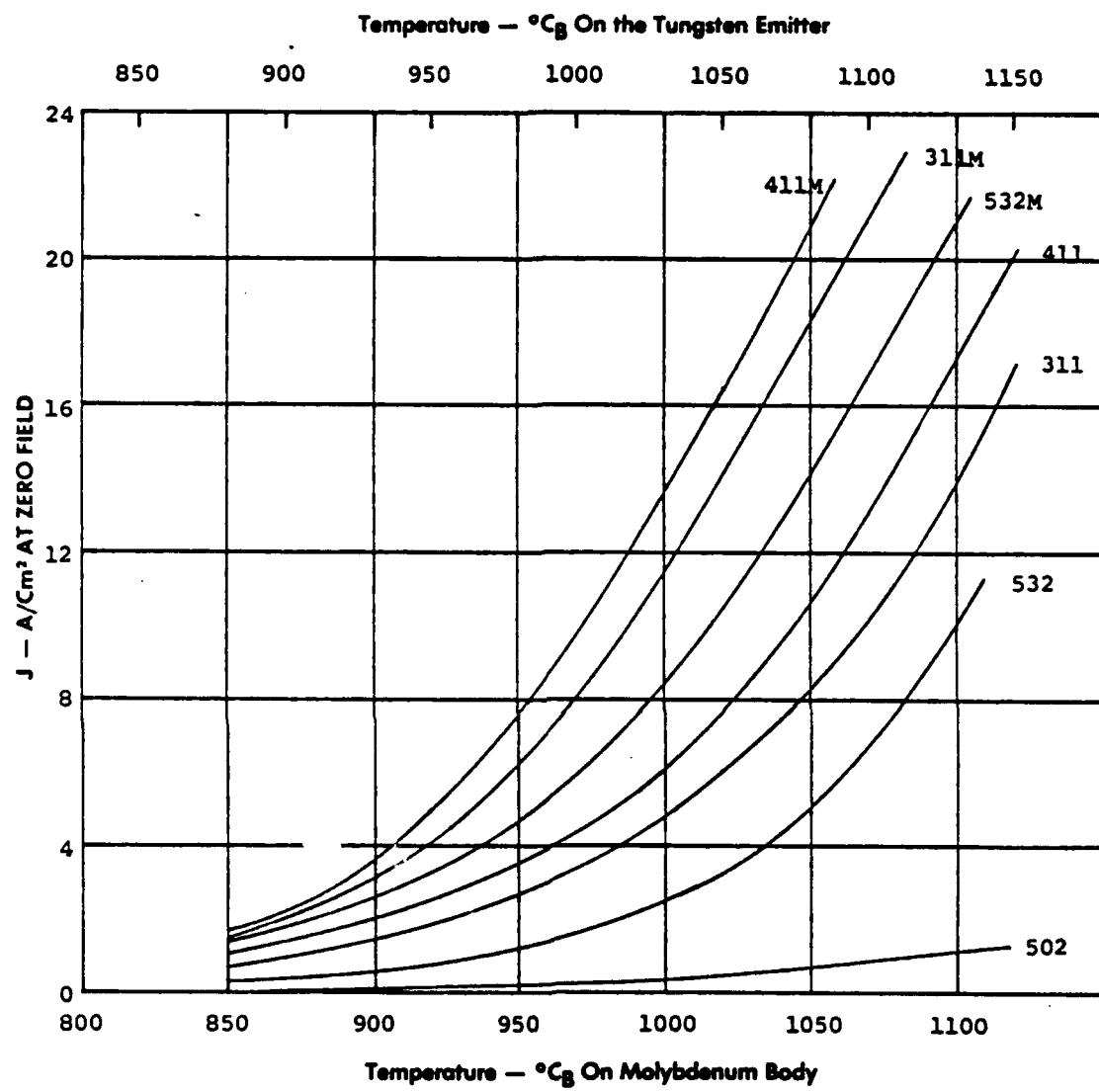
Figure 26. Emission of various tungsten dispenser cathodes: [Ref. 32]

IV. EXPERIMENTAL EQUIPMENT

The experimental equipment consists of Varian vacuum system producing high vacuum in a chamber, power supplies for the source heater, and measuring instrumentations. The ion-and electron sources are installed with device properly designed, to be investigated or simulated in the vacuum chamber.

A. VACUUM SYSTEM
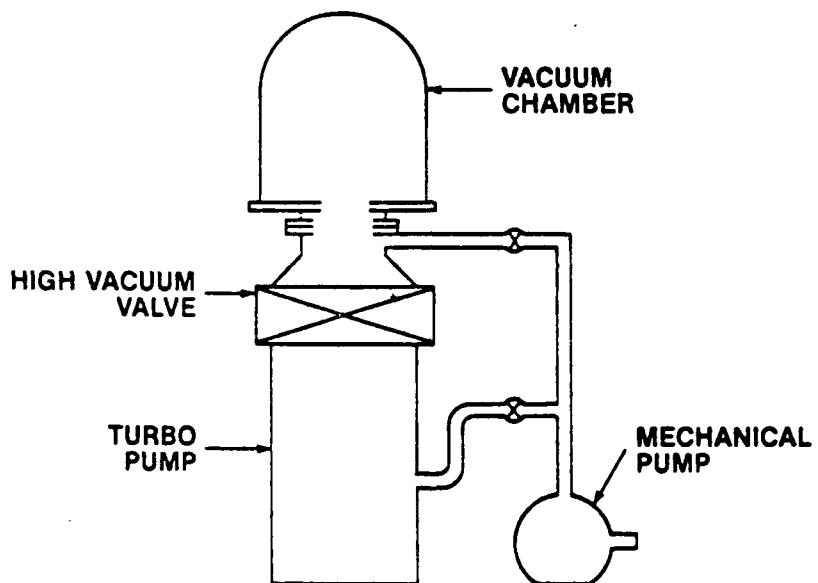
Figure 27.   Varian vacuum system

Figure 27 shows the major parts of the Varian vacuum system. This system consists of two pumps and bell jar vacuum chamber. A Rotary Vane Oil-Sealed Mechanical Pump is used to produce rough pumping; pressure range 760 torr to 10^{-3} torr (760 torr

49

= 1 atm.). A Turbomolecular pump (V 1000) is used for high vacuum pumping; pressure range 10^{-3} to 10^{-8} torr.

The required minimum pressure for the experiment is approximately 10^{-6} torr, which can be considered as a high vacuum condition. The pressure is strongly related to the cleanliness of the installations in the chamber. The pressure tended to increase when the sources were heated, apparently due to outgassing from the sources.

The operating procedure for the system is important because two pumps should be started properly. In order to start this experiment, the bell jar should be evacuated to the order of 10^{-6} torr. It usually takes several hours to reach the desired pressure range of the vacuum chamber, and up to 24 hours pumping to assure complete outgassing. When the source and device have been exposed to atmosphere, it is desirable to allow vacuum system to pump down at least overnight before attempting to heat the source.

We used a dessicator to keep the lithium ion and electron sources temporarily outside the chamber. It helps to conserve the sources from interaction with atmosphere. A simple mechanical pump used to make a partial vacuum for the dessicator.

B. VACUUM CHAMBER

A copper mesh is mounted just inside of the bell jar, which takes the important role of plasma sheath in the laboratory space. There are several electrical feedthrough for permitting the electrical lines and apparatus to measure the physical properties in the chamber. There is a window through the metal covering protector which surrounds outside the bell jar. This window is to observe the device mounted in the chamber and measure the surface temperature of sources with an optical pyrometer.

The lithium ion and electron sources, which are mounted on space shuttle tile (see Appendix), are heated by power supplies with proper device and geometry according to requirements. The characteristics of induced current flows and observable physical properties are measured and investigated for the purpose of controlling spacecraft charging. Several diagrams of these chamber interiors will be shown in the Figures for each experimental procedure.

C. POWER SUPPLY

We used four kinds of power supplies to heat the sources. Two HP 6030A DC power supplies which have a maximum output of 1000 W (0-200 V, 0-17 A) were used. They were used to heat the lithium ion sources. The electron source needed a current of more than the maximum value of 17 A for heating up to the normal operating temperature. The problem was solved by connecting both in parallel to get sufficient current.

A Sorensen DCR 300-3B (0-300 V, 0-3 A) was used to bias the grid for collecting an induced current, or to be biased the screen copper mesh.

Several smaller supplies were also used.

D. MEASURING INSTRUMENTATION

Two Varian Type 0531 thermocouples were used to measure the pressure in the rough vacuum range, and Varian 880RS vacuum ionization gauge was used to measure the high vacuum pressure.

Two kinds of Keithley (195A, 196 DMM) digital multimeters and Fluke (handheld 75, 85) multimeters were used to measure the ion or electron currents in the system, and

to read the bias. A Keithley 230 programmable voltage source was available to set bias voltages to various elements of the system.

The temperature of the sources was measured with a Leeds & Northrup optical pyrometer. The measured values represent the surface temperature of heated sources, called *surface brightness temperature* .

V. EXPERIMENTAL PROCEDURES AND RESULTS

A. SIMULATION OF CHARGED SPACECRAFT WITH 0.6 INCH LITHIUM ION SOURCE

1. Introduction

Previous research at NPS verified that the lithium ion source can be a possible device for potential control on a positively charged spacecraft. A lithium ion emitter of 0.25" diameter was used in these initial tests. The emission current was about 2.0 μA through 200 hours of life time period at an input power of 20 W. It was difficult to demonstrate the control of differential charging with the small source because of low current levels. [Ref. 33]

In geosynchronous orbit, the spacecraft potential is approximately $+10$ V in sunlight, with a photoelectron current of about 10 μA. Therefore, an emission current of 2~10 μA can reduce the spacecraft potential to near zero. This is useful for scientific satellites, which are platforms for low energy plasma measurement.

As a completion of the previous study, we extended the work with a 0.6" diameter lithium ion source.

2. Simulation of a Positively Charged Spacecraft

We arranged the chamber interior, as shown in Figure 28. The 0.6 inch lithium ion source was mounted on space shuttle tile in an 8 inch long by 5 inch diameter structure allowed simulation of the source mounted on a spacecraft. The screen mesh (copper) simulates the sheath of plasma in space with distance of 15 cm from the source,
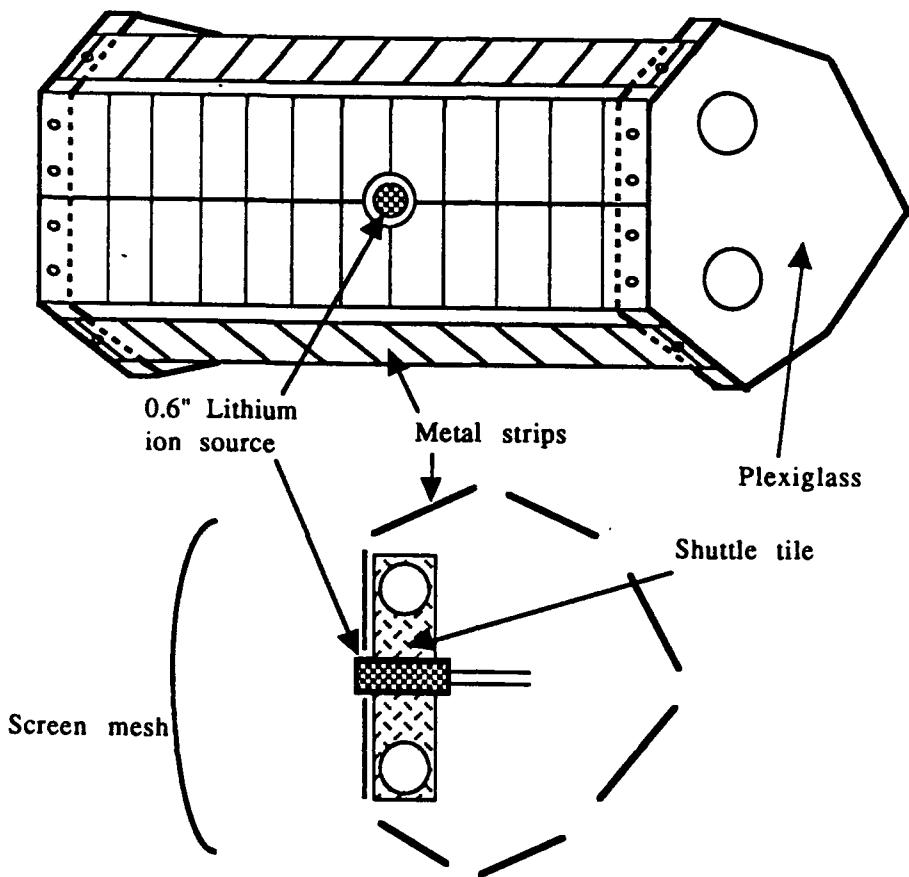
Figure 28. Diagram of chamber interior for simulation

and the metal (stainless steel) strips around the source simulate the spacecraft surface.

The front strip is a solid stainless steel plate with a hole for mounting the source at the

center. The other 6 strips are set separately with small gaps between them.

Figure 29 shows the diagram of circuit for simulation of a positively charged

spacecraft. All strips were electrically connected as a surface of spacecraft to be biased

with equal potential. The source and strips were grounded to the base plate. The screen
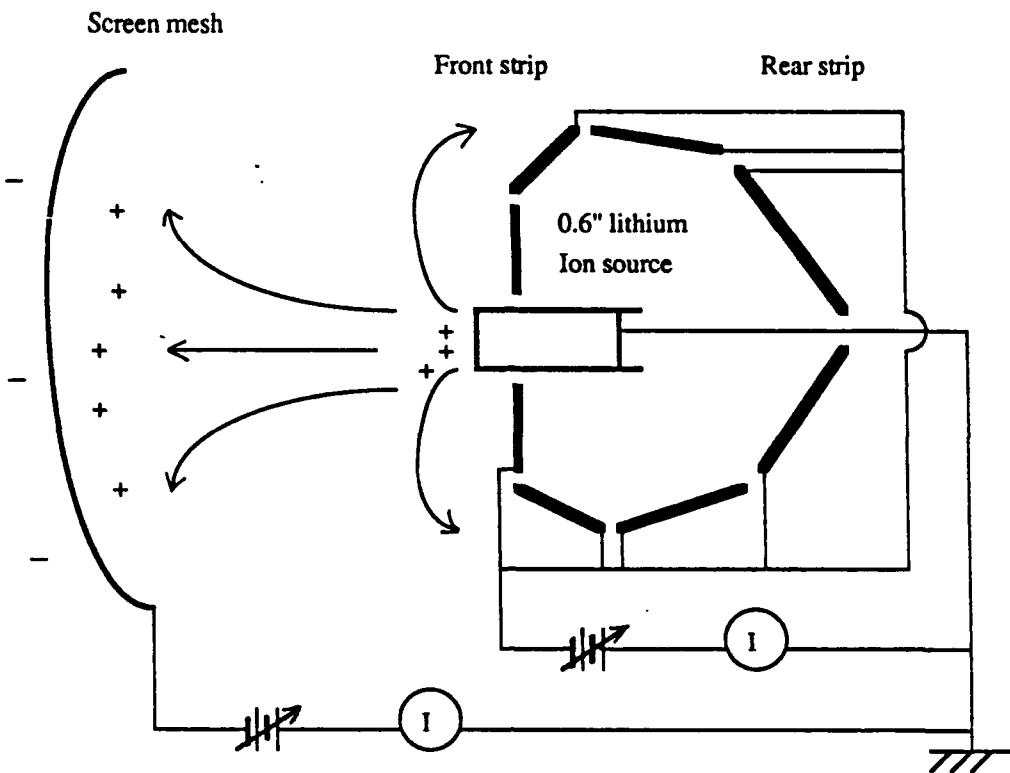
Figure 29. **Diagram of circuit for simulation:** of a positively charged spacecraft.

mesh and strips were biased negatively with respect to the source. Induced Currents
from the source to the screen and strips were measured as a function of bias voltage and
heater power.

Figure 30 (top) shows that the current induced to the screen is linearly pro-
portional to the strip bias voltage varying from -5 V to -100 V. The copper mesh
(screen) surrounded the chamber system, and it was biased with fixed voltages of -100
V and -200 V. The induced current to strips shows a little different behavior, as seen in
Figure 29 (bottom). The strip current was not linearly dependent upon its bias voltage.
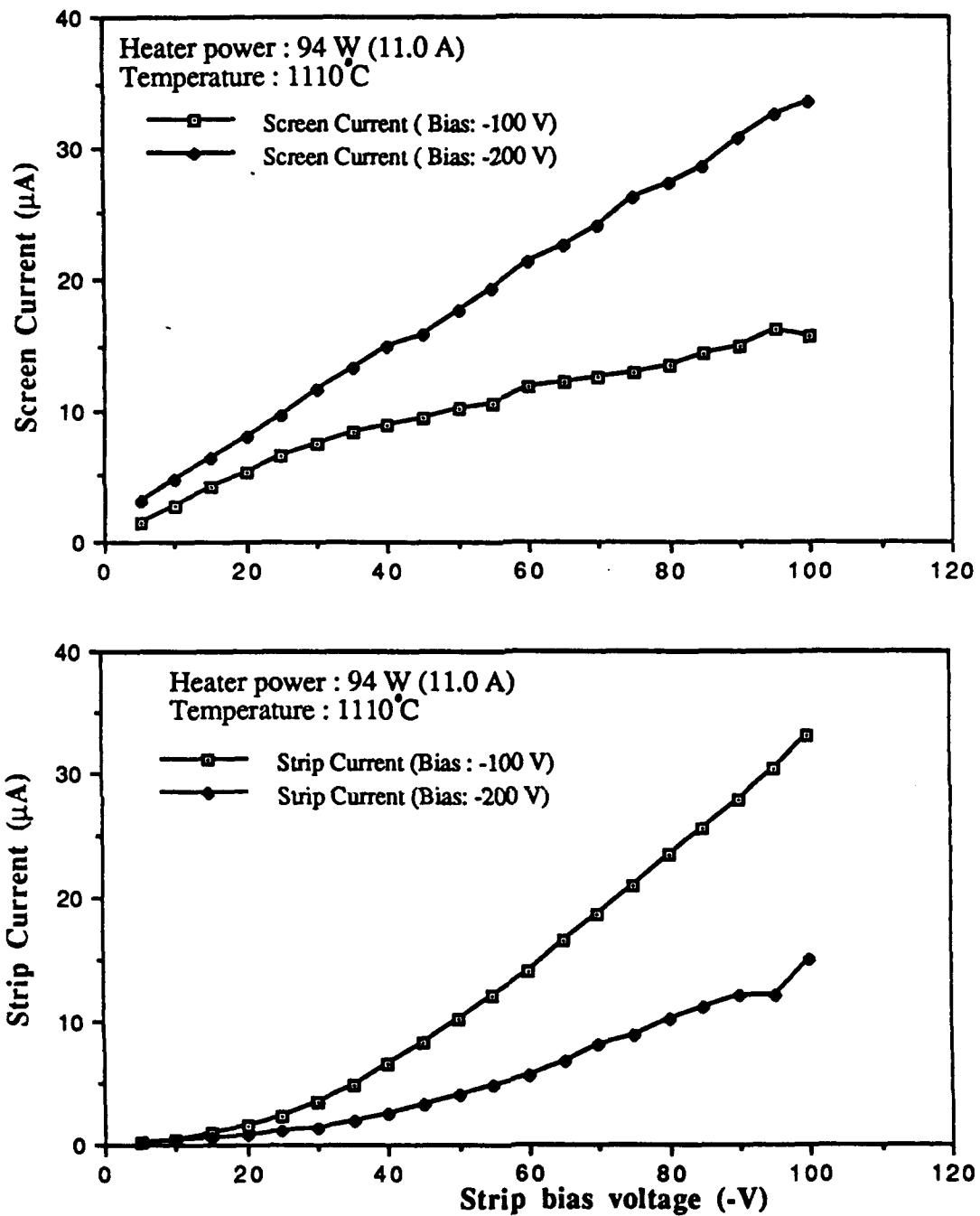
Figure 30.   Induced current to the screen (top) and strips (bottom):   as a function

of bias voltage (negative) to strips

56
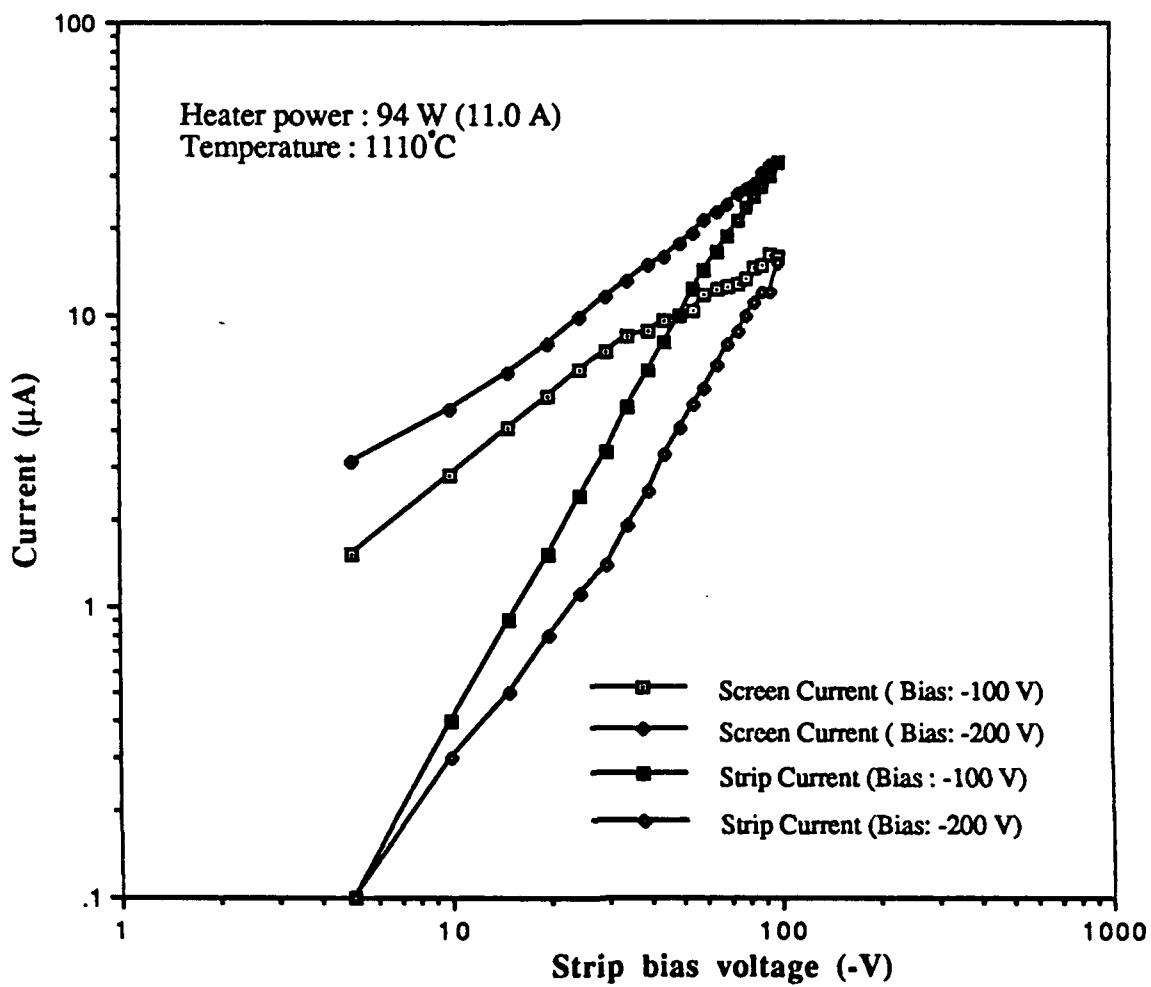
Figure 31. Induced current to the screen and strips (log-log scale): as a function of strip bias voltage.

Figure 31 clearly shows the currents on a log-log scale. The slopes are quite different. The strip current was apparently space charge limited, since the slope of ~1.7 corresponds to the classical value. The screen current was not as obviously space charge limited with a slope of 1.0. At the highest bias voltage on strips (-100 V), both

currents were almost the same value. The maximum current was about 33 μA at a heater power of 94 W (11.0 A, 8.55 V) and screen bias voltage of -200 V. The surface temperature of the source was about 1100°C, which was almost the upper limit of operating temperature.

Figure 32 shows the ion current induced from the source to the screen and strips as a function of bias voltage to the screen. The heater power was 94 W (11.0 A, 8.55 V) and temperature was 1110 °C. Screen bias voltages were varied from zero to -200 V and strip bias voltages were fixed at -10 V and -20 V. We measured currents of below 10 μA. The screen mesh was separated by over 15 cm from the source. Therefore, the low current level is not surprising. The screen current (top) rapidly increased at lower bias voltages of $\sim$50V. The slopes and breakpoint were greater for higher strip bias voltage.

Figure 32 (bottom) shows the current induced to the strips. The current initially increases from a value of several μA, then decreases rapidly as the ions move toward the outer mesh. There was a critical point of current flow between the screen and strips around -50 V of bias voltage. The applied negative bias voltage to the screen strongly attracted positive ions to the screen.

Figure 33 shows both currents to the screen and strips and their sum. The sum of currents increased gradually from about 4 μA to 9 μA according to the screen bias voltage. All strips were biased with -20 V constantly. It showed that positive ions from the source were attracted by the bias voltage, and the total current tended to increase slowly according to the bias voltage. But, the sum remained reasonably constant. There might be a slight chamber effect.
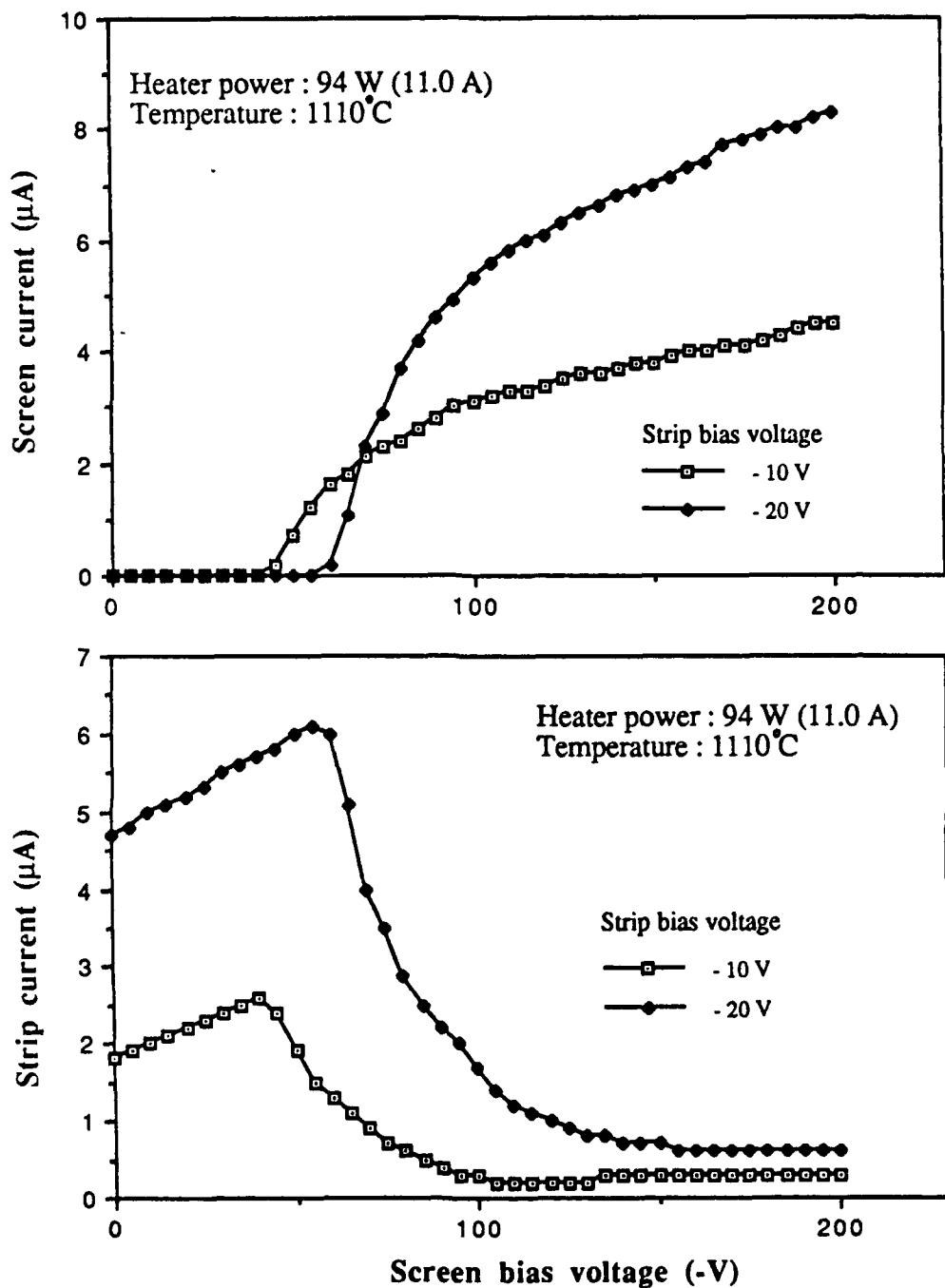
Figure 32. Induced current to the screen (top) and strips (bottom): as a function of bias voltage to the screen.
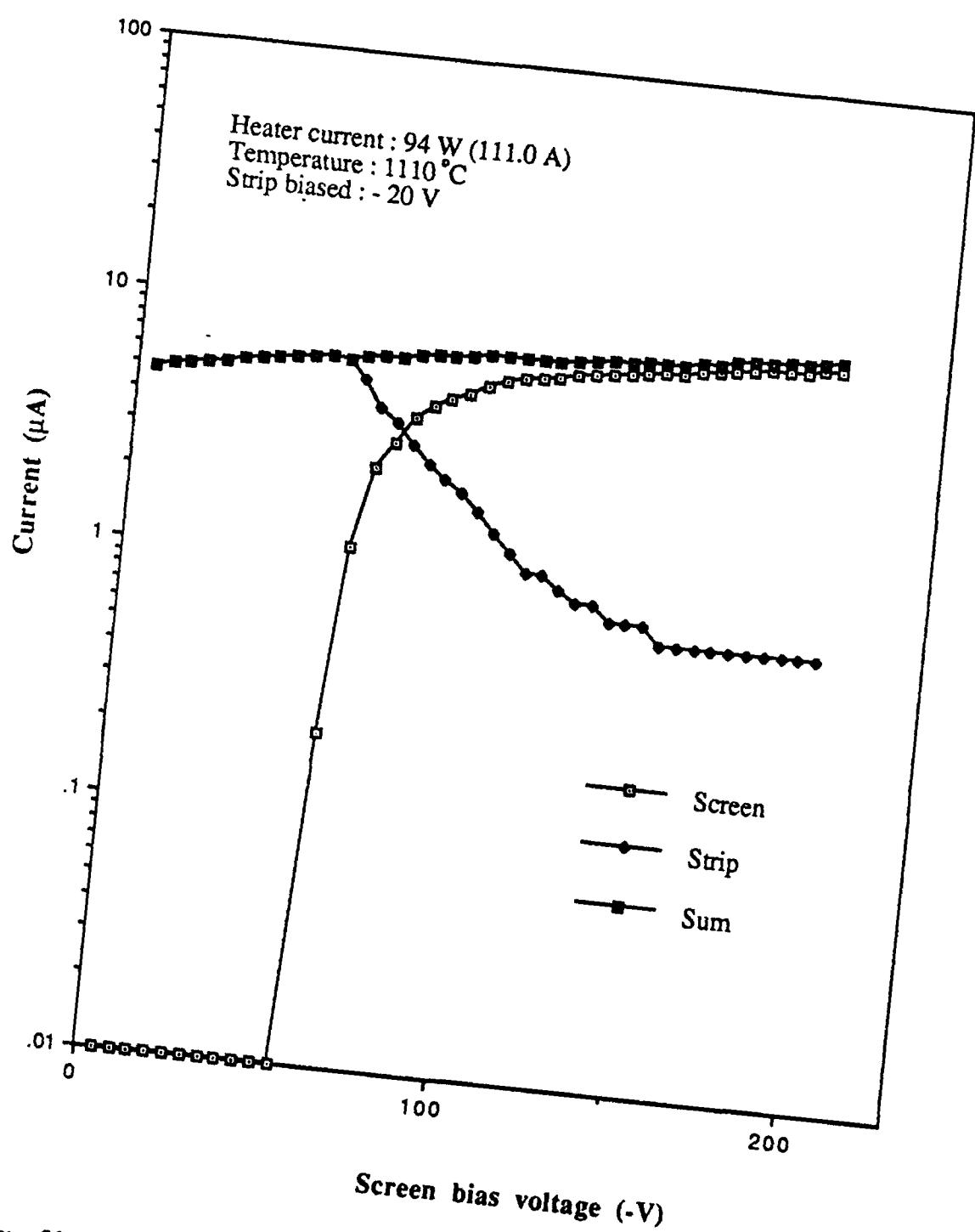
Figure 33. Induced current to the screen and strips and their sum: as a function of screen bias voltage.

60

3. Simulation of Differential Charging

Figure 34 shows the diagram of circuit to simulate differential charging with the same geometry used previously. In order to investigate the current induced from the 0.6″ lithium ion source to a differentially charged surface, the front and rear strip should be at different potentials. The two rear strips were connected electrically, but they were isolated from the others.
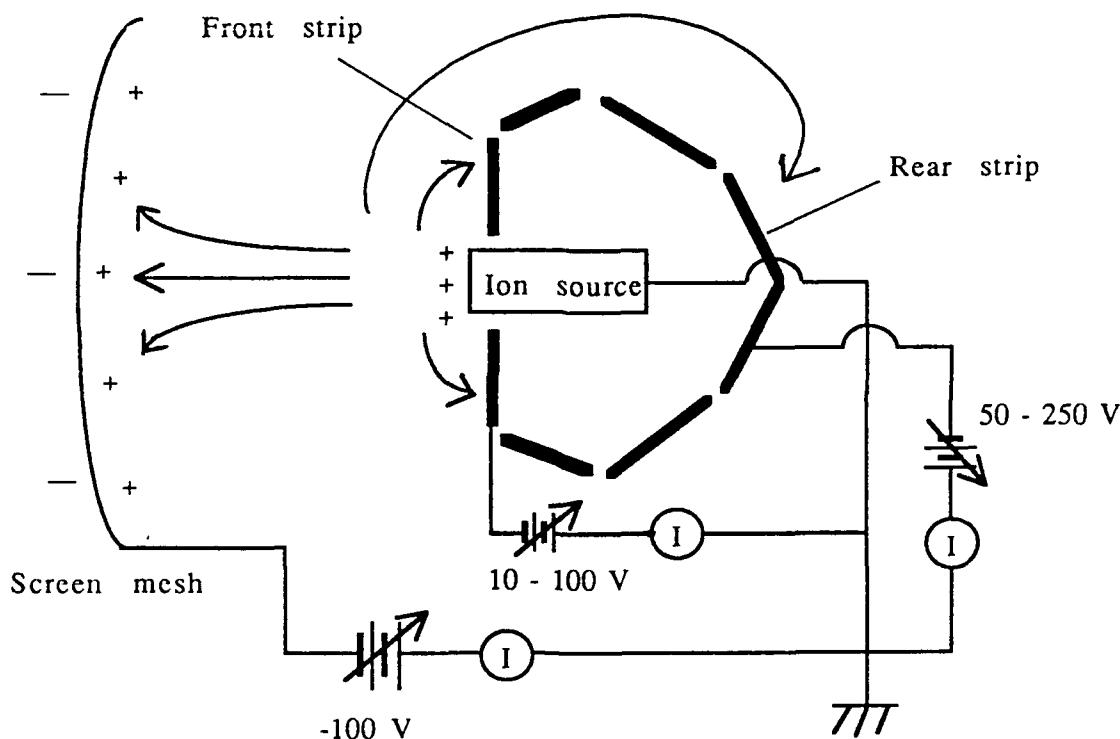
Figure 34.   Diagram of circuit for simulation of differential charging

We simulated the differential charging with various bias voltages applied to the isolated front and rear strips. The bias voltages on the front strip were varied from -10 V to -100 V, and -50 V to -250 V for the rear strip. The screen was biased -100 V con-
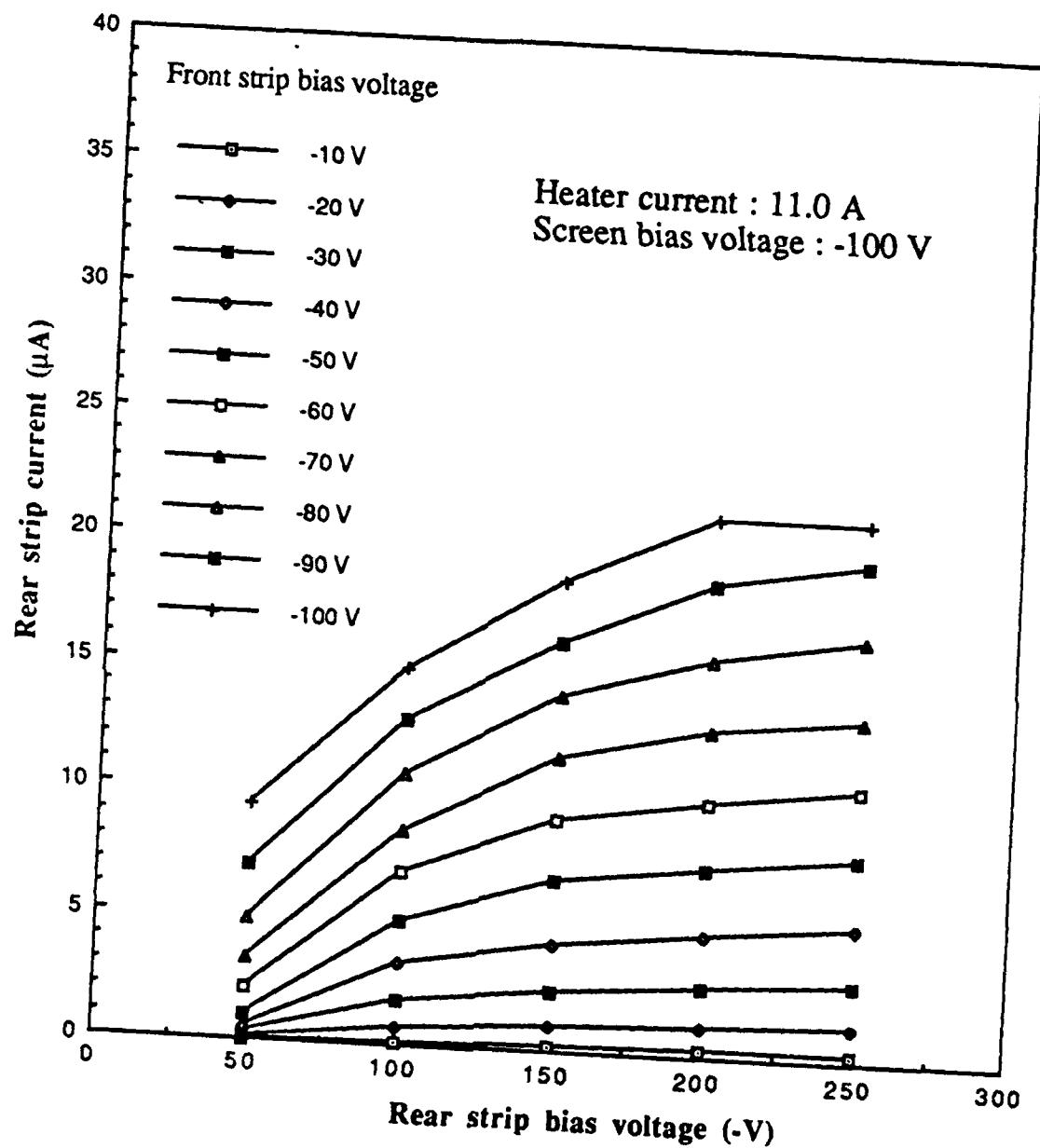
Figure 35. Induced current to the rear strip: as a function of its bias voltage.

stantly through measurements to simulate a net 'positive' spacecraft condition. Figure 35 shows the induced current to the rear strip as a function of its bias voltage with the heater power of 94 W (11.0 A). The maximum current measured to the rear strip was 21 μA for the bias voltage of -250 V. We worried about some possible ion current leakages through the hole around the source, but there was not a noticeable current leakage. We verified this with a gasket which was durable for the high temperature. These current levels would be adequate to discharge differentially charged surfaces on high altitude satellite.

The current to the rear and front strip and their relation is shown in Figure 36. The current to both strips were strongly related with their bias voltages. The more (relative) potentials on rear strips, the more (relative) currents induced. We obtained induced currents of 25 μA and 15 μA to the front and rear strip respectively, when the screen and both strips were equally biased with -100 V. This was quite a significant result compared to the 0.25″ lithium ion source under the same simulating condition. The maximum rear strip current was over 20 μA when biased with -200 V.

From these results above, we conclude that the 0.6″ lithium ion source could be a suitable device to control the potential of differentially charged surfaces on spacecraft in geosynchronous orbit.

B.   INVESTIGATION OF ELECTRON SOURCES

1.   Tungsten Dispenser Cathode

We mounted the newly designed 31180 tungsten dispenser cathode to examine the behavior of electron current and its effect on ion current. Figure 37 shows the diagram of chamber interior for operating the ion source in conjunction with electron
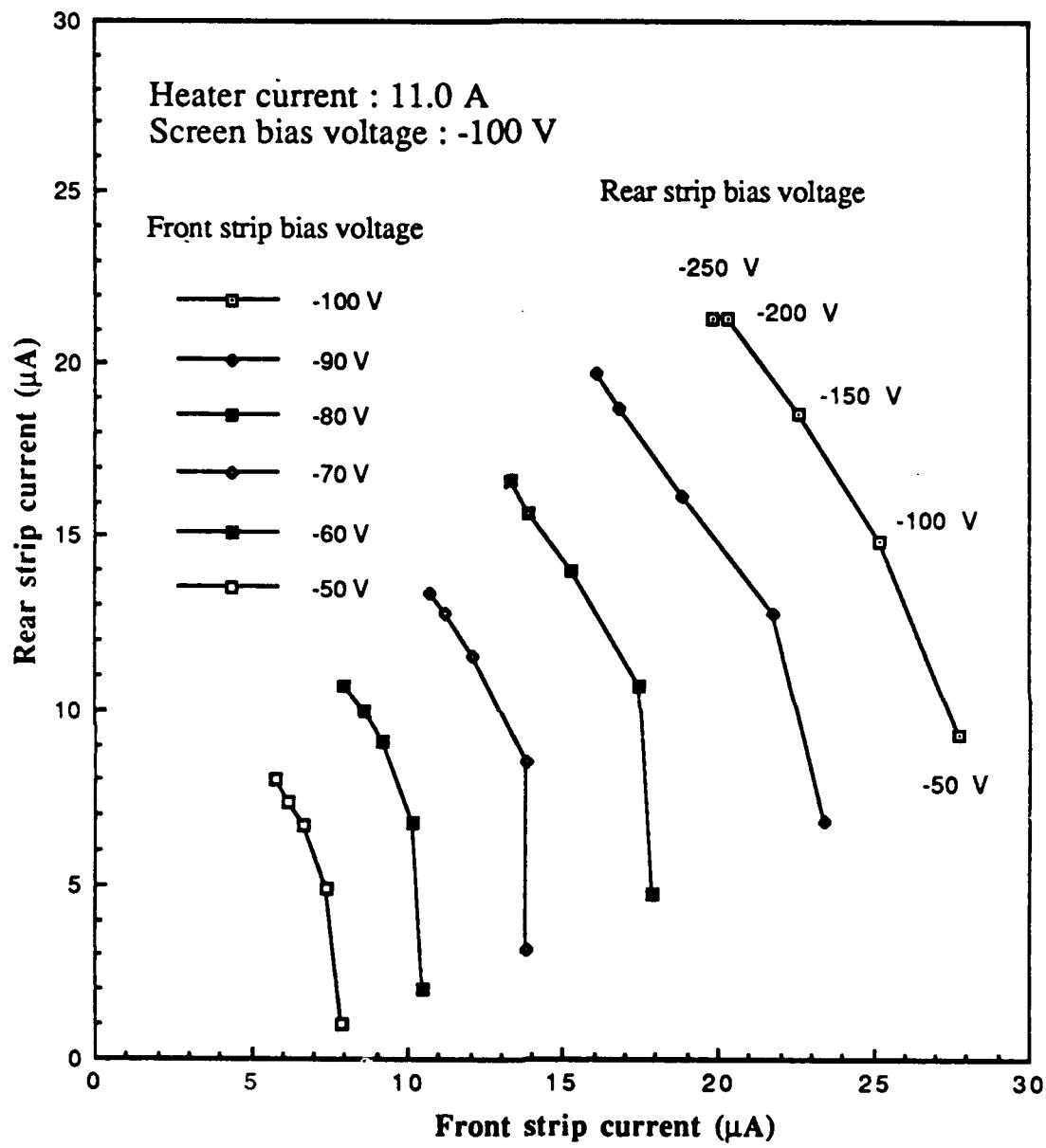
Figure 36. Induced current to the rear and front strips and their relation: as functions of their biased voltages.
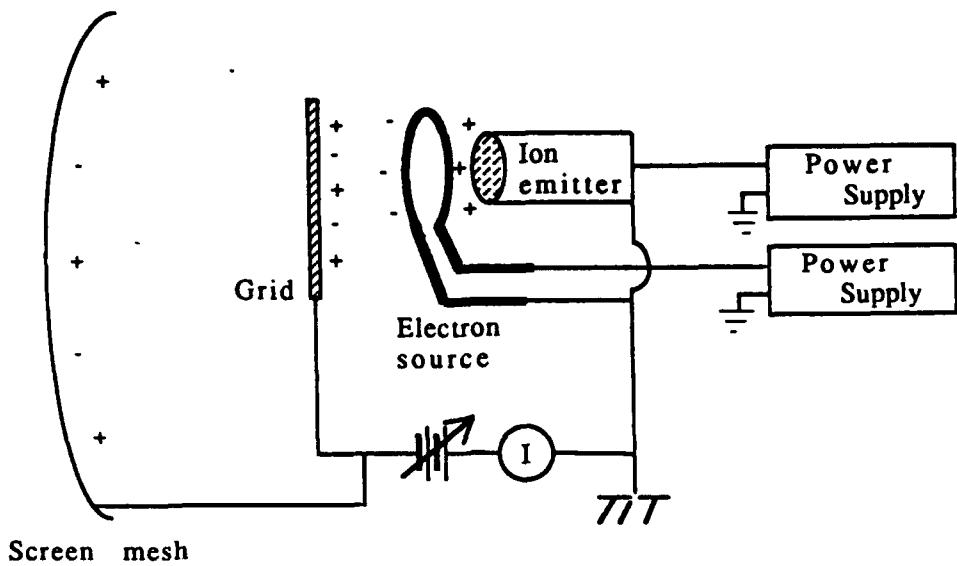
Figure 37. **Diagram of chamber interior:** for operating ion source in conjunction with tungsten dispenser cathode.

source. The grid for collecting current was mounted between the electron source and screen mesh with separation of 32 mm from the electron source. The electron source was installed between the grid and ion source with separation of 7 mm from the ion source to accelerate positive ions and to overcome space-charge limiting effects.

First, we operated only the electron source to investigate its characteristics. Figure 38 shows the induced electron current as a function of input power and surface temperature. The grid was biased with 100 V positive. The currents were surprisingly low.
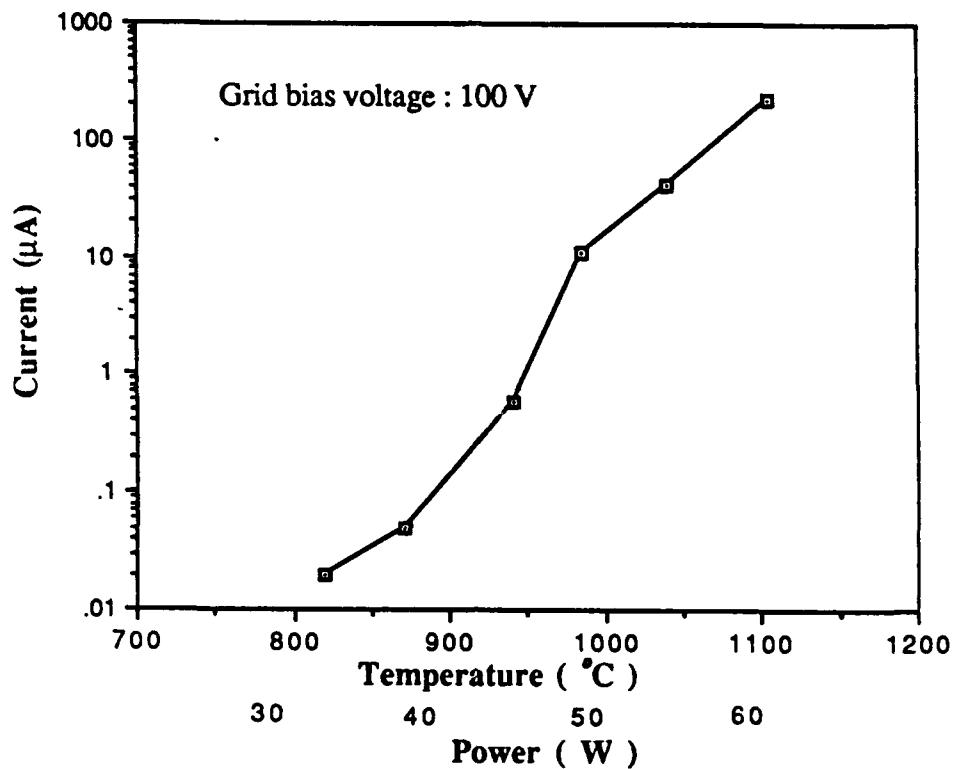
Figure 38. Electron current vs. input power and temperature: for tungsten dispenser cathode.

The electron current varied greatly with time particularly during the initial source heating. Currents were measured immediately after setting the power because they quickly decreased. The maximum current was over 200 μA at the temperature of 1080°C and power of 56.4 W, as shown in Figure 38, from early tests.

Figure 39 shows the dependence of the current on time. The power was set for the peak allowable temperature (1080°C), and the grid was biased 100 V positive. The first value of 1.2 μA was taken in the first few seconds after starting the source.
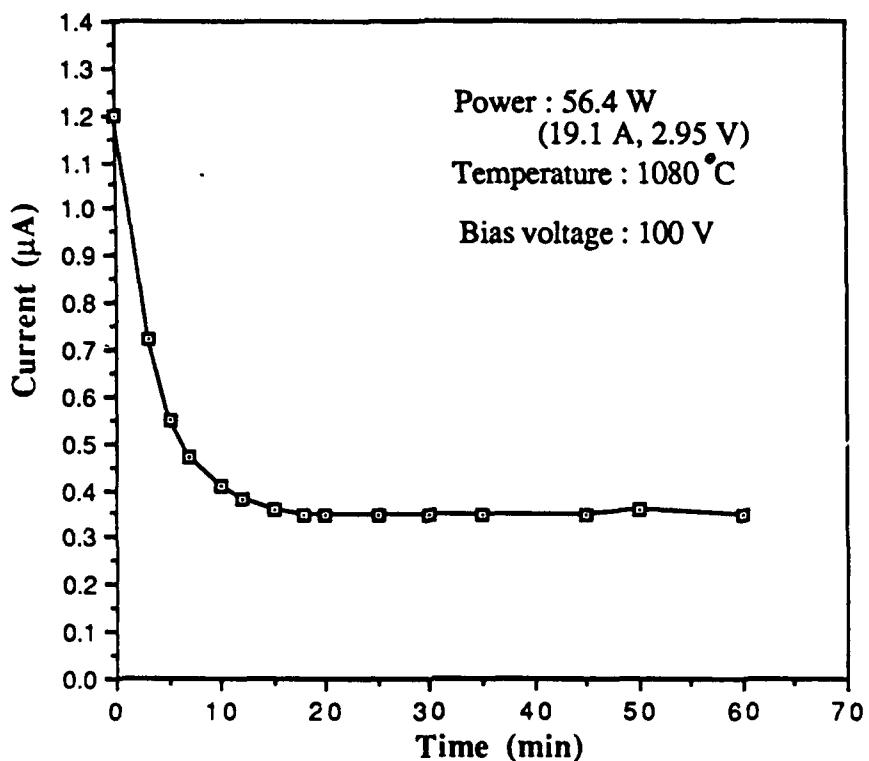
Figure 39. Electron current vs. time (saturation): for tungsten dispenser cathode.

We measured a saturation electron current of order 0.35 μA after 20 minutes. This is a very small amount of electron current. The saturation current can be considered as below the needed value for later applications.

Figure 40 shows the electron current as a function of bias voltage on the grid. Temperature of the source was 1080°C and heater power was 56.4 W. The current was not obviously space charge limited, with a slope of 0.23 for higher rarge of extraction potentials.
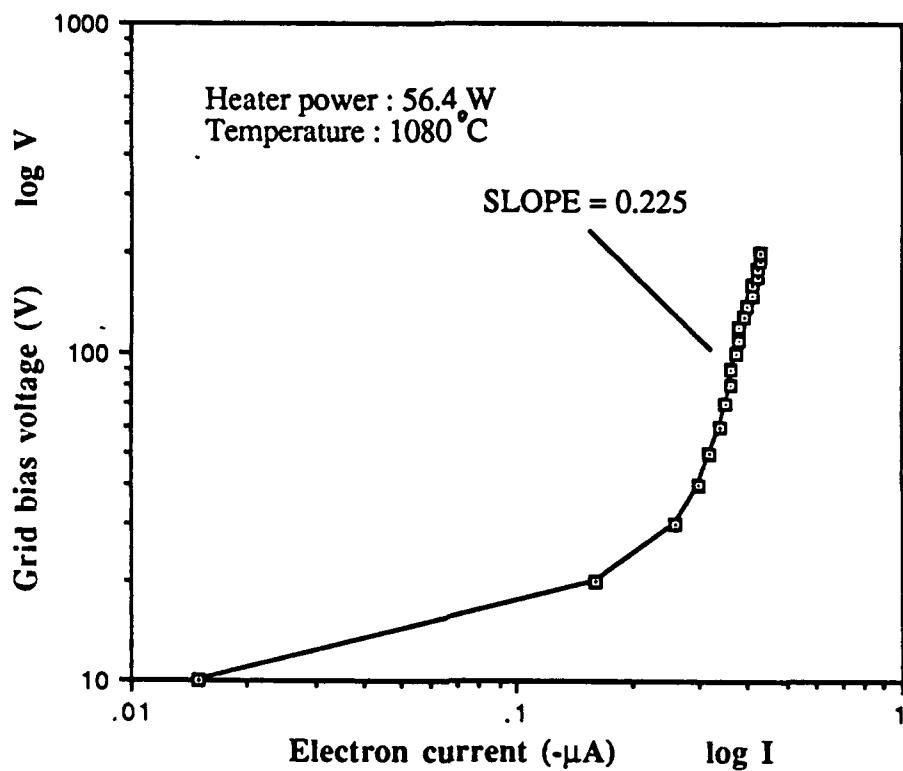
Figure 40. Emission characteristics of tungsten dispenser cathode: as a function

of bias voltages on the grid.

These results indicate that this source is not operating in the desired fashion.

The porous tungsten is not properly supplying fresh oxide to the surface. This may be

due to oxygen or other contaminates of the surface, or manufacturing irregularities.

Unfortunately, two of the three, fragile, electron sources purchased for this project were

broken during installation. There was not sufficient time to order more of these special-

ized devices. The staggering amount of power required to heat the source for operating

already makes them nearly useless for our application (space), so this design will not be

pursued further.

2. Filament Electron Source

As a result of the above problems, a new source was pursued. We prepared a filament-type electron source from an old ionization gauge. The configuration of this source is shown in Figure 41. We mounted the filament electron source to investigate its electron emission characteristics and the effect on ion emission from the 0.6 inch lithium ion source. The electron source was mounted between the ion source and grid with seperation of 5 mm and 20 mm respectively, as shown in Figure 42.
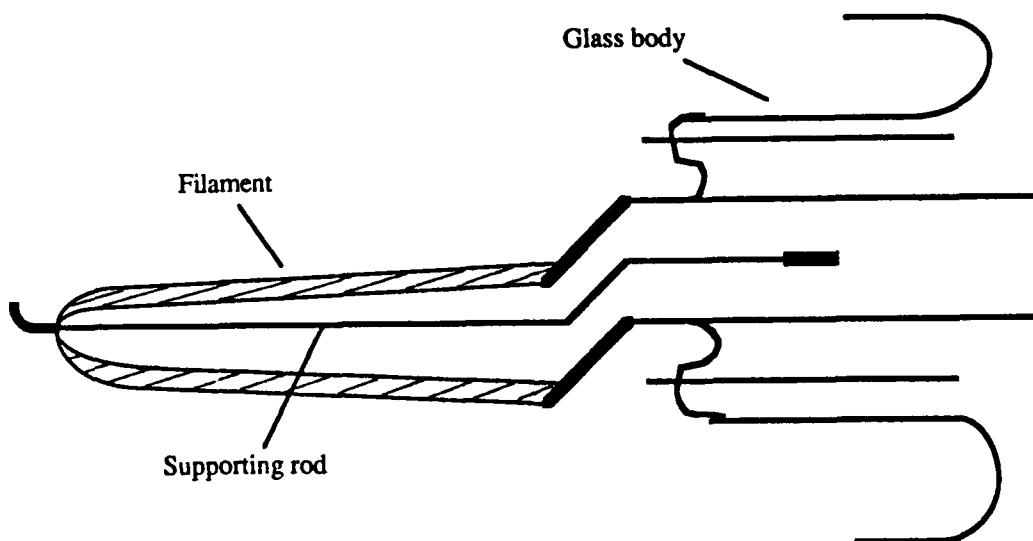
Figure 41. Filament-type electron source

Figure 43 shows that the emission characteristics of filament-type electron source as functions of input power and surface brightness temperature. Grid bias voltage was fixed at 100 V positive. Power of 10-20 W was needed to reach the temperature of range 900-1200°C. The electron current increased with power and temperature and no obvious maximum was reached in the power and temperature range we used. The
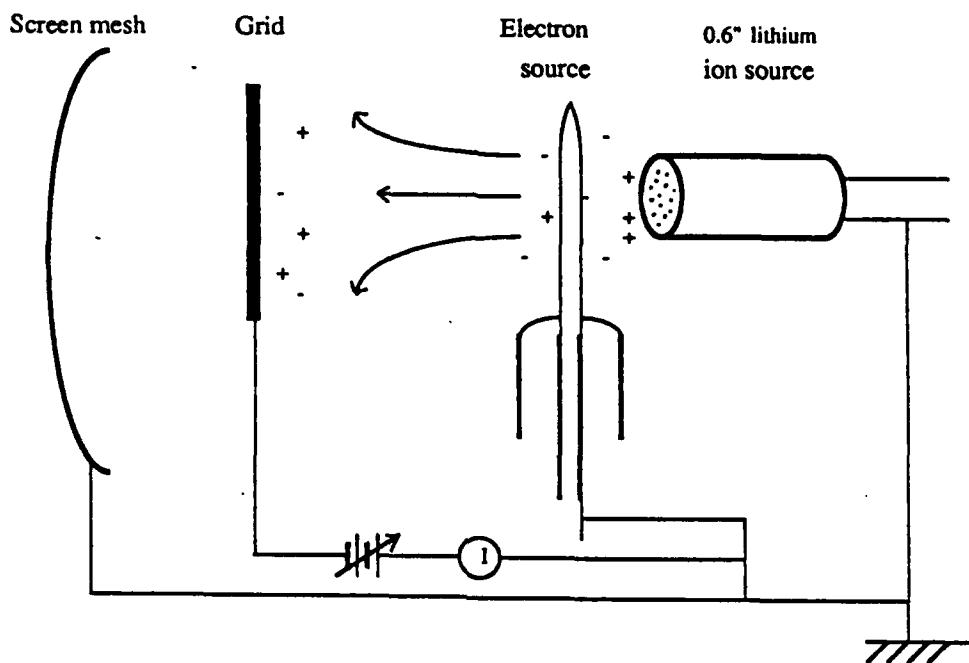
Figure 42. **Diagram of chamber interior:** for operating ion source with a filament-type electron source.

electron source performance drifted with time, presumably due to continued cleaning of the source by the ongoing operations, and other poorly determined factors.

Early on, we measured the time dependence of the electron current, with power set at 19.6 W, and a temperature of 1150°C, as shown in Figure 44. Bias voltage was fixed at +100 V on the grid. The current continuously increased with time for 25 minutes. This drift complicated measurements, as shown below, but could be compensated for.
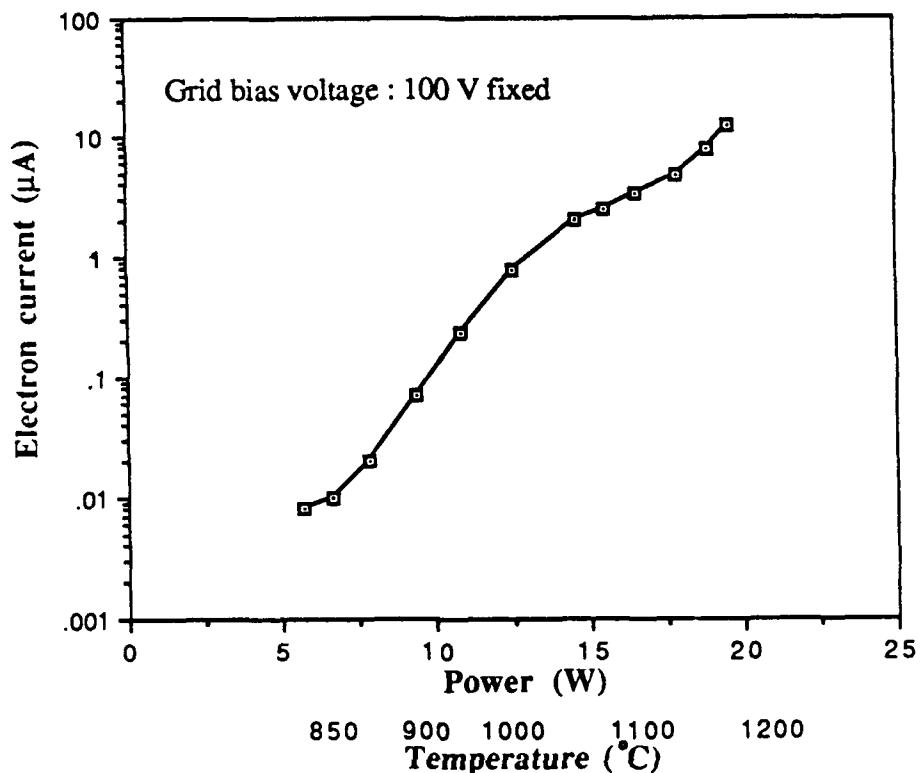
Figure 43. **Electron current vs. power and temperature:** for filament electron source.

Figure 45 shows the electron current as a function of the bias voltage on the grid. The current for high voltage region was not space charge limited with a slope of 0.19. The lower voltage region apparently did exhibit space charge limited current, with a slope of 1.10.
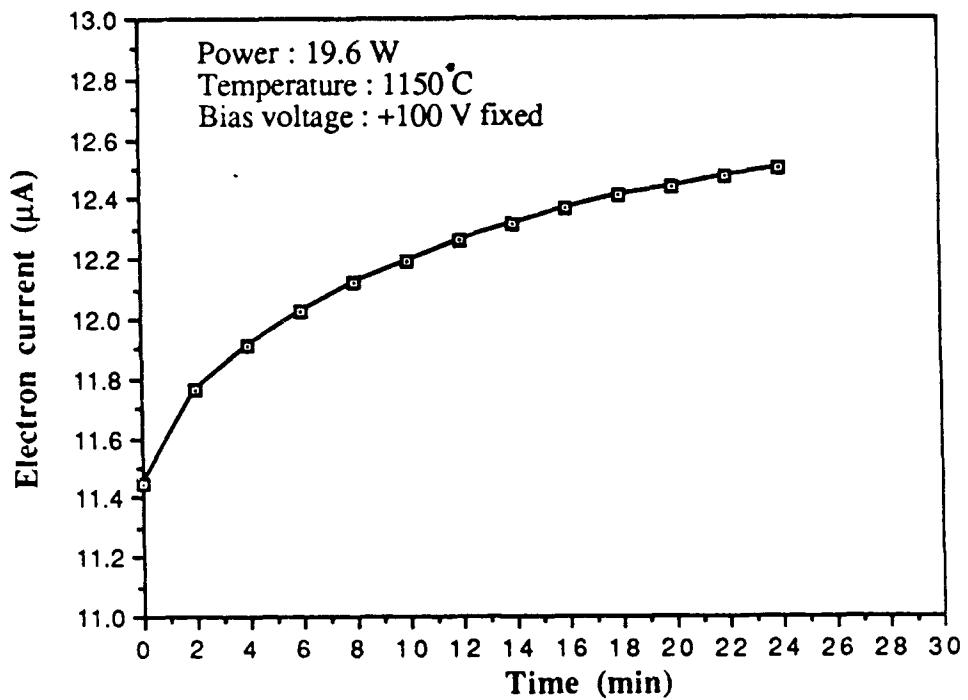
Figure 44. Current vs. time for filament electron source

C. COMBINED ELECTRON AND ION SOURCE BEHAVIOR

1. Operation of 0.25 Inch Ion Source with Tungsten Dispenser Cathode

In spite of the low electron current provided by the dispenser cathode, exper-
iments were run with it and the 0.25″ ion source to see if space-charge effects could be
reduced.

The chamber interior was shown in Figure 37. The electron source was
mounted between the grid and ion source. The distances between them were varied to
try and optimize the coupling (neutralization of space charge). During the last set of
experiments, the separation between the grid and electron source was 18 mm. The
electron source was separated 3 mm from the ion source.
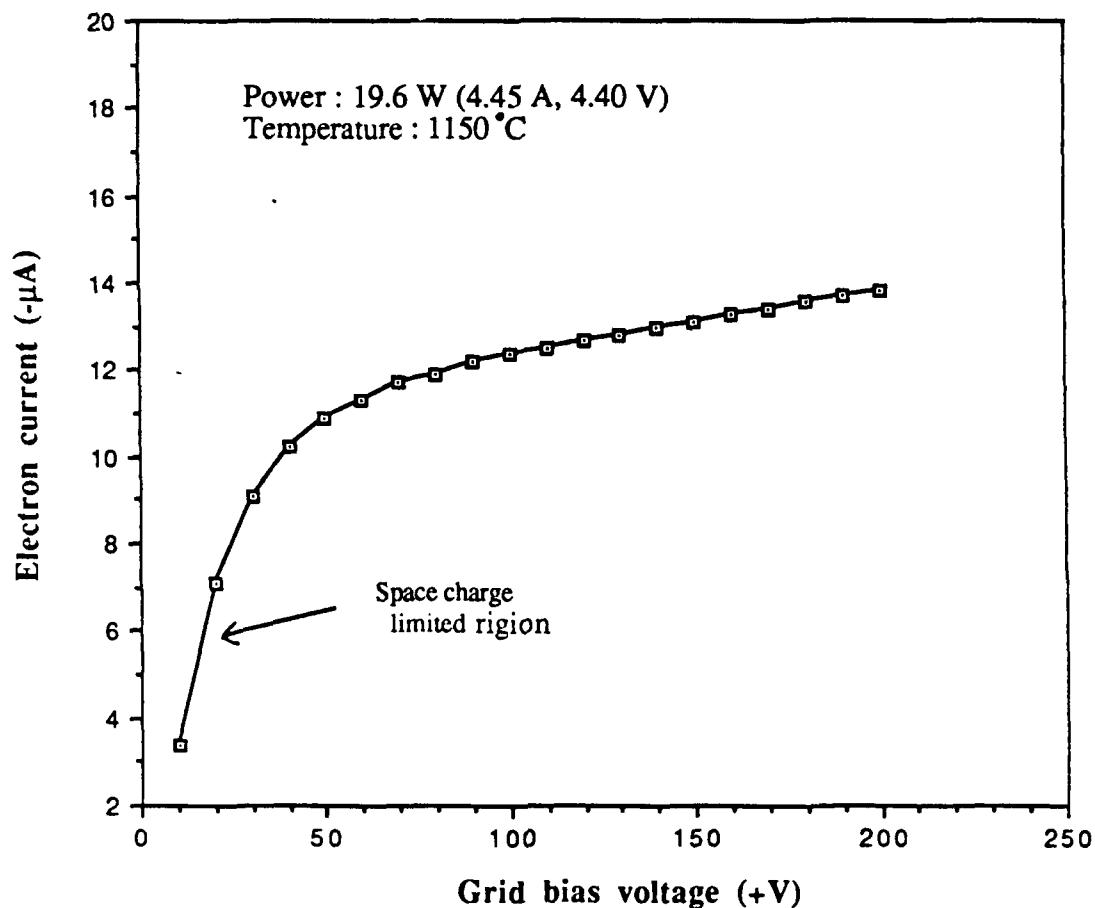
Figure 45. Emission characteristics of filament-type electron source: as a function of bias voltage on the grid.

The two sources were connected to different power supplies, and we could heat the sources independently. We first measured the ion and electron currents separately. We then measured the positive ion current with the electron source on. Figure 46 shows the behavior of induced ion current as a function of bias voltages on the grid which were varied from -10 V to -200 V. Input powers of the heater for the ion and electron sources

were 23 W (2.55 A, 9.10 V) and 61 W (19.10 A, 3.20 V) respectively. The temperatures of ion and electron sources were 1150°C and 1120°C.

The ion current was slightly increased by operation of the tungsten dispenser cathode. The space charge limited region of ion current was not largely improved by this type of electron source. The average increase in current was approximately 50 %. We could get a maximum ion current of 5.6 μA with the aid of the tungsten dispenser cathode.

Figure 47 shows the behavior of the electron current when the ion source was operated. We measured the electron current with the ion source on, and then shut off the power to the ion source. The electron current decreased slowly with time.

We concluded that ion current could be increased by operation of a tungsten dispenser cathode, but the effect was not large.

2. Operation of 0.6 Inch Ion Source with Filament Electron Source

We investigated the emission characteristics of the filament-type electron source. The electron current showed this type source could largely be effected on the ion current. Figure 42 showed that the chamber interior to operate the 0.6″ ion source in conjunction with the filament electron source. We first measured the ion and electron currents separately. Then, we tried to observe the relation and effects. The electron current and neutralized ion current were time varying. To reduce these effects the sources were switched on, and allowed to operate at 1100°C for ~4 hours before running tests. Special attention was to given the region of space charge limited current collection, using low extraction potentials.
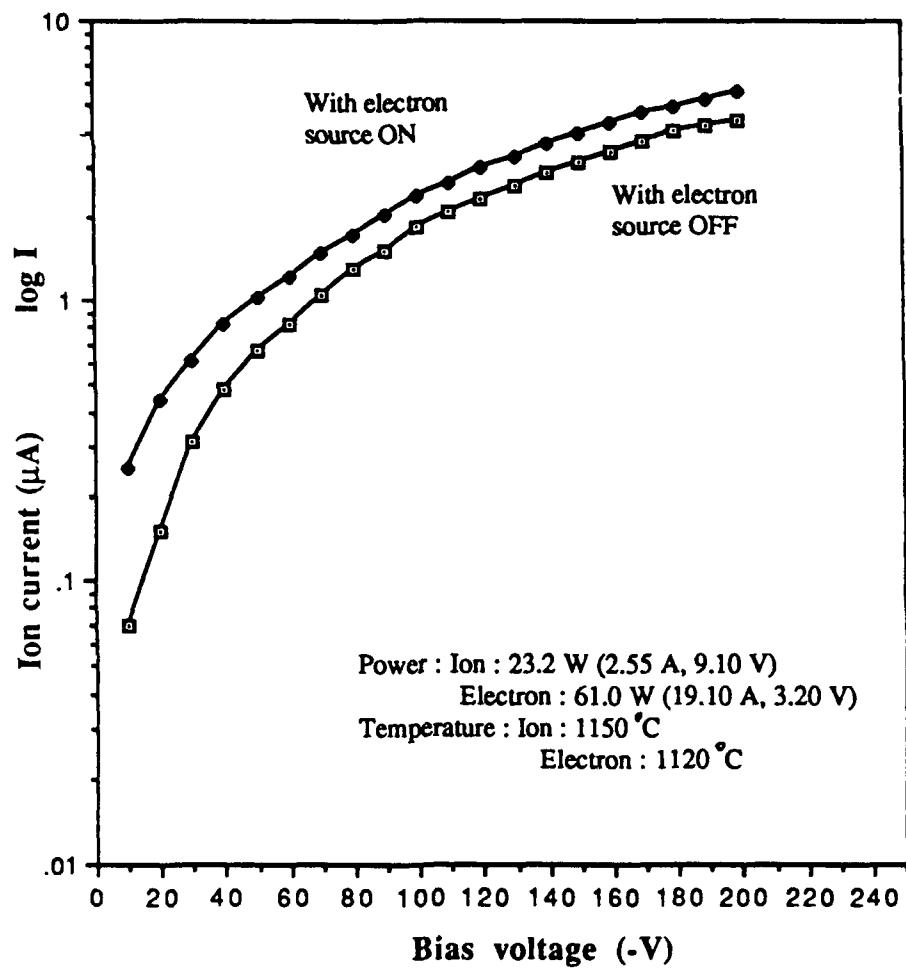
Figure 46. Ion current with tungsten dispenser cathode: as a function of bias voltage on the grid.
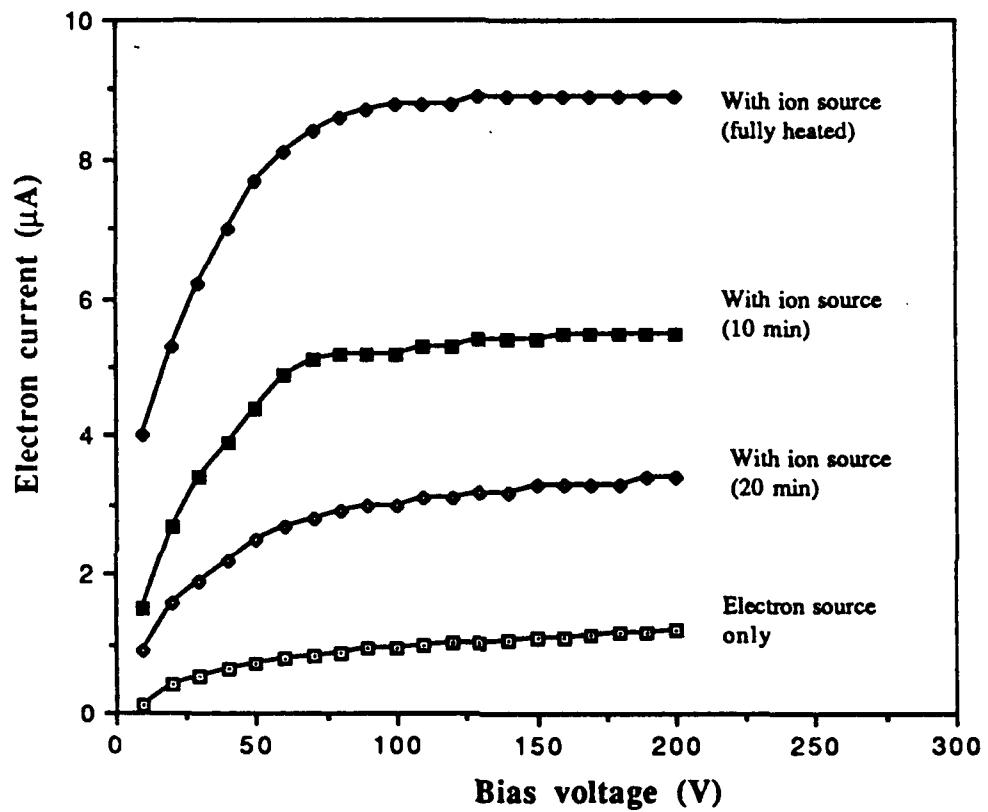
Figure 47. Electron current affected by ion source with time: as a function of positive bias voltage on the grid.
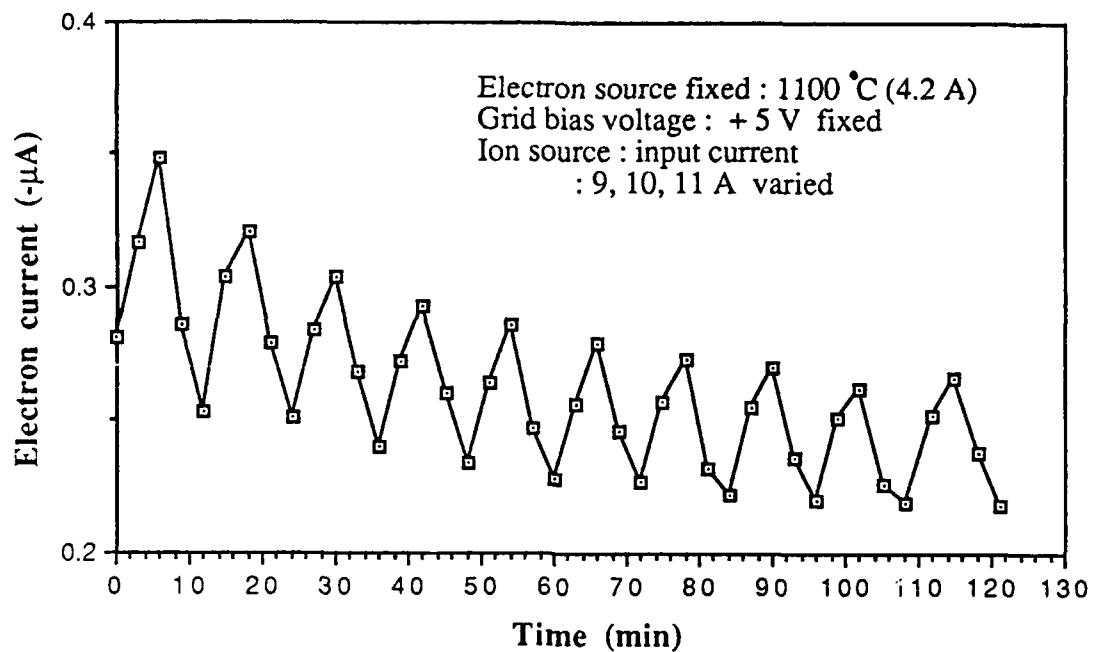
Figure 48. Behavior of cyclic electron currents: with varying ion emission and
time.

Figure 48 shows the behavior of electron currents while varying the electron

source (temperature). The grid bias voltage was fixed at 5 V positive for these tests.

The electron source was fixed at the temperature of 1100°C (4.2 A, 4.6 V). We applied

the input power for the ion source cyclically (9 A, 10 A, 11 A, 10 A, 9 A). These input

currents corresponded to temperatures of the ion emitter of about 950, 1000, and

1100°C respectively. The electron current was effected by the ion source. We measured

large currents for high temperature of the ion source, and small currents for low. The

current decreased slowly during the 2 hour period required for these measurements.

77
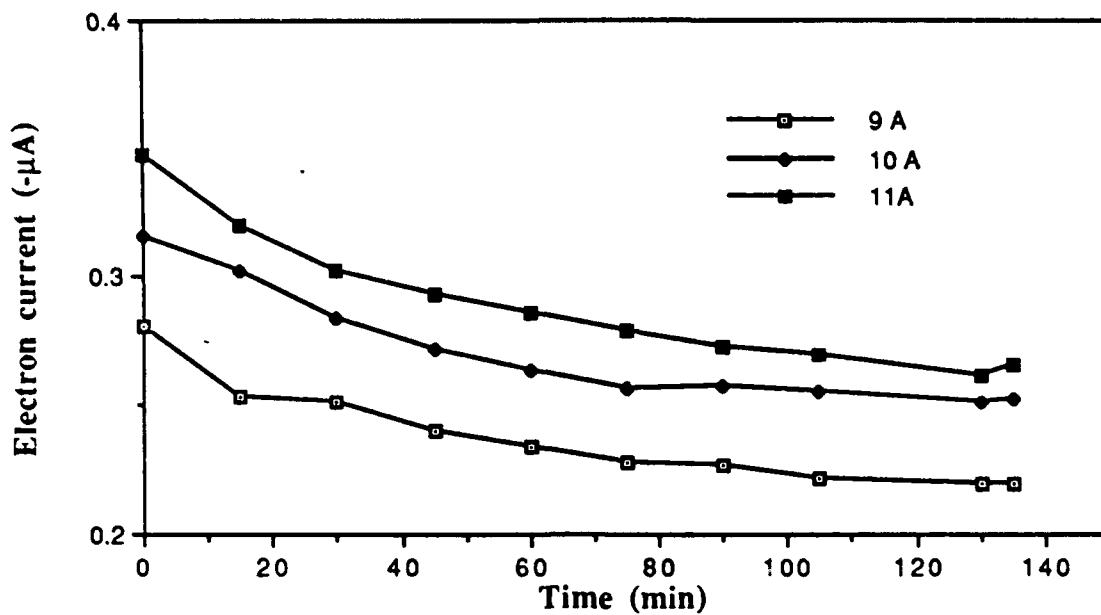
Figure 49. Electron current with varying ion emission and time

Figure 49 shows the electron currents for 3 cases. The electron current was space charge limited at low bias voltages ($\lesssim 50V$). The space-charge limited electron current was improved by ion emission at the bias voltage of +5 V.

We measured the ion currents with varying electron emission currents, as shown in Figure 50. The 0.6" lithium ion source was fixed at the temperature of 1110°C (11.0 A, 8.45 V). The input power for heating the electron source was cyclically varied with 3.0, 3.7, and 4.2 A. These input currents corresponded to filament temperatures of 900, 1000, 1150°C respectively. The grid bias voltages were fixed at -5 V and -10 V.

Figure 50 shows that the ion current increased with the aid of the filament electron emission. We measured a large current (0.6~1.0 μA) for high potential (-10 V),
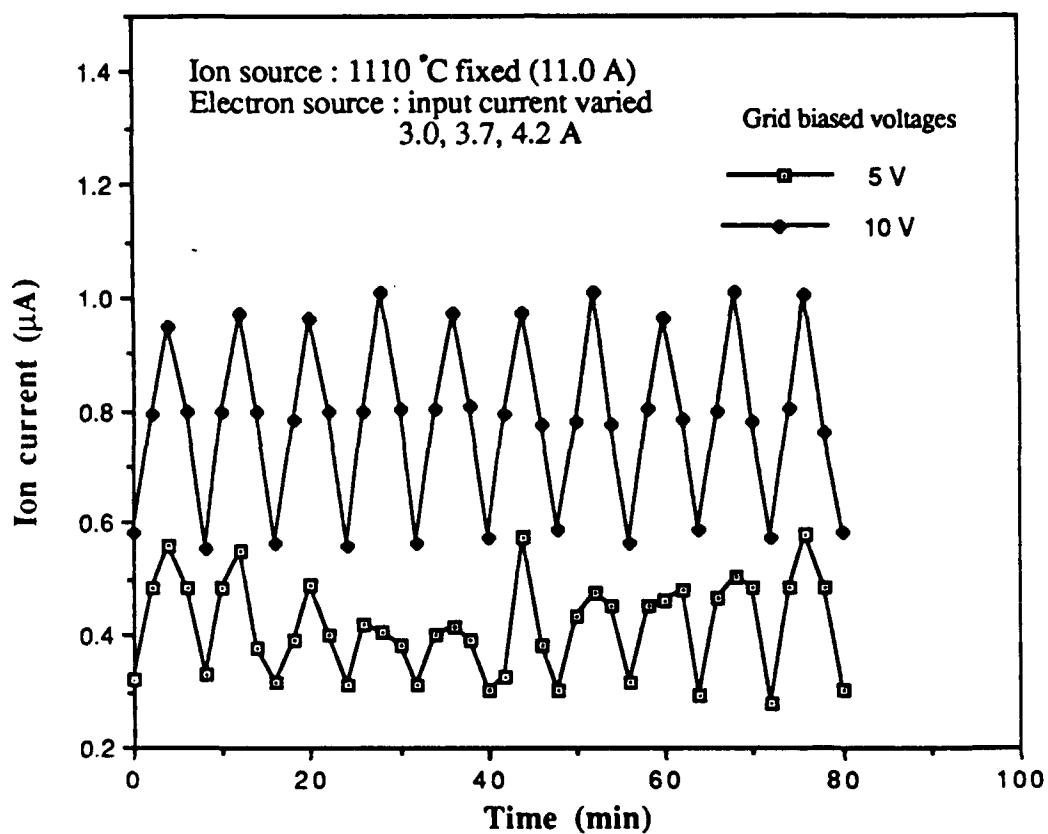
Figure 50.   Ion current with varying electron emission and time

and small (0.3~0.6 μA) for low potential (-5 V). The currents at -10 V bias were much

easier to measure, and less erratic.

Figure 51 shows that the ion current from 0.6" ion source with and without the

filament electron source heating as a function of bias voltages on the grid. The input

powers for the ion and electron sources were 94.6 W (11.00 A, 8.60 V) and 17.0 W (3.90

A, 4.35 V) respectively. The temperature of both sources was 1100°C. The currents
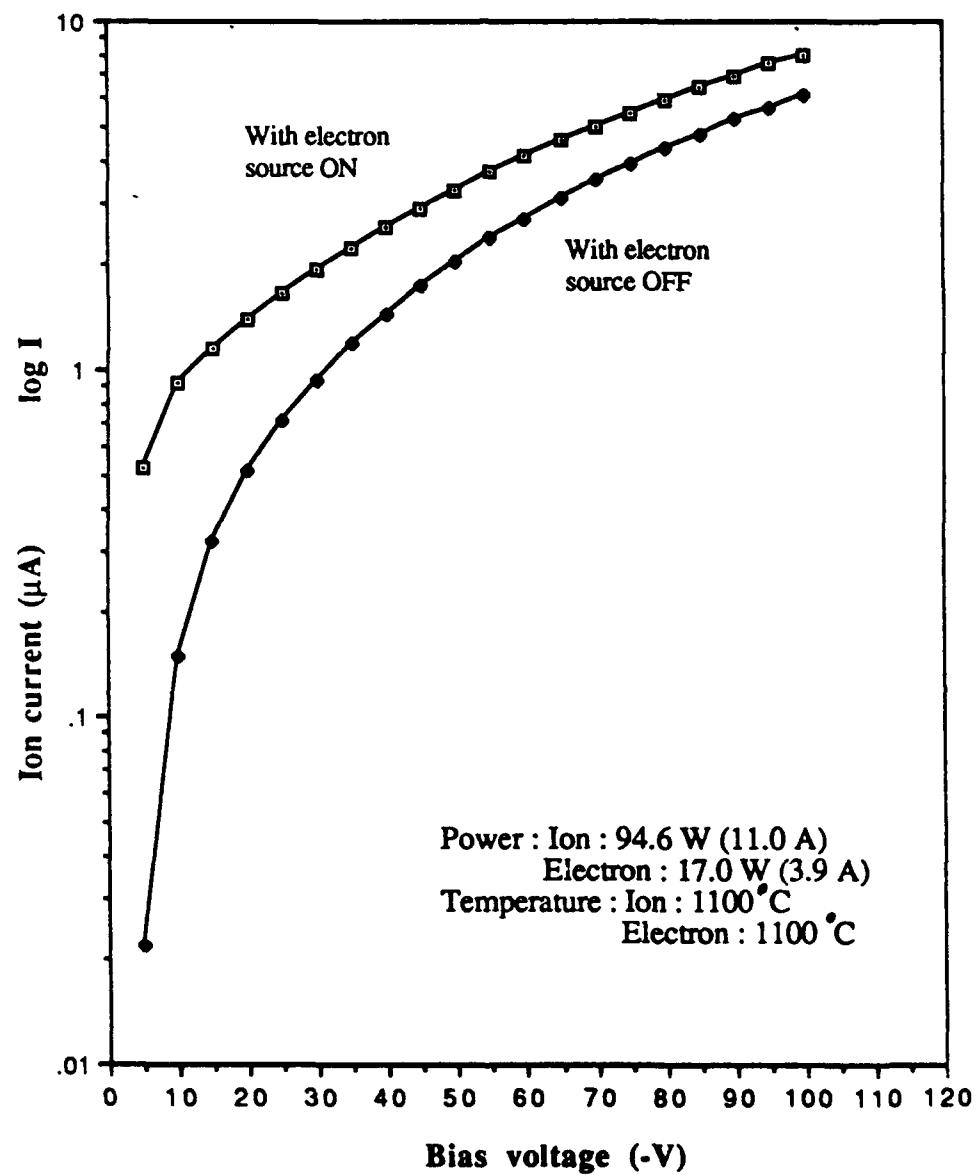
Figure 51. Ion current in conjunction with filament electron source: as a function of bias voltage on the grid.

greatly increased for the lower potential region ($\lesssim 50V$). The average increase in current for this region was about 4 times of original value (376 %). For higher extraction potential region, the ion current not greatly affected (40 % for 50~100 V, 20 % for 100~200 V). We measured the maximum induced current of 19 μA with the aid of the filament electron source at the bias voltage of -200 V and temperature of 1100°C.

We measured the ion current with the filament electron source heating for the region of low extraction potentials of 0~20 V, as shown in Figure 52. The ion current was approximately space charge limited at the lower voltages. A large level of ion current was induced by the neutralization with electrons from the filament-type electron source. The average increase in current for this region was 523 %. A typical increase was 400 % at 10 V.

We concluded that the ion current from the 0.6" lithium ion source was increased by operation of the filament-type electron source. The electron source overcame the space-charge limiting effect in the vacuum chamber for this experiments.
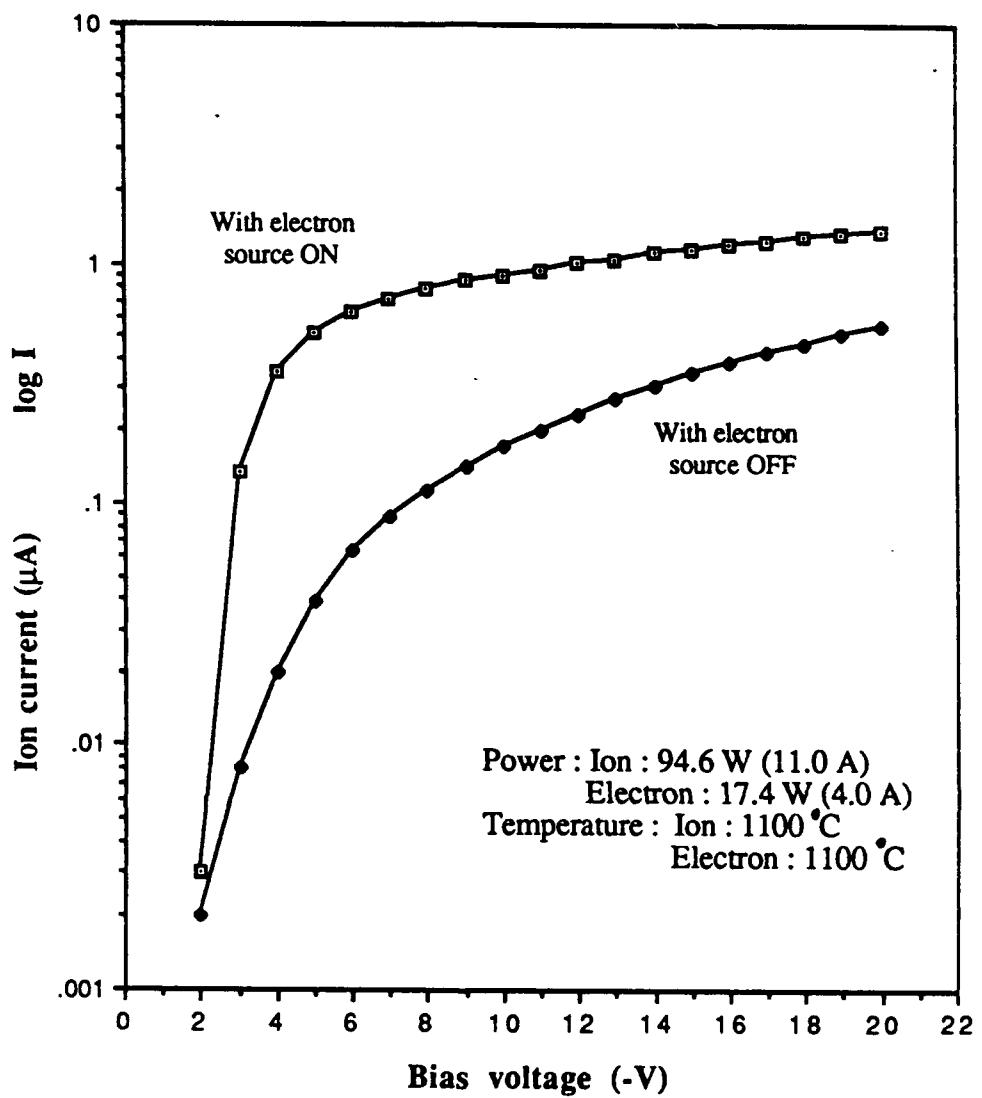
Figure 52. **Ion current for the space charge limited region:** in conjunction with the filament electron source as a function of bias voltage on the grid.

VI. SUMMARY AND DISCUSSION

The objective of this experiments was to verify that the lithium ion source can be used for spacecraft charge control. We simulated a positively charged spacecraft and differential charging with a 0.6 inch lithium ion source. The emission currents of 0.6 inch ion source were measured under various condition with various geometries. The tungsten dispenser cathode and filament electron source were operated with the ion source to overcome space-charge limiting effects. The properties of the ion currents in conjunction with these electron sources were investigated.

A. SUMMARY OF RESULTS

1. Simulation of Charged Spacecraft

The copper mesh simulates the sheath of plasma in space, and the metal strips around the source simulate the spacecraft surface. All strips were electrically connected as a surface of a positively charged spacecraft to be biased with equal potential. Induced currents from the source to the screen and strips were measured as functions of input power, temperature, and various conditions of bias voltage. The induced strip current was about 33 μA at a power of 94 W (1100°C) and strip bias voltage of -100 V. The screen bias voltage was -200 V.

We simulated differential charging with the same source and geometry. The front and two rear strips were electrically disconnected and differentially charged with various potentials. The maximum current measured to the rear strip was 21 μA for the bias voltage of -250 V. We obtained induced currents of 25 μA and 15 μA to the front

83

and rear strip respectively, when the screen and both strips were equally biased with -100 V. The currents induced to the front and rear strips were strongly related with their magnitude of bias voltages.

2. Combined Ion and Electron Source Behavior

a. *0.25 inch ion source and tungsten dispenser cathode*

The electron source was mounted between the current collecting grid and ion source to accelerate the positive ions (neutralization of space charge). We first investigated the emission characteristics of the tungsten dispenser cathode. We measured saturation electron currents of order 0.35 μA from the tungsten dispenser cathode. The electron current, as a function of bias voltage on the grid, was not obviously space charge limited with a slope of 0.23.

The tungsten dispenser cathode was coupled with 0.25 inch lithium ion source for neutralizating the ions between the grid and emitting surface of the ion source. The average increase in ion current was approximately 50 %, but the space charge limited current was effectively not overcome by this electron source. The input power was 61 W (19.10 A, 3.20 V) and the temperature of the electron source was 1120°C.

b. *0.6 inch ion source and filament electron source*

The filament-type electron source from an old ionization gauge was investigated with the 0.6 inch lithium ion source. Low powers of 10~20 W were needed to reach the temperature of range 900~1200 °C. The lower voltage region ($\lesssim$50 V) did exhibit space charge limited current, approximately, with a slope of 1.10. The electron

current was increased by ion emission at the bias voltage of +5 V which was in its space charge limited potential region.

The ion currents from the 0.6 inch ion source were greatly increased by the operation of the filament electron source. The average increase in current for the region (0~20 V) of space charge limited potentials was 523 % (376 % for 0~50 V). We measured a maximum current of 19 μA at the bias voltage of -200 V. The filament electron source showed a large effect on the ion currents in the space charge limited regime.

B. DISCUSSION OF RESULTS

The simulation of positively charged spacecraft and differential charging were successfully conducted with the 0.6 inch lithium ion source in a simple geometry. We obtained sufficient ion currents to modify the floating potential of a spacecraft in geosynchronous orbit. The ion current was sufficient to reduce the charge on differentially charged surfaces of geosynchronous satellites. The characteristics of current vs. voltage showed that the ion source satisfied the Child-Langmuir law only at low currents.

A tungsten dispenser cathode was designed for this project. This electron source did not show appropriate emission properties. The effects on the ion production of the 0.25 inch lithium source were contrary to our hopes. The electron source needed a large input power (of order 60 W) for a surface brightness temperature of 1100°C.

We obtained better results from a filament electron source. This electron source needed less power (15~20 W). Operation of the filament source with the 0.6" lithium source did show favorable effects on ion emission. Even with the electron source on,

85

however, relatively low currents were produced at 10-20 V extraction potentials, e.g., currents of order 1 μA.

VII. CONCLUSIONS

A simulation using the lithium ion source and investigation of the currents from the ion sources in conjunction with the electron sources were successfully conducted in a small bell jar vacuum system.

The tungsten dispenser cathode required too much power to be used in space and did not produce sufficient currents. It was too fragile and may have been contaminated during the experiment. The tungsten dispenser cathode was not a good design for this purpose.

The filament electron source demonstrated neutralization of spacecraft charging in conjunction with the 0.6" lithium ion source. However, the current was still not high enough to control spacecraft charging with the low extraction voltage required in space. This means that naturally occuring space electric fields will not be sufficient to extract currents at the 10 μA level. Some sort of lens structure will be needed to produce a low energy ion beams, which can then be used for charge control on satellites. Flight experiments are recommended in the future to test this technology.

APPENDIX   SPACE SHUTTLE TILE CHARACTERISTICS

When NASA's space shuttle orbiters re-enter earth's atmosphere from space, they will encounter temperatures as high as 2300°F. To protect the orbiters and their passengers from such temperatures, Lockheed Missiles & Space Company has developed a high-purity silica fiber insulation that sheds heat quickly.

They manufactured in two forms; LI-900 (9 lbs per cubic foot) and LI-2200 (22 lbs per cubic foot). The basic raw material for LI-900 and LI-2200 is a short-staple, 99.7% pure amorphous silica fiber that is derived from common sand. A slurry containing fibers mixed with water is frame cast to form soft, porous blocks to which a colloidal silica binder solution is added. When dried and sintered, a rigid block of LI-900 is produced. Coatings of silica frit are baked on in 15 mm thickness. Tiles for high temperature (up to 2300°F) use a black Class 2 reaction-cured boro-silicate glass coating (RCG). For lower temperature use at 750-1200°F on upper surface, a white Class 1 silica compound is used with shining alumina oxide. The data sheet for LI-900, which used in our experiment, is attached at following pages. [Ref. 34]

Lockheed Missiles & Space Co., Inc. developed LI-900 as a unique new rigid insulation material for the Space Shuttle Thermal Protection System. When protected by a black reaction cured glass (RCG) coating, LI-900 tiles attached to the underside of the space shuttle can withstand the searing heat of 100 reentry cycles without damage. The coating reradiates approximately 90 percent of the heat generated during each reentry back into deep space or the upper atmosphere. The tile insulation material absorbs the remaining energy, preventing the aluminum surface of the orbiter from exceeding 350°F.

Summarized below are the principal properties of LI-900; the values cited were obtained in connection with the Shuttle Program.

- **Low Conductivity.** LI-900 conductivity at 500°F is only 0.52 $BTU\text{-}in./ft^2$ $\text{-}hr\text{-}°F$, compared to a value of 0.30 $BTU\text{-}in./ft^2\text{-}hr\text{-}°F$ for still air.

- **Low Density.** LI-900 has a density of only 9 lb per cubic foot.

- **Purity.** LI-900 is 99.7 percent pure SiO_2. It has no organic constituents that will outgas to contaminate parts or equipment.

- **Long Life In Cyclic Applications to 2300°F.** LI-900 does not degrade with cyclic exposure to 2300°F. It can withstand limited exposure to 2650°F.

- **Rigidity.** LI-900 can maintain shape and support light mechanical loads while providing thermal insulation.

- **Consistency of Product.** Processed to exacting specifications, all LI-900 material meets minimum strength and conductivity requirements.

- **Dimensional Stability to 2300°F.** LI-900 has an extremely low coefficient of thermal expansion (3.2×10^{-7} in./in./°F from 0 to 2000°F).

- **Unusual Thermal Shock Resistance.** Because of its low coefficient of thermal expansion, LI-900 heated to 2300°F can be immediately immersed in cold water without damage.

- **Inert.** LI-900 does not react with most fluids and substances.

- **Nonflammable.** LI-900 does not burn; the material softens above 2500°F and melts at about 3100°F.

- **Low Dielectric Constant.** The relative (to vacuum) dielectric constant for LI-900 is less than 1.15 over the temperature range to 2100°F.

- **High Diffusivity.** LI-900 contains over 90 percent voids by volume and offers minimal resistance to the passage of gases during pressure equalization.

LI-900 is a cast material with anisotropic properties. The higher mechanical properties are in the in-plane direction, whereas the high "insulation" (or lower thermal conductivity) properties are in the through-the-thickness direction.

RF characteristics and mechanical properties at room temperature and thermophysical properties over a range of temperatures are shown in Tables 1 through 3. Mechanical properties remain relatively constant up to 1600°F, where a gradual reduction in strength begins. Mechanical properties at cryogenic temperatures are generally somewhat higher than room temperature properties. The room temperature standard deviation for tensile strength, based on approximately 2,000 tests, is 5 psi in the through-the-thickness direction and 10 psi in the in-plane direction.

Table 1 REPRESENTATIVE RF CHARACTERISTICS AT 10 GHz (ROOM TEMPERATURE)

	DIELECTRIC CONSTANT	LOSS TANGENT
LI-900 RCG Coating	1.13 4.80	0.0004 0.0030

Table 2 TYPICAL LI-900 MECHANICAL PROPERTIES AT ROOM TEMPERATURE

DIRECTION	PROPERTY	VALUE (psi)
In-Plane	Tensile Strength	68
	Tensile Modulus of Elasticity	25000
	Compressive Strength	70
Through-The-Thickness	Tensile Strength	24
	Tensile Modulus of Elasticity	7000
	Compressive Strength	28

Table 3 TYPICAL LI-900 THERMOPHYSICAL PROPERTIES

MEAN TEMPERATURE (°F)	THROUGH-THE-THICKNESS THERMAL CONDUCTIVITY (BTU-in./ft²-hr-°F) PRESSURE (ATM)					SPECIFIC HEAT (BTU/LB-°F)	THERMAL EXPANSION ($\Delta L/L_0$)
	10^{-4}	10^{-3}	10^{-2}	10^{-1}	1		
-250	0.06	0.08	0.16	0.26	0.28	0.070	-0.6×10^{-4}
-150	0.07	0.10	0.20	0.28	0.30	0.106	-0.5×10^{-4}
0	0.09	0.12	0.22	0.30	0.33	0.150	-0.1×10^{-4}
250	0.11	0.15	0.27	0.38	0.41	0.210	$+0.4 \times 10^{-4}$
500	0.15	0.20	0.33	0.48	0.52	0.252	1.4×10^{-4}
750	0.21	0.26	0.39	0.59	0.64	0.275	2.2×10^{-4}
1000	0.28	0.33	0.47	0.72	0.79	0.288	3.4×10^{-4}
1250	0.37	0.42	0.59	0.87	0.94	0.296	4.4×10^{-4}
1500	0.50	0.55	0.74	1.05	1.13	0.300	5.0×10^{-4}
1700	0.64	0.70	0.88	1.22	1.31	0.302	5.6×10^{-4}
2000	0.88	0.94	1.13	1.52	1.63	0.303	6.2×10^{-4}
2300	1.16	1.23	1.39	1.86	2.00	0.303	–

NOTE: TOLERANCES ARE:
1. THERMAL CONDUCTIVITY ±15% OR ±0.04, WHICHEVER IS GREATER
2. SPECIFIC HEAT ±10% OR ±0.02, WHICHEVER IS GREATER
3. THERMAL EXPANSION ±12% OR ±0.3×10⁻⁴ WHICHEVER IS GREATER

For the Space Shuttle , LI-900 is provided with hard borosilicate glass coatings on the outer surface. These coatings increase material durability and resist rain impingement, fluid contamination, sand and dust impingement, fungus and ozone exposure, salt spray exposure, and handling damage. The coatings also control optical properties such as emittance and solar absorptance. Typical optical, thermophysical, and mechanical properties for the coatings currently in use on the shuttle orbiter tiles are given in Tables 4 through 6. Class 1 (white) coating is used on the upper surfaces of the orbiter, while RCG (black) coating is used on the bottom surfaces.

Table 4 TYPICAL COATING OPTICAL PROPERTIES

COATING	PROPERTY	VALUE	TEMPERATURE RANGE (°F)
Class 1 (to 1200°F)	ϵ_{TH}	0.82	-170 to 75
		0.74	750
		0.70	1000
		0.66	1200
	α_S/ϵ_{TH}	0.35	-170 to 135
RCG (to 2300°F)	ϵ_{TH}	0.8	-170 to 2300
	α_S/ϵ_{TH}	0.9 to 1.1	-170 to 250

NOTES: ϵ_{TH} = Total hemispherical emittance

α_S = Solar absorptance

RCG = Reaction Cured Glass

LI-900 can be easily cut with a band saw or machined. Machining must be performed with diamond-tipped tools because the hardness of the fibers in the material quickly dulls conventional tool cutters.

Table 5 TYPICAL RCG COATING THERMOPHYSICAL PROPERTIES

PROPERTY	VALUE	TEMPERATURE RANGE (°F)
Coefficient of Thermal Expansion (10^{-6} in./in.°F)	0.57	70 to 1500
	0.56	70 to -100
	0.46	70 to -200
	0.41	70 to -250
Thickness (in.)	0.014	

Table 6 TYPICAL COATING MECHANICAL PROPERTIES AT ROOM TEMPERATURE

PROPERTY	VALUE (psi)
Tensile Strength	4000
Tensile Modulus of Elasticity	4,000,000
Compressive Strength	10000

LIST OF REFERENCES

1. Deforest, S. E., *Spacecraft Charging at Synchronous Orbit* , Journal of Geophysical Research, vol. 77, p. 651, 1972.

2. R. C. Olsen, and C. K. Purvis, *Observations of Charging Dynamics* , Jounal of Geophysical Research, vol. 88, No. 47, p. 5657-5667, 1983.

3. R. C. Olsen, *Record Charging Events from Applied Technology Satellite* , Journal of Spacecraft and Rockets, vol. 24, No. 4, p. 362, 1987.

4. Fredricks, R. W., and Scarf, F. L., *Observation of Spacecraft Charging Effects in Energetic Plasma Regions (photon and particle interactions with surfaces in space)* , ed. R.J.L. Grard, D. Reidel Publishing Co., 1972.

5. Grard, R., K. Knott, and A. Pederson, *Spacecraft Charging Effects* , Space Science Reviews, vol. 34, p. 289, 1983.

6. Henry B. Garrett, and Charles P. Pike, *Space Systems and Their Interactions with Earth's Space Environment ; Spacecraft Charging: A Review(H. B. Garrett)* , vol. 71, p. 167-226, Progress in Astronautics and Aeronautics, New York, 1980.

7. ASPOC Scientific/Technical Plan., *Positive for an Active Spacecraft Potential Control Experiment (ASPOC)-ion emitter- for the Stop Cluster Mission* , IWF Oesterreichische Akademie der Wissenschaften, Inffeldgasse 12, A-8010 Graz. Austria, 1988.

8. W. D. Deininger, G. Aston, and L. C. Pless, *Hollow Cathode Plasma Source for Active Spacecraft Charge Control* , Review of Scientific Instruments, 58(6), p. 1053, 1987.

9. Otto Heinz, and R. T. Reaves, *Lithium Ion Emitter for Low Energy Beam Experiments* , The Review of Scientific Instruments, vol. 39, p. 1229, 1968.

10. R. T. Reaves, and S. M. Jarrett, *Directly Heated Tungsten Dispenser Cathodes for Ion Laser Application* , Laser Journal, A.Z. Publishing Co., 1969.

11. James D. Combine, *Gaseous Conductors (Theory and Engineering Applications)* , Dover Publishing Inc., New York, p. 123-128, 1958.

12. C. R. Chappell, *The Convergence of Fact and Theory on Magnetospheric Convection* , D. Reidel Pubshing Co., 1974.

13. M. S. Gussenhoven, E. G. Mullen, and D. A. Hardy, *Artificial Charging of Spacecraft due to Electron Beam Emission* , IEEE Distributions, Air Force Geophysics Lab., MA, 1987.

14. E. L. Chaffee, *Theory of Thermionic Vacuum Tubes* , McGraw-Hill Book Co., Inc., p. 66-71, New York, 1933.

15. I. Langmuir, *The Interaction of Electron and Positive Ion Space Charge in Cathode Sheaths* , Physics Review, vol. 33, p. 954-990, 1929.

16. F. M. Johnson, *Studies of The Ion Emitter Beta-Eucryptite* , RCA Review, p. 427-437, 1962.

17. R. C. Olsen, *Experiments in Charge Control at Geosynchronous Orbit, ATS-5 and ATS-6* , Journal of Spacecraft and Rockets, vol. 22, p. 254-264, 1985.

18. R. C. Olsen, *Modification of Spacecraft Potentials by Plasma Emission* , Journal of Spacecraft and Rockets, vol. 18, p. 462-469, 1981.

19. R. C. Olsen, and E. C. Whipple, *Operations of the ATS-6 Ion Engine* , USAF/NASA Spacecraft Technology Conference, USAF Academy, Colorado, 31 Oct. - 2 Nov., 1978.

20. J. P. Blewett, and E. J. Jones, *Filament Sources of Positive Ions* , Physical Review, vol. 50, p. 464, 1936.

21. Technical Bulletin #118, *Ion Sources* , Spectra-Mat, Inc., CA, 1980.

22. D. C. Lorents, G. Black and O. Heinz, *Charge Transfer Between Li Ions and Li Atoms in the 14-1000 eV Energy Region* , Physical Review, vol. 137, No. 4A, p. 1045-1053, 1965.

23. M. Remy and R. Haug, *A Lithium Ion Source Using the Surface Ionization Process* , Review of Scientific Instruments, vol. 41, No. 5, p. 650-652, 1969.

24. Howard L. Daley and Julius Perel, *Lithium and Sodium Surface Ionization Ion Surface Operation and Efficiency* , Review of Scientific Instruments, vol. 42, No. 9, p. 1324-1328, 1971.

25. R. K. Feeney, Willam E, Sayle, and J. W. Hooper, *Aliminosilicate Sources of Positive Ions for Use in Collision Experiments* , Review of Scientific Instruments, vol. 47, p. 964, 1976.

26. S. Kita, H. Hubner, W. Kracht, and R. Duren, *Beam Source for Moderately Fast Neutral Alkali Atoms* , Review of scientific instruments, vol. 52, p. 684-688, 1981.

27. G Conforti, F Del Giallo, F Pieralli, G Ventura, G Zaccanti, E D' Anna, and G Leggieri, *An Alkali Ion Gun for Use in Collision Experiments* , Journal of Physics E: Scientific Instruments, vol. 15, p. 827-830, 1982.

28. D. M. Thomas, W. P. West, and K. McCormick, *Low-divergence, High-brightness Lithium Ion Source for Plasma Diagnostics* , Review of Scientific Instruments, vol. 59, p. 1736-1737, 1988.

29. A. H. W. Beck, *High-current-density Thermionic Emitters: A Survey* , The Institution of Electrical Engineering, No. 213.6, p. 372-390, 1958.

30. J. L. Cronin, *Modern Dispenser Cathodes* , IEE Review of PROC., vol. 128, Pt. I, No. 1, Feb 1981.

31. R. T. Reaves, and S. M. Jarrett, *Directly Heated Tungsten Dispenser Cathodes for Ion Laser Application* , Laser Journal, A.Z. Publishing Co., 1969.

32. Technical Bulletin #117, *Emission Characteristics - Dispenser Cathodes (Performance Characteristics of the "M" Type Cathode* Spectra-Mat, Inc., CA, 1978.

33. Song, Tae Ik, *Lithium Ion Source for Satellite Charge Control* , Physics Dept.(NOT Published), NPS, Monterey, CA, June 1990.

34. Data Sheet for LI-900: Lockheed's All-Silica Insulation Material, Lockheed Missiles & Space Company, Inc., Sunnyvale, CA, 1987.

INITIAL DISTRIBUTION LIST

		No. Copies
1.	Defense Technical Information Center Cameron Station Alexandria, VA 22304-6145	2
2.	Library, Code 52 Naval Postgraduate School Monterey, CA 93943-5002	2
3.	Department Chairman, Code Ph Department of Physics Naval Postgraduate School Monterey, CA 93943-5000	2
4.	Professor R.C. Olsen, Code Ph/Os Department of Physics Naval Postgraduate School Monterey, CA 93943-5000	20
5.	Professor Otto Heinz, Code Ph/Hz Department of Physics Naval Postgraduate School Monterey, CA 93943-5000	1
6.	Professor S. Gnanalingam, Code Ph/Gm Department of Physics Naval Postgraduate School Monterey, CA 93943-5000	1
7.	Yi, Chong Man SMC # 2917 Naval Postgraduate School Monterey, CA 93943	1
8.	Ryu, Chong Uk 62-68, JungGok 4-dong, SungDong-Gu, Seoul-city, 133-224 Republic of Korea	5
9.	Ryu, Chong Soo 225-3, YunBan 4-Gu(JunKi-Ri), SukGok-Myun GokSung-Gun, JunNam-Do, 543-850 Republic of Korea	4
10.	Library Kum-Oh Institute of Technology 180-1, ShinPyung 1-Dong	1

KuMi-city, KyungBook-Do, 730-070
Republic of Korea

11. Library   1
    P.O. Box 77, GongNeung-Dong
    DoBong-Gu, Seoul-city, 132-240
    Republic of Korea

12. Army Central Library   1
    Army Headquarter, BuNam-Ri, DuMa-Myun
    NonSan-Gun, ChungNam-Do, 320-919
    Republic of Korea

13. Park, Nai Soo   1
    193-26, DoGok 1-Dong
    KangNam-Gu, Seoul-city, 130-270
    Republic of Korea

14. Park, Seong Seung   1
    625-113, 6-Tong 5-Ban, DoBong 2-Dong
    DoBong-Gu, Seoul-city, 139-012
    Republic of Korea

15. Song, Tae Ik   1
    451, PalDal-Dong, Buk-Gu
    DaeGu-city, 702-290
    Republic of Korea

16. Jung, Young Je   1
    SMC # 2240
    Naval Postgraduate School
    Monterey, CA 93943

17. Jung, Dong Seung   1
    23, JangDong 4-Ri, DaeDeuk-Gu
    DaeJun-city, 306-110
    Republic of Korea

18. Choi, Byung Gook   1
    SMC # 1587
    Naval Postgraduate School
    Monterey, CA 93943

19. Park, Hyun Kyoo   1
    SMC # 2820
    Naval Postgraduate School
    Monterey, CA 93943

20. Choi, Nag Jung   1
    SMC # 2853
    Naval Postgraduate School
    Monterey, CA 93943

21. Lee, Kyung Taek   1
    SMC # 2990
    Naval Postgraduate   School
    Monterey, CA 93943

22. Kim, Chang Ho   1
    SMC # 1671
    Naval Postgraduate School
    Monterey, CA 93943

23. R. Gracen Joiner   1
    Office of Naval Research, Code 1114
    800 North Quincy Street
    Arlington, Virginia 22217-5000

24. Dr. E. C. Whipple   1
    Center for Astrophysics and Space Science
    University of California at San Diego
    La Jolla, CA 92093

25. Dr. C. E. Mcllwain   1
    Center for Astrophysics and Space Science
    University of California at San Diego
    La Jolla, CA 92093

26. Dr. T. E. Moore, ES53   1
    NASA Marshall Space Flight Center
    Huntsville, Alabama 35812

27. Dr. K. Torkar   1
    Institute fur Weltraumforschung Oesterreichische
    Akademie der Wissenschaften
    Inffeldgasse 12
    A-8810 Graz, Austria

28. Dr. Paul Wilbur   1
    Department of Mechanical Engineering
    Colorado State University
    Ft. Collins, Colorado 80523

29. Mr. Kim Gunther   2
    Spectra-Mat, Inc.
    100 Westgate Drive,
    Watsonville, CA 95076